

Sensitivity Analysis of a Mixed-Phase Chemical Mechanism using Automatic Differentiation

Yang Zhang¹, Christian H. Bischof², Richard C. Easter¹ and Po-Ting Wu²

¹Environmental and Energy Sciences Division, Battelle, Pacific Northwest National Laboratory
Richland, WA 99352

²Mathematics and Computer Science Division, Argonne National Laboratory
Argonne, IL 60439

Argonne Preprint ANL/MCS-P680-0897

(submitted to Journal of Geophysical Research on June 6, 1997)

Abstract

A mixed-phase chemistry box model is applied to study heterogeneous chemistry and its effect on tropospheric gas-phase chemistry, particularly on photochemical production of O₃ and photochemical indicators for O₃-NO_x-hydrocarbon sensitivity, under a variety of atmospheric conditions ranging from remote marine to heavily-polluted atmospheres. A subsequent sensitivity analysis of the mixed-phase chemical mechanism is conducted using the novel automatic differentiation ADIFOR tool, which calculates the local sensitivities of species concentrations in gas, aqueous and aerosol phases with respect to a variety of model parameters. The main chemical reaction pathways in all phases, interfacial mass transfer processes, and ambient physical parameters that affect tropospheric O₃ formation, O₃-precursor relations and photochemical indicators under all modeled conditions are identified and analyzed.

The results show that the presence of clouds and aerosols not only reduces many gas-phase species concentrations and the total oxidizing capacity but alters O₃-precursor relations. Cloud chemistry is the dominant heterogeneous process under the remote and marine atmospheres. Aerosols are important scavengers for gaseous species in polluted atmospheres when the total aerosol surface area is larger than 1000 $\mu\text{m}^2 \text{ cm}^{-3}$. Decreases in concentrations and formation rates of O₃ can be up to 27% and 100%, respectively, depending on the initial atmospheric conditions and preexisting surfaces. The significant decreases in photochemical O₃ formation are primarily caused by the aqueous-phase reactions of O₂⁻ with dissolved HO₂ and O₃ under most cloudy conditions and heterogeneous uptake of O₃, HCHO, HO₂, H₂O₂ and NO₂ in the presence of aerosols. Heterogeneous chemical processes also affect the photochemical indicators and their sensitivities to many model parameters in a variety of ways.

1. Introduction

Air pollution models have provided the most effective means to quantify the impact of human activities on the atmosphere and to develop balanced and cost-effective emission control strategies for air pollutants such as tropospheric ozone (O_3) during the last several decades. The effectiveness of these abatement strategies depends on the reliability of model predictions, which is further built upon the accurate understanding and appropriate parameterization of a variety of atmospheric processes in current air quality models. Sensitivity analysis of these models is a valuable diagnostic tool capable of identifying the most influential model parameters and predicting the changes in the responses due to arbitrary perturbations in the parameters. In particular, it can evaluate the relative importance of various physical and chemical processes, the influence of the model input and mechanistic parameters, and the role of individual species and their correlations in the atmospheric system as a whole, thus providing scientific insights and suggesting research priorities for laboratory and field studies. While sensitivity analysis of 3-D models can acquire scientific information that is useful in long range scientific and regulatory analysis regarding air pollutant abatement, sensitivity analysis of atmospheric chemistry box models provides scientific insights into the detailed chemical mechanisms, on which the condensed mechanisms typically used for 3-D models are based.

Among many uncertain model mechanistic and input parameters, the representation of atmospheric chemistry used in the models is of large uncertainty. While the basic set of reactions that leads to O_3 production has been identified, different chemical representations produce different O_3 predictions. For a given chemical mechanism containing a large number of chemical reactions, model predictions of key species are sensitive to the rate parameters and product yields, which may have large uncertainties when they are based upon limited experiments or estimation (Stockwell et al., 1993). The uncertainties of the system will greatly increase in the presence of various atmospheric condensed phases (e.g., clouds, aerosols, fog, rain, and snow). A growing number of studies have shown the importance of these heterogeneous processes. For example, the heterogeneous oxidation of SO_2 on aerosols may account for nearly 60% of the tropospheric sulfate formation in marine environments (Luria and Sievering, 1991). Aerosols may be an important sink for HO_2 and influence the tropospheric H_2O_2 level (Ross and Noone, 1991). Clouds may decrease the gas-phase NO_x , O_3 , OH , HO_2 and $HCHO$ by 10-85 % in the global troposphere (Lelieveld and Crutzen, 1990). The decrease in O_3 formation is due to aqueous-phase radical reactions in typical urban polluted atmospheres (Walcek et al., 1997). However, many factors such as the reaction probability and product yields for these important heterogeneous reactions remain unknown, which creates several orders of magnitude higher uncertainties in mixed-phase chemistry than in gas-phase chemistry.

Rigorous sensitivity and uncertainty analyses of chemical mechanisms in 3-D comprehensive chemistry and transport models are rarely performed because of the computational limitation. Previous studies on chemical mechanisms and their sensitivity using 0-2D models have largely focused on limited numbers of species and model parameters for a given chemical mechanism that contains either gas-phase or aqueous-phase chemistry only. Milford et al. (1992) compared two gas-phase mechanisms: the LCC of Lurmann et al. (1987) and the CBM-IV of Gery et al. (1989) through evaluating sensitivities of model-predicted O_3 , H_2O_2 and $HCHO$ to initial concentrations and various reaction rate constants. Gao et al.

(1995) conducted a sensitivity and uncertainty analysis for the gas-phase mechanism in the second-generation Regional Acid Deposition Model (RADM2, Stockwell et al., 1990) and identified the most influential reactions to overall model predictions. Pandis and Seinfeld (1989) developed a full aqueous-phase mechanism for cloud chemistry and derived a condensed mechanism through sensitivity analysis without simulating gas-phase reactions. Since there are few models capable of realistically simulating atmospheric heterogeneous processes due to many uncertain parameters and pathways associated with these processes, the sensitivity of overall model predictions to these heterogeneous processes has been seldom quantified. To improve our understanding of heterogeneous chemistry and the associated uncertainties, a state of the art representation of all known or suspected heterogeneous chemical processes needs to be incorporated into existing atmospheric chemical mechanisms. A comprehensive sensitivity analysis based on such a mixed-phase chemical mechanism will be extremely valuable for investigating the effect of heterogeneous chemistry on photochemical processes and providing guidance for field and laboratory studies of important heterogeneous chemical reactions.

In this paper, we applied a mixed-phase chemistry box model MaTChM (Zaveri, 1997; Zhang et al., 1996) to study the effects of heterogeneous processes associated with clouds and aerosols on tropospheric gas-phase chemistry. A subsequent comprehensive sensitivity study of MaTChM was conducted using the automatic differentiation ADIFOR 2.0 tool (Bischof et al., 1992, 1996a). The sensitivities of individual species and photochemical indicators with respect to a variety of model input and mechanistic parameters are calculated and evaluated under a broad range of atmospheric conditions. Our primary objectives are to (i) quantify the impact of clouds and aerosols on tropospheric photochemistry; (ii) evaluate the sensitivity of overall model predictions to model parameterizations and inputs in the absence/presence of clouds and aerosols; (iii) identify the most important reactions in the condensed phases and the most influential model parameters under typical atmospheric conditions. The particular emphasis will be directed towards the evaluation of chemical pathways and parameters that affect tropospheric O₃ formation, O₃-precursor relations and the measurable “indicators” that indicate the sensitivity of O₃ to emissions of nitrogen oxides (NO_x) or reactive organic gases (ROG).

2. Mixed-Phase Chemistry Box Model

2.1 Mixed-Phase Chemical Mechanism

The time-dependent mixed-phase Mass Transfer with Chemical Reactions Box Model (MaTChM) treats gas and aqueous phase chemistry, heterogeneous surface reactions on aerosols, and the dynamic exchange of species between gas and condensed phases in a homogeneous parcel of air containing cloud droplets and aerosol particles. Emission, dilution, transport and deposition processes are neglected. The model includes 57, 58, and 29 species in the gas, aqueous and aerosol phases, respectively, as shown in Table 1. The mixed-phase chemical mechanism is designed to be applicable in a variety of atmospheric conditions ranging from remote marine to heavily-polluted. It consists of 125 gas-phase reactions, 120 aqueous-phase reactions, 47 dissolution and dissociation equilibria and 29 aerosol surface reactions. The gas and aqueous-

phase chemistry was taken from the earlier version of MaTChM developed by Zaveri (1997), in which a condensed dimethyl sulfide (DMS) chemistry was derived based on the comprehensive DMS chemistry of Yin et al. (1990) and combined with the condensed Carbon Bond Mechanism IV(CBM-IV) of Gery et al. (1989) and the full aqueous-phase chemistry of Pandis and Seinfeld (1989). In Zaveri (1997), the combined gas and aqueous phase chemistry was further modified for simulations in relatively clean atmospheres through explicitly treating the lesser reactive methane and ethane, and their intermediate radicals in CBM-IV and adding the aqueous-phase oxidations of DMS and DMSO by dissolved oxidants. In addition, the mass transfer between gas and aqueous phases was simulated based on the two-resistance theory of Astarita (1967). A list of gas and aqueous-phase reactions taken from the earlier work of Zaveri (1997) is given in Appendix A-1 through A-4. It is noted that these mechanisms are partially different from the current work of Zaveri (1997) in which some rate constants have been updated and additional reactions have been included. In this work, we extended the earlier version of MaTChM of Zaveri (1997) to include heterogeneous uptake of gaseous species on aerosols to explore the effect of aerosols on photochemistry and to compare it with the effect of clouds. The heterogeneous uptake on aerosols is treated as a pseudo first-order mass transfer process (Li et al., 1993; Dentener et al., 1996). The model parameterization is described in detail below.

2.2 Mathematical Description

The governing equation for the mixed-phase chemical system can be given as:

$$\frac{d\bar{G}_i}{dt} = P_{Gi} - D_{Gi}\bar{G}_i - H_i K_{Li} \left(\frac{3}{a} \right) V_c \left(\bar{G}_i - \frac{\bar{A}_i N_{avo}}{1000 H_i} \right) - K_{pi} \bar{G}_i \quad (1)$$

$$\chi \frac{d\bar{A}_i}{dt} = \chi (P_{Ai} - D_{Ai}\bar{A}_i) + H_i K_{Li} \left(\frac{3}{a} \right) V_c \left(\bar{G}_i - \frac{\bar{A}_i N_{avo}}{1000 H_i} \right) \quad (2)$$

$$Y \frac{d\bar{P}_i}{dt} = K_{pi} \bar{G}_i \quad (3)$$

where, \bar{G}_i is the bulk or average gas-concentrations of species i , \bar{A}_i and \bar{P}_i are the average aqueous- and aerosol-phase concentrations of species i , respectively (defined as the total amount of species in the aqueous or aerosol phases divided by the total volume of water in clouds or aerosols, respectively). P_{Gi} , D_{Gi} , P_{Ai} , and D_{Ai} are the chemical production and destruction terms for the gas and aqueous phases, respectively. a is the radius of cloud droplets which is assumed to be monodisperse, H_i is the effective Henry's Law constant, V_c is the liquid water content, and N_{avo} is Avogadro's number. K_{Li} is the overall mass transfer coefficient accounting for gas-phase diffusion, interfacial mass transfer, aqueous-phase diffusion and reactions in clouds; K_{pi} is the pseudo-first-order rate coefficient which describes the overall net heterogeneous loss rate of gas-phase species on aerosol surfaces. χ is the conversion factor from moles L^{-1} to molecules cm^{-3} , $= 10^{-3} N_{avo} V_c$. Y is the conversion factor from $\mu g m^{-3}$ to molecules cm^{-3} , $= 10^{-9} (R T C_{air} / P M_i)$, where R is the gas

constant in $\text{atm m}^3 (\text{Kmol K})^{-1}$, T is the temperature in K, P is the pressure in atm, C_{air} is the air concentration in molecules cm^{-3} , and M_i is the molecular weight of species i .

K_{Li} can be calculated based on the two-film theory of Astarita (1967) (Zaveri, 1997):

$$\frac{1}{K_{Li}} = \frac{1}{k_{li}} + \frac{H_i}{k_{gi}} \quad (4)$$

$$\text{with } \frac{1}{k_{gi}} = \frac{a}{D_{gi}} + \frac{4}{\alpha_i \bar{v}} \quad \text{and} \quad k_{li} = \frac{D_{li}}{\delta_{li}}$$

where k_{li} is the liquid-side mass-transfer coefficient with chemical reaction for species i ; k_{gi} is the combined gas-phase and interfacial mass-transfer coefficient for species i ; D_{gi} and D_{li} are the gas-phase and liquid-phase diffusion coefficients for species i , respectively; α_i is the mass accommodation coefficient (i.e., sticking coefficient) for species i ; \bar{v} is the mean molecular speed; and δ_{li} is the liquid-side hypothetical film thickness for species i . It depends on the cloud droplet radius and the effective aqueous-phase first-order reaction rate constant, $D_{Ai} - P_{Ai} / \bar{A}_i$. A detailed description of the mass transfer treatment can be found in Zaveri (1997).

The net removal rate on aerosols, K_{pi} , can be given as (Heikes and Thompson, 1983):

$$K_{pi} = \int_{r_1}^{r_2} k_{di}(r) \cdot n(r) dr \quad (5)$$

where $k_{di}(r)$ is the gas-to-particle diffusion rate constant of species i for a particle of radius r . It can be calculated by the Fuchs and Sutugin interpolation equation (Fuchs and Sutugin, 1970):

$$k_{di} = \frac{4\pi r D_{gi} V}{1 + K_n (\lambda + 4(1 - \gamma_i) / 3\gamma_i)} \quad (6)$$

where the variable V represents ventilation factor which is close to 1, K_n is the Knudson number, defined as the ratio of the effective mean free path of a gas molecule in air, λ , to the particle radius r , γ_i is the uptake coefficient (i.e., reaction probability) for species i . $n(r)dr$ is the aerosol number density between radii r and $r+dr$. It can be described using the lognormal size distributions for three aerosol modes (i.e., nucleation (0.001-0.1 μm), accumulation (0.1-1 μm), and coarse modes (>1 μm)) (Jaenicke, 1993):

$$\frac{dN(r)}{d(\log r)} = \sum_{j=1}^3 \frac{n_j}{\sqrt{2\pi} \log \sigma_j} \exp\left\{-\frac{(\log r/R_j)^2}{2(\log \sigma_j)^2}\right\} \quad (7)$$

where $N(r)$ is the cumulative number concentration for particles with radius larger than r , n_j , R_j and σ_j are the number density, mean radius and standard deviation of mode j , respectively.

2.3 Mass Accommodation Coefficient and Uptake Coefficient

The mass accommodation coefficient α is a fundamental parameter for heterogeneous uptake of gaseous species on particles. It represents the probability that a gas molecule reaching the particle surface will adhere to it. The sticking molecule may remain on or penetrate the surface or be desorbed back to the gas phase. The net flux to the surface can be described by the uptake coefficient γ (i.e., reaction probability), which is defined as the fraction of collisions that leads to irreversible loss of gaseous species on the particle surface. The distinction between α and γ becomes important when desorption occurs. γ represents a lower limit to α when the various processes can not be separated. Although α and γ for various species have been extensively measured during the last several years, there are still large discrepancies among measured values, with the uncertainty factors ranging from 2-3 and 2-10, respectively (DeMore et al., 1994). Thus, a constant value is usually assumed for all species in current model studies (e.g., Pandis and Seinfeld, 1989; Dentener, 1993; Li et al., 1993). Since the magnitudes of α or γ for various species vary from 10^{-8} to 1, however, this simplified treatment may introduce significant errors when estimating the effects of heterogeneous processes on photochemistry.

In this study, we incorporate the best-guessed individual mass accommodation coefficients, α_i , either from measurements or indirectly derived from kinetic measurements, to calculate the overall mass transfer coefficients K_{Li} between gas-phase and cloud droplets, as shown in Eq. (4). In the light of the increasing measurements of α_i and γ_i , it is assumed that all gaseous species that can be transferred to cloud droplets may undergo similar heterogeneous uptake and reactions on deliquescent aerosols. As an initial study indicating the effect of aerosols on tropospheric chemistry, these removal processes are assumed to be irreversible. The individual uptake coefficients γ_i measured or assumed based on the measured α_i are used to calculate the irreversible heterogeneous loss rate K_{pi} of gases on aerosols, as shown in Eq. (5). Table 2 and 3 show α_i and γ_i of condensing species used in the model and the resulting K_{pi} under the five modeled conditions, which will be described in the next section. K_{pi} is a strong function of available aerosol surfaces. It ranges from 1.0×10^{-2} to $1.0 \times 10^{-10} \text{ s}^{-1}$ and is up to 2-3 orders of magnitude higher under the polluted conditions than those under relatively clean conditions.

2.4 Model Inputs and Simulation Approaches

The sensitivities of overall model predictions are calculated along with the base simulations under a broad range of atmospheric conditions including heavily-polluted (Heavily-polluted), polluted (Urban), moderately-polluted (Rural), marine (Marine) and remote marine (Remote) conditions. The initial conditions are given in Table 4. Most initial concentrations are mainly based on literature values and the initial composition of hydrocarbon species is from Stockwell et al. (1990). The initial NO_x concentrations range from 0.1 ppb under the Remote conditions to 110 ppb under the Heavily-polluted conditions, and the corresponding initial ROG ranges from 1.0 to 1100 ppb, with a ratio of ROG/NO_x of 30 for the Urban conditions and 10 for other conditions. Under each condition, we further evaluate four scenarios: clear air (Gas) with only gas-phase reactions included, gas+aerosol (Aerosol) with gas-phase and aerosol surface

reactions included, gas+cloud (Cloud) with gas- and aqueous-phase reactions included, and gas+cloud+aerosol (Cloud+Aerosol) with all reactions included. A constant cloud droplet radius of 10 μm and a volumetric water content of 4×10^{-7} are assumed for all simulations under cloudy conditions. These values are based on the measurements of the most common cloud types (e.g., stratus and cumulus) in the boundary layer and the free troposphere (Pruppacher and Klett, 1980; Heymsfield, 1993). The resulting total droplet number density is about 95 cm^{-3} , with total surface area of $1.2 \times 10^{-5} \mu\text{m}^2 \text{ cm}^{-3}$. Different aerosol size distributions measured under different atmospheric conditions (e.g., Whitby, 1978, Jaenicke, 1993 and Fitzgerald, 1991) are used in this work. The total aerosol surface area available for surface uptake varies from a few tens $\mu\text{m}^2 \text{ cm}^{-3}$ under relatively clean conditions to a few thousands $\mu\text{m}^2 \text{ cm}^{-3}$ in polluted atmospheres.

All simulations began at local noon and were run for 2 hours. During this period of time, the atmospheric mixing, generally in equilibrium with emissions, has minimum effect on distribution and ambient concentrations of species. With maximum photolysis rates, peak ozone levels can be reached at approximate 2-4 p.m. From gas-aqueous mass transfer standpoint, the gas and aqueous-phase equilibria can be established as rapid as within a few minutes and a 2-hr period is sufficient to simulate the aqueous-phase reactions and predict their feedback to gas-phase chemistry, as shown in Pandis and Seinfeld (1989). A constant temperature of 280 K and a relative humidity (R.H.) of 80% are used for all simulations. While the high R.H. is associated with most cloudy conditions and pollution episodes, it also warrants ambient aerosols in deliquescent state with certain amounts of liquid water on the surface. A temperature of 280 K reflects a lower limit of the observed values in the boundary layer clouds. The photolysis rates are calculated continuously throughout the simulation period at a latitude of 40° N under summer time conditions. Clouds and aerosols are assumed to remain all the time for Aerosol, Cloud and Cloud+Aerosol cases. The set of ordinary differential equations (ODEs) describing the mass balances is solved using LSODE (Livermore Solver for Ordinary Differential Equations) software package (Hindmarsh, 1983). An integration time step of 1 minute is used.

3. Sensitivity Analysis Method

The system of ODEs for gas, aqueous and aerosol phase concentrations shown in Eq. (1) through (3) can be written in a generalized form:

$$\frac{dc_k}{dt} = r_k(\mathbf{c}, t, \mathbf{q}) \quad \mathbf{c}(t_0) = \mathbf{c}_0 \quad (8)$$

where \mathbf{c} is the N-dimensional vector of concentrations, \mathbf{q} is the M-dimensional time-independent vector of model parameters, c_k is the concentration of the k^{th} species, r_k is the reaction rate of the k^{th} species and is dependent on \mathbf{c} , \mathbf{q} , and the time t , \mathbf{c}_0 is the initial condition on \mathbf{c} .

The sensitivities of the concentration of the k^{th} species with respect to the l^{th} parameter

$$S_{kl} = \frac{\partial c_k}{\partial q_l} \quad (9)$$

can be computed using a variety of techniques including the brute force method, Green's function analysis (Cho et al., 1987), adjoint Green's function analysis (Hall and Cacuci, 1983), and several variations of the direct decoupled methods (Dunker, 1984). Most sensitivity studies of 3-D atmospheric models have been conducted using the so-called brute force method, i.e., a number of model parameters are varied and the simulation results are then compared. This approach is closely related to finite-difference approximations of derivatives, where the derivatives $\partial c_k / \partial q_l$ are approximated as $[c_k(q + h e_l) - c_k(q)] / h$, where e_l is a vector that is all zero except for an entry of unity in its l^{th} component. This method becomes less viable as the model becomes more comprehensive because of the large computational burden. In addition, a suitable choice of the stepsize h may not be obvious. An alternative technique for sensitivity study is automatic differentiation (AD). This approach is superior to finite difference approximation of the derivatives because the numerical values of the computed derivatives are guaranteed to be accurate to machine precision and the computational effort can be significantly lower (Griewank and Corliss, 1991). In our work, we employ the ADIFOR (Automatic Differentiation in FORTRAN) tool (Bischof et al., 1992, 1996a), to compute a complete set of sensitivities for all species with respect to all model parameters.

3.1 Introduction for ADIFOR

Automatic differentiation is an approach to computing sensitivities which relies on the fact that every function, no matter how complicated, is executed on a computer as a sequence of elementary operations such as additions, multiplications, and elementary functions such as \sin and \cos (e.g., Rall, 1981; Griewank and Corliss, 1991; Berz et al., 1996). By applying the chain rule of derivative calculus over and over again to the composition of those elementary operations, one can compute, in a completely mechanical fashion, derivatives of a function f that are correct up to machine precision. Traditionally, two approaches to AD have been developed: the so-called forward and reverse modes, which are distinguished by how the chain rule is used to propagate derivatives through the computation. The two approaches are briefly summarized below. A detailed description can be found in Bischof et al. (1996a) and the references therein.

Assume that we have a code for the computation of a function f , $f : q \in R^M \mapsto c \in R^N$ we wish to compute S_{kl} in Eq. (9), i.e., the derivatives of the dependent variables c_k with respect to independent variables q_l . The forward mode propagates derivatives of intermediate variables with respect to the independent variables and follows the control flow of the original program. By exploiting the linearity of differentiation, the forward mode allows us to compute arbitrary linear combinations $J \cdot U$ of columns of the Jacobian $J = dc / dq$. For an $N \times p$ matrix U , the effort required is roughly $O(p)$ times the runtime and memory of the original program. In particular, when U is a vector u , we compute the directional derivative

$$J * u = \lim_{h \rightarrow 0} \frac{f(q + h \cdot u) - f(q)}{h}.$$

In contrast, the reverse mode of AD propagates derivatives of the final result with respect to an intermediate quantity, in a fashion that is closely related to discrete adjoint techniques. To propagate adjoints, one must be able to reverse the flow of the program, and remember or recompute any intermediate value that nonlinearly affects the final result. However, if these technical difficulties can be overcome, for a

$z \times M$ matrix W , the reverse mode allows us to compute the row linear combination $W \cdot J$ with $O(z)$ times as many floating-point operations as required for the evaluation of f . When W is a row vector w , we compute the derivative $\partial(w^T * c) / \partial \mathbf{q}$.

The ADIFOR 2.0 system, jointly developed by Argonne National Laboratory and Rice University (Bischof et al., 1996a), provides the directional derivative computation possibilities associated with the forward mode of AD. ADIFOR has several novel features:

- It employs a hybrid scheme that combines the forward mode overall with the reverse mode at the statement level;
- The SparsLinC subsystem allows transparent exploitation of sparsity in derivative objects, without any a-priori knowledge of sparsity structure (Bischof et al., 1996b);
- The ADIntrinsics subsystem provides complete and user-configurable handling of all Fortran 77 intrinsics;
- ADIFOR supports almost all of Fortran 77, in particular, the differentiation of codes using any or all of the real or complex single or double precision-valued data types.

ADIFOR has been applied to sensitivity analysis in a variety of problem domains as described in Bischof et al. (1996a). In particular, ADIFOR has been used for sensitivity analysis of atmospheric models including 0-D Sulfur Transport Eulerian Model (STEM-II) (Carmichael et al., 1997) and MM5, a 3-D finite-difference weather model for meso- and regional-scale studies (Bischof et al., 1996c). Application of ADIFOR to a code requires that the user designate the independent and dependent variables with respect to differentiation, and provide the location of the source files containing the subroutines to be differentiated. ADIFOR then generates a new FORTRAN code that computes both the original simulation and its derivatives. The user then provides a derivative driver that selects at runtime what derivative is to be computed (this corresponds to the instantiation of the matrix U mentioned above) and invokes the ADIFOR-generated code. Similar functionality has been recently developed for ANSI-C programs with the ADIC tool (Bischof et al., 1996d) and that a survey of available automatic differentiation tools can be found at http://www.mcs.anl.gov/Projects/autodiff/AD_Tools.

3.2 Application of ADIFOR to MaTChM

To compute the sensitivities S_{kt} in Eq. (9), we applied ADIFOR directly to the MaTChM code, which basically consists of the code for LSODE and the code for rate equations. That is, we considered the MaTChM code as a “black box” that, given an initial concentration c_0 and input parameters \mathbf{q} , produced concentration of species k at time t , c_{kt} . Nominating \mathbf{q} as independent variables and \mathbf{c} as dependent variables, ADIFOR then automatically produces a code that computes the desired sensitivity coefficients.

Carmichael et al. (1997) applied such a black-box approach to the STEM-II model using a quasi-steady state approximation (QSSA) integrator. They showed that for a fixed-stepsizes QSSA integrator this

black-box approach delivered results that are comparable to those obtained by integrating the ODE's for S_{kl} that would be obtained by differentiation of Eq. (8). In general, though, the automatic differentiation of sophisticated numerical integrators requires some care. In particular, Eberhard and Bischof (1996) showed that for integrators with adaptive stepsize control (such as LSODE) some postprocessing may be required to recover the desired sensitivities. They observed that the *algorithmic* sensitivities (which are computed by AD) may reflect the impact of numerical artifacts such as stepsize control and showed the relation of these algorithmic sensitivities with the *analytic* sensitivities that are desired. In the case of LSODE, it turned out that the stepsize control did not affect the AD-computed derivatives as described in Eberhard and Bischof (1996). However, under cloudy conditions, we had to adjust the so-called “internal stepsize” parameter of LSODE to obtain the desired derivatives. We are continuing our studies on the interplay of AD and sophisticated numerical algorithms. So far initial work has been done on integrators (Carmichael et al., 1997; Eberhard and Bischof, 1996) and certain classes of nonlinear solvers (Griewank et al., 1993), but much remains to be done.

To compare sensitivities with dependent and independent variables of different orders of magnitude, the dimensionless sensitivities (i.e., normalized local sensitivities) is calculated:

$$\bar{S}_{kl} = \frac{q_l}{c_k} \frac{\partial c_k}{\partial q_l} = \frac{\partial \ln c_k}{\partial \ln q_l} \quad (10)$$

The sign of \bar{S}_{kl} gives the sense of response of c_k upon the relative variation of q_l . The positive values indicate that c_k increases with the increase in q_l , while the negative values mean a reversed change in c_k when increasing q_l . The magnitude of \bar{S}_{kl} gives the relative change in c_k due to one unit change (i.e., doubling its value) in q_l . For instance, a value of $\bar{S}_{kl}=0.5$ can be interpreted to mean that doubling q_l will lead to a 50% increase in concentration of species k .

Applying ADIFOR to MaTChM, we computed the sensitivities of 144 gas, aqueous and aerosol species concentrations with respect to 404 model parameters at every integration time step. The model parameters include 245 reaction rate constants; 134 mass transfer parameters; 21 species initial concentrations, and 4 physical parameters (temperature, R.H., cloud water content and droplet radius). While it is easy to compute derivatives with AD and recompute derivatives in response to changes in the code (we actually found a bug in the code of MaTChM through inspection of the ADIFOR-computed sensitivities), large-scale sensitivity analysis is still computationally expensive. For example, the undifferentiated model required 0.72MB of memory and 1.3 minutes on an IBM RS/6000 workstation with 128MB RAM running at 62.5 Mhz. On the same machine, the sensitivity analysis with respect to all 404 parameters required 197 MB of memory and roughly 10.6 hours CPU time. For every run, we computed 404 parameters x 144 concentrations x 60 time steps = 3,490,560 sensitivities. Using ADIFOR “out of the box,” it was feasible to compute this large number of sensitivities with little human effort, and the time required to compute the derivatives mattered little in comparison to the effort required to interpret the 27.7 Mbytes of data produced by one run.

We note, however, that AD and the associativity of the chain rule allow for various ways of decreasing the computational cost, both with respect to memory and runtime. Derivatives can be computed in parallel (Bischof et al. 1994; Bischof and Wu 1997), cost can be reduced by techniques such as interface contraction (Hovland et al., 1997; Bischof and Haghighat, 1996), the number of derivatives can be reduced via “shaped” perturbations (Bischof et al., 1996c), or the understanding of the mathematical underpinnings of a particular algorithm may make it possible to avoid differentiation of parts of the code (Griewank et al., 1993; Carle and Fagan, 1996).

Given the sensitivities of individual species, the sensitivities of the ratio of the concentrations of the i^{th} species to the j^{th} species with respect to the arbitrary parameter q_l can be easily derived as the difference of the two individual sensitivities:

$$\bar{s}_{r_{ijl}} = \frac{q_l}{(c_i / c_j)} \frac{\partial(c_i / c_j)}{\partial q_l} = \frac{q_l}{c_i} \frac{\partial c_i}{\partial q_l} - \frac{q_l}{c_j} \frac{\partial c_j}{\partial q_l} = \bar{s}_{il} - \bar{s}_{jl} \quad (11)$$

The sensitivity of lumped concentrations of two (or more) species can also be calculated as the sum of products of the concentration fraction and the sensitivity coefficient of each species:

$$\bar{s}_{s_{ijl}} = \frac{q_l}{(c_i + c_j)} \frac{\partial(c_i + c_j)}{\partial q_l} = \frac{c_i}{(c_i + c_j)} \bar{s}_{il} + \frac{c_j}{(c_i + c_j)} \bar{s}_{jl} \quad (12)$$

Using Eq. (11) and (12), we calculated the sensitivities of several lumped species (e.g., NO_x , NO_z , R_xO_y , defined in Table 1) and photochemical indicators (e.g., NO_y , O_3/NO_z , and $\text{H}_2\text{O}_2/\text{HNO}_3$) with respect to all model parameters under all conditions. Instantaneous sensitivities at selected time steps and the sensitivities averaged during the last hour simulation along with base simulation results are analyzed and discussed below.

4. Results and Discussions

4.1 The Base Simulations

4.1.1 Heterogeneous Effects on Gas-Phase Species

Table 5 shows the average concentrations and percent changes in concentrations of 12 major gas-phase species and total sulfate and nitrate formed in all phases during the last hour simulation under various conditions. The heterogeneous processes associated with clouds and aerosols can affect these species in a variety of ways, either increasing or reducing their concentrations. The changes in species concentrations range from a few percent to several times, depending on properties of species (e.g., gas-phase diffusivity, interfacial mass accommodation coefficient or uptake coefficient, effective solubility, diffusivity, and

reactivity in the aqueous-phase) and properties of pre-existing particles (e.g., liquid water content and size distribution).

Under cloudy conditions, HNO_3 , HCHO , HO_2 , and H_2O_2 experience significant reduction (10.4-100%) in their gas-phase concentrations due to their high solubilities (with Henry's law constants greater than 100 M atm^{-1}). Although OH , SO_2 , and H_2SO_4 have relatively small Henry's law constants, these species can undergo rapid aqueous-phase reactions and/or dissociations, which greatly enhances their effective solubility and results in large concentrations decreases (6.8-100%). Under aerosol conditions, various species undergo irreversible reactions on aerosols with a pseudo first-order rate ranging from 1×10^{-10} to $1 \times 10^{-2} \text{ s}^{-1}$, which depends on gas-phase diffusivity, pre-existing aerosol surface and individual species uptake coefficient. When the surface areas are greater than $1 \times 10^2 \mu\text{m}^2 \text{ cm}^{-3}$ (i.e., Rural), aerosols are found to have appreciable effects (decrease by 6.6- 43.9%) on many species including HNO_3 , PAN, H_2SO_4 , HCHO , OH , HO_2 , and H_2O_2 . They become very effective scavengers when the available surface areas are greater than $1 \times 10^3 \mu\text{m}^2 \text{ cm}^{-3}$ (i.e., Urban and Heavily-polluted), with decreases in many species concentrations comparable or even larger than those under cloudy conditions.

In the presence of both clouds and aerosols, heterogeneous uptake and chemistry on both surfaces occur, competing for the available condensing gases. The combined heterogeneous effects are a nonlinear function of their individual effects. The magnitude of these effects is determined by the scavenging efficiencies of clouds and aerosols, which vary with the initial gas-phase concentrations, the assumed cloud parameters and aerosol size distributions. In the Marine and Remote atmospheres, cloud processes control losses of almost all species, because the total surface area of cloud droplets is $1.2 \times 10^5 \mu\text{m}^2 \text{ cm}^{-3}$, which is at least four orders of magnitude higher than the total aerosol surface areas. Aerosol surface uptake becomes increasingly important with increasing surface areas. Under the Heavily-polluted and the Urban conditions, the large aerosol surface areas result in rapid heterogeneous loss rates for many condensing species. Consequently, aerosols serve as a very effective sink for many species including OH , HO_2 , HCHO , PAN, and O_3 , while both clouds and aerosols contribute significantly to the loss of HNO_3 , SO_2 , H_2SO_4 , and H_2O_2 . The effect of aerosols can be comparable or even overwhelming to that of clouds. For instance, under the Heavily-polluted conditions, more than 80% of decrease in O_3 and PAN concentrations is due to aerosols surface uptake processes.

As a consequence of the decreases in concentrations of many gaseous precursors and reactive radicals, the predicted concentrations of O_3 and PAN are consistently reduced in the presence of clouds and/or aerosols. Figure 1 shows concentrations of O_3 and PAN as a function of time under various polluted conditions. The decreases in O_3 concentrations at the end of the 2-hour simulation range from 0.6-5.1 ppb (~3-9%), 0.2-24.2 ppb (~0.3-27%) and 0.6-24.5 ppb (~3-26.8%) due to cloud chemistry, aerosol surface uptake, and the combined cloud and aerosol chemistry, respectively. While the magnitude of cloud effect on O_3 is similar under various conditions due to constant cloud water content and droplet size, the aerosol surface area and O_3 formation are anti-correlated, i.e., the magnitude of O_3 reduction appreciably increases as the air becomes increasingly polluted (i.e., the surface areas become larger). Under moderately-polluted and relatively clean conditions, the decreases in O_3 due to aerosol surface reactions are negligible (< 2%). The aerosol surface uptake processes become important and dominate the decreases in O_3 concentrations under

the Urban and the Heavily-polluted conditions. The relative changes in PAN concentrations under various conditions are even larger, with decreases of 0.1-0.7 ppb (~8-69.2%), 0.003-1.7 ppb (~2-38%) and 0.15-2.1 ppb (33-69.2%) at the end of simulation due to cloud chemistry, aerosol surface uptake and their combination, respectively.

Clouds and aerosols are not always a sink for gas-phase species. Their presences actually help increase gas-phase budgets of some insoluble or less soluble reactive nitrogen and organic species including NO, NO₂, PAR, OLE, ETH, TOL, XYL and ISOP. Since the reactions of these species with many oxidants and radicals are usually the major sinks, the decrease in the concentrations of oxidants and radicals reduced these sinks. For example, lower OH and HO₂ can lower the depletion rates of NO, PAR, OLE, ETH, TOL, XYL, and ISOP via reactions G28, G52, G57, G61, G63, G69 and G76, respectively. As a result, these species remain in the gas-phase with higher concentrations when there are clouds and/or aerosols. The effects of clouds and aerosols are complicated for NO₂, with a decreased concentration under the Remote and Heavily-polluted conditions and an increased one under other conditions, reflecting a competition between its sink and source reactions. In addition, the heterogeneous oxidation of SO₂ and NO_x associated with clouds and aerosols is shown to be a dominant pathway, resulting a higher total sulfate formation under all cloud and/or aerosol conditions and a higher nitrate formation under the Heavily-polluted conditions as compared to those in clear air.

Dentener and Crutzen (1993) reported a net decrease in yearly-averaged concentrations of NO_x (by 50%), O₃ (by 25%) and OH (by 30%) due to heterogeneous reactions of NO₃ and N₂O₅ on aerosols using a 3-D global model. While consistent results are found for O₃ and OH, our results also show the concentrations of NO_x could be higher (rather than lower) when aerosol chemistry is included. The different aerosol effects on NO_x can be attributed to two reasons. First, the uptake coefficients that we use for NO₃ and N₂O₅ are 1×10^{-3} and 5×10^{-3} , respectively (Thomas et al., 1989; Kirchner et al., 1990), which are lower limits of available measurements. Dentener and Crutzen adopted the value of 0.1 for both species, which is the upper limit of measurements. While these two studies provide the variation range of the observation, the rate of denitrification due to NO₃ and N₂O₅ reactions on aerosols is several orders of magnitude faster in their work. Secondly, Dentener and Crutzen neglected other possible aerosol surface reactions such as uptake of OH, HO₂ and H₂O₂ in their calculations. OH levels are likely overpredicted when these processes are ignored. The lowered OH levels predicted in this work can further reduce the rate of NO_x sinks (e.g, G26 and G28), resulting in higher gaseous NO_x.

4.1.2 Heterogeneous Effects on Photochemical Indicators

Scientific understanding of the relationships between O₃ and its precursors NO_x and ROG is essential in the development of more effective O₃ abatement strategies. A fundamental factor that leads to difficulties and ineffectiveness in attainment of O₃ is that O₃ is not directly emitted but is formed by a complex set of photochemical reactions involving nonlinear interactions among NO_x, ROG, and CO. In the past, evaluations of O₃-NO_x-ROG sensitivity have largely relied on 3-D photochemical model simulations, which are highly dependent upon model assumptions and thus possibly lead to inaccurate predicted sensitivity.

Recent studies have established the use of measurable photochemical indicators in determining the O_3 - NO_x -ROG sensitivity in order to effectively control O_3 at non-attainment regions. This approach is based on direct measurements of individual species or species ratios that consistently assume different values under NO_x - and ROG-sensitive conditions. Milford et al. (1994) have found that O_3 is ROG-sensitive in regions where afternoon NO_y concentrations are higher than a threshold value ranging from 10-25 ppb, whereas it becomes NO_x -sensitive with NO_y concentrations lower than the threshold. Sillman (1995) has linked ROG-sensitivity chemistry to afternoon conditions with $NO_y > 20$ ppb, $O_3/NO_z < 7$, $HCHO/NO_y < 0.28$, and $H_2O_2/HNO_3 < 0.4$, lower NO_y and higher ratios correspond to NO_x -sensitive O_3 . Other indicators include O_3/NO_y , O_3/HNO_3 , H_2O_2/NO_y (Trainer et al., 1993 ; Sillman, 1995) and $(HNO_3/H_2O_2) / (NO_x/ROG)$ (Stockwell, 1986). All these indicators and corresponding threshold values are established under the clear air conditions. The theoretical rational for use of these species and ratios as indicators for O_3 - NO_x -ROG sensitivity is described in several literatures (e.g., Milford et al., 1994; Sillman, 1995).

The calculated indicators under various polluted conditions are shown in Table 6. The relative changes represent the perturbation in the indicators due to clouds and/or aerosols relative to the values under the clear air conditions. According to the aforementioned threshold values of indicators, O_3 is ROG-sensitive and NO_x -sensitive under the Heavily-polluted and the Rural clear air conditions, respectively. O_3 chemistry exhibits a transition between the two regimes under the Urban conditions, with $10 < NO_y < 20$ ppb but values of O_3/NO_z , $HCHO/NO_y$ and H_2O_2/HNO_3 higher than the thresholds. While cloud and aerosol chemistry can always increase O_3/NO_z and O_3/HNO_3 , decrease NO_y , H_2O_2/NO_y , $HCHO/NO_y$, and $(HNO_3/H_2O_2)/(NO_x/ROG)$ under all modeled conditions, it can cause either an increase or a decrease in O_3/NO_y and H_2O_2/HNO_3 . Some changes are so substantial that they can cause a controversy or even failure of the above criteria developed for determination of O_3 - NO_x -ROG sensitivity. For example, the value of O_3/NO_z under the Heavily-polluted conditions changes from 6.48 to 14.1 and 13.2 in the presence of clouds and aerosols, respectively, which exceeds the range of ROG-sensitive regime. Other indicators NO_y , $HCHO/NO_y$ and H_2O_2/HNO_3 still fall in the ROG-sensitive regime. Exclusion of heterogeneous chemistry could cause the incorrect model predictions of indicators and the inaccurate determination of threshold values for different chemical regimes. Therefore, the established criterias of indicators under clear air conditions are not applicable to regions where the large cloud coverage or high aerosol loading are frequently observed.

4.2 Sensitivity Analysis

The base simulation results show that heterogeneous chemistry can significantly change concentrations of many important gas-phase species and reduce the total tropospheric oxidizing capability (TOC) (i.e., the total burden of principal oxidants such as O_3 , H_2O_2 , and OH radicals) under typical atmospheric conditions. To further study the correlation of O_3 and its precursors and to evaluate the relative importance of the homogeneous and heterogeneous pathways, we conduct several sets of sensitivity analysis for the mixed-phase chemical mechanism by excluding or including heterogeneous chemistry under the five

conditions using automatic differentiation ADIFOR tool. The results are presented and discussed in the following sections.

4.2.1 Gas-Phase Chemistry

4.2.1.1 Sensitivity to Gas-Phase Reaction Rate Constants

The 30 most influential reactions for O_3 concentrations under the five conditions are ranked along with the 1-hr average sensitivities of O_3 to these reaction rate constants in Table 7. These reactions could have either positive or negative influences depending on the signs of their sensitivities. O_3 predictions are more sensitive (by a factor of a few to several hundreds) to reaction rate constants under various polluted conditions (i.e., Rural, Urban and Heavily-polluted) than relatively clean conditions (i.e., Marine and Remote) for one unit change in the rate constants. For instance, when the rate constant of R1 doubles, the predicted O_3 concentration will increase by 1.86%, 4.13% and 27.7 % under the Remote, Rural and Heavily-polluted conditions, respectively. This is because O_3 formation rate in the lower atmosphere is proportional to the TOC. The TOC is much higher under polluted conditions, resulting in higher reaction rates of most species. Higher sensitivities reflect higher influence of these reactions and larger model responses to uncertainties in the rate constants.

Under the Remote and Marine conditions, the most important reactions contributing to O_3 production are $NO+HO_2$ (G28), $NO_2+h\nu$ (G1), CH_4+OH (G116), $NO+CH_3O_2$ (G117), $H_2O_2+h\nu$ (G34), $CO+OH$ (G36), $HCHO+h\nu$ (G38), $C_2O_3 + NO$ (G46), the photolysis of O_3 (G9) and the subsequent reaction of $O(^1D)+H_2O$ (G11). G28 and G117 are major pathways for conversion of NO to NO_2 . Followed by G1, they generate $O(^3p)$, which directly produces O_3 . The photolysis of H_2O_2 (G34), $HCHO$ (G38) and O_3 (G9) are the major sources of OH and HO_2 . A higher rate constant of G9 decreases O_3 but increases $O(^1D)$, which contributes to O_3 production via generation of OH (G11). The increase in O_3 via G11 compensates the decrease via G9. Thus, G9 has a net positive impact on O_3 . OH can be converted to HO_2 and CH_3O_2 by reacting with CO (G36) and CH_4 (G116), respectively. These radicals then convert NO to NO_2 via G28, G117 and G46. The generation and inter-conversion of these radicals thus increase O_3 by increasing the TOC. Compared to the Remote conditions, O_3 formation under the Marine conditions is more affected by the photolysis of $HCHO$ (G38) by one order of magnitude, due to a much higher initial $HCHO$. The reactions contributing to O_3 destruction include $NO+O_3$ (G3), $HO_2+CH_3O_2$ (G118), NO_2+OH (G26), $2HO_2+H_2O$ (G33), HO_2+HO_2 (G32), $O(^1D)\rightarrow O(^3p)$ (G10), O_3+HO_2 (G13), O_3+OH (G12), $ALD_2 + OH$ (G43), and $C_2O_3 + NO_2$ (G47). O_3+NO (G3) is the predominant destruction pathway for O_3 . G10 reduces O_3 via reducing $O(^1D)$, a major source of OH. Representing the major sink for OH, HO_2 , and CH_3O_2 , the formation of peroxides (G118, G33 and G32), HNO_3 (G26) and PAN (G47 following G43) reduces the TOC thus decreases O_3 . O_3 can also be directly destroyed by OH (G12) and HO_2 (G13).

Under various polluted conditions, G28, G32, G33, G116-118 become less important or unimportant because of the relatively lower HO_2 and CH_3O_2 . O_3 predictions are highly sensitive to ROG chemistry. This is consistent with the results from photochemical indicator calculations in section 4.1.2. $HCHO+h\nu$

(G38), $\text{ALD}_2 + \text{OH}$ (G43), $\text{OLE} + \text{OH}$ (G57) become the most important positively-influential reactions under the Urban and the Heavily-polluted conditions, with their effects comparable or even higher than other important inorganic reactions such as G1 and G3. Other important positively-influential ROG reactions include reactions of C_2O_3 with NO and NO_2 (G46 and G47), photolysis of ALD_2 and MGLY (G45 and G74), $\text{OLE} + \text{O}_3$ (G58), $\text{NO} + \text{TO}_2$ (G64) and reactions of HCHO, PAR, ETH, TOL, XYZ and ISOP with OH (G37, G52, G61, G63, G69, and G76). A higher rate constant of G58 directly decreases O_3 but simultaneously increases odd hydrogen R_xO_y and O_3 precursors HCHO and ALD_2 , which eventually give rise to O_3 via G1 and G2. The increase in O_3 due to these pathways suppresses the direct decrease, thus G58 shows a net positive impact. Other ROG reactions (i.e., G37, G45, G46, G52, G57, G61, G63, G64, G69, and G74) contribute to O_3 formation by producing HCHO, ALD_2 , HO_2 and RO_2 . G43 and G47 are dominant negatively-influential ROG reactions. G39 also contributes to O_3 destruction by competing with the positively-influential reaction G38 and consuming HCHO. These results are consistent with the sensitivity analyses of other gas-phase mechanisms such as RADM2, CBM-IV, LLM and STEM-II under smog chamber and urban plume conditions by Milford et al. (1992), Gao et al. (1995) and Carmichael et al. (1997).

Photochemical indicators are mainly discovered based on theoretical rational and case studies using 3-D models, therefore their applications involve large uncertainties arising from model assumptions or omissions. While being verified by growing observational dataset, the sensitivity of these model-based indicators to model parameters have not been fully explored. Our sensitivity analysis shows that NO_y and O_3/NO_y are relatively insensitive ($\bar{S}_{kl} < 0.01$) to most model parameters (e.g., reaction rate constants), whereas other indicators involving H_2O_2 , HNO_3 , HCHO and NO_z are highly sensitive to changes in many model parameters. Figure 2 shows the 1-hr average sensitivities of O_3/NO_z and $\text{H}_2\text{O}_2/\text{HNO}_3$ with respect to gas-phase reaction rate constants under various polluted conditions. Both O_3/NO_z and $\text{H}_2\text{O}_2/\text{HNO}_3$ are much more sensitive to these rate constants than O_3 itself, with their sensitivities as large as 0.6.

While the most influential reactions for these indicators are almost the same as those for O_3 , their relative impacts are different both in signs and amplitudes. For example, the photolysis of HCHO (G38) has a positive impact on O_3 , but a negative impact on O_3/NO_z and $\text{H}_2\text{O}_2/\text{HNO}_3$. While a higher rate constant of G38 increases O_3 and H_2O_2 formation via generation of HO_2 , it also increases the denominator NO_z and HNO_3 . The net effect is the decrease in both O_3/NO_z and $\text{H}_2\text{O}_2/\text{HNO}_3$. Such a decrease can be up to 10-55% when doubling the reaction rate constant of G38. Similar to O_3 , the indicators generally exhibit higher sensitivities on basic $\text{O}_3\text{-NO}_x\text{-CO}$ reactions (G9-G11, G26, G28, G29, G32-34, and G36) under the Rural conditions, and higher (by a factor of 2-30) sensitivities on various ROG reactions (G38, G39, G43, G45-G47, G52, G57, G58, G61, G69, and G74) under the Urban and the Heavily-polluted conditions. This coincides with the nature of the indicators as good markers for the $\text{O}_3\text{-NO}_x\text{-ROG}$ sensitivity. For instance, the sensitivities of O_3/NO_z and O_3 to G38, G45, and G58 under the Heavily-polluted conditions are higher than those under the Rural conditions by a factor of 4.0, 16, and 29, and a factor of 18, 68, and 168, respectively, indicating that ROG chemistry is dominant under the Heavily-polluted conditions. Lower

sensitivities to ROG reactions and higher sensitivities to O_3 - NO_x -CO reactions under the Rural conditions indicate a NO_x -dominant chemistry.

4.2.1.2 Sensitivity to Species Initial Concentrations

The O_3 predictions are also sensitive to species initial concentrations. The initial O_3 always has the predominant positive impact on the predicted O_3 . Doubling initial O_3 will result in an increase of 73-100% in predicted O_3 under various conditions. Figure 3(a) shows the sensitivity of O_3 with respect to initial species concentrations under the five conditions at the end of the 2-hr simulation. The O_3 -precursor relations are different at various conditions. Under relatively-clean conditions, O_3 production increases with increasing NO_x but is insensitive to ROG (except for HCHO and ALD_2 under the Marine conditions). At various polluted conditions, O_3 formation increases rapidly with increasing ROG (except for ALD_2) and decreases with increasing NO_x . The sensitivities of O_3 to positively-influential ROG species increase as the air becomes increasingly polluted. Other O_3 precursors such as H_2O_2 , CO, and CH_4 have relatively large impact on O_3 production under the Remote, Marine and Rural conditions. Being a major source of OH, H_2O_2 helps produce O_3 under these conditions. CO and CH_4 always tend to increase O_3 via G36 and G116 followed by G28, G1 and G2.

Since O_3 production rate is proportional to reactions of ROG with OH radicals under most atmospheric conditions (Sillman, 1995), the different O_3 -precursor relations under various conditions can be interpreted by relative importance of reactions of odd hydrogen, R_xO_y ($=OH+HO_2+CH_3O_2+ETHP+C_2O_3+ROR+TO_2+CRO$, see Table 1), as shown in Table 8. Under the Remote and Marine conditions, formation of peroxides via HO_2+HO_2 (G32), $2HO_2+H_2O$ (G33) and $HO_2+CH_3O_2$ (G118) are the major sinks for R_xO_y . The fate of OH is mainly governed by the inter-conversion of OH, HO_2 , and CH_3O_2 via $NO+HO_2$ (G28), CH_4+OH (G117), $CO+OH$ (G36), and $HCHO+OH$ (G37). OH decreases with a higher HCHO (due to G37) under both conditions and other ROG species including ALD_2 , PAR, OLE, C_2H_6 , ETH and TOL (due to G37, G43, G47, G51, G52, G57 and G61) under the Marine conditions. Thus, O_3 production is insensitive to most ROG (only HCHO exists under the Remote conditions), because increases in ROG coincide with decreases in OH. As a predominant pathway for O_3 production, the conversion of NO by HO_2 (G28) results in a higher O_3 followed by G1 and G2 (see Table 7). $NO+HO_2$ (G28) and $NO_2+h\nu$ (G1) compete with $NO+O_3$ (G3) and NO_2+OH (G26), with less NO_x available for the latter reactions. In addition, OH increases with increasing NO_x (due to G28). Thus, a higher NO_x always causes a higher O_3 under both conditions.

Under various polluted conditions, the reactions of $NO_2+h\nu$ (G1), $NO+O_3$ (G3), NO_2+OH (G26), $HCHO+h\nu$ (G38), ALD_2+OH (G43), and $NO_2+C_2O_3$ (G47) are the overwhelming pathways affecting O_3 production. Both $NO+HO_2$ (G28) and NO_2+OH (G26) are the predominant pathways for R_xO_y . While an increase in NO consumes more O_3 and HO_2 via G3 and G28, a higher NO_2 results in a lower OH (due to G26). Therefore, an increase in NO_x leads to a lower O_3 . Increases in individual ROG species either increase or decrease OH, but the net overall effect is a slight increase in OH, reflecting that ROG reactions

could be a source of R_xO_y . Thus, O_3 increases with increases in most ROG species. When present, ALD_2 always has a negative influence on O_3 (up to 11% decrease) because it acts as a sink for NO_x via G43 and G47. G43 generates C_2O_3 , which either reduces NO_2 through G47 or converts NO to NO_2 via G46. Being a sink for NO_2 , G47 is relatively more important to the source G46. Correspondingly, O_3 decreases with higher rate constants of G43 and G47 but increases with a higher rate constant of G46 (see Table 7), causing the anti-correlation between O_3 and the initial ALD_2 . The negative impact of ALD_2 on O_3 formation has also been reported by Carmichael et al. (1997) under similar conditions, by Carter and Atkinson (1989) under low NO_x conditions and by Milford et al. (1992) under the smog chamber conditions with higher ROG to NO_x ratios.

Figure 3 (b) through (d) show the 1-hr average sensitivities of NO_y , O_3/NO_z and H_2O_2/HNO_3 to species initial concentrations under various polluted conditions. These indicators are affected in a variety of ways. NO_y is predominantly correlated to initial NO_x and almost insensitive to initial concentrations of other species. O_3/NO_z is anti-correlated to initial H_2O_2 , NO , $HCHO$, ALD_2 , OLE , TOL , XYL and $ISOP$, and positively-correlated with initial O_3 , PAR , CO and CH_4 . The impacts of NO_2 and ETH are complicated and can be either way. For H_2O_2/HNO_3 , the positively-influential species include H_2O_2 , ALD_2 , PAR , CO and CH_4 , and the negatively-influential species are O_3 , NO_x , $HCHO$ and XYL . The impacts of OLE , ETH and TOL can be either negative or positive. These relations are much more complicated relative to O_3 -precursor relations. The interpretation requires an understanding of the chemical behaviors of the individual indicator species. Although an increase in various ROG species (other than ALD_2) can always increase O_3 production, only a few of them (e.g., PAR) can increase O_3/NO_z . Most ROG species negatively affect the indicator because they simultaneously increase the denominator NO_z to the extent of exceeding the increase in O_3 . Whether the species have positive or negative impacts depends on the relative importance of their reactions and the signs of the predominant reactions. For instance, G1, G26 and G28 are important reactions for NO_2 . Under the Rural and Urban conditions G26 and G28 are the predominant reactions and both have a negative sign. Under the Heavily-polluted conditions, G1 is predominant and has a positive sign. Correspondingly, O_3/NO_z and NO_2 are positively-correlated under the Heavily-polluted conditions but anti-correlated under the Rural and Urban conditions.

4.2.1.3 Sensitivity to Temperature and Relative Humidity

Most species are very sensitive to changes in temperature and relative humidity (R.H.) under all modeled conditions, as shown in Table 9. Under all conditions, a higher temperature always results in higher HNO_3 , H_2SO_4 , OH , HO_2 , PAN and O_3 due to an increase in their formation rates and lower SO_2 due to an increase in its destruction rate. A higher temperature will decrease H_2O_2 and increase O_3 , NO_z and HNO_3 , with the net effects of increasing NO_y and decreasing the other two indicators. O_3 (under relatively-clean conditions), SO_2 (under all conditions), and NO_y (under polluted conditions) are less sensitive to changes in temperature, with their sensitivities at least one order of magnitude lower than those of other species and indicators. For example, an increase of 2.8 K in temperature will increase O_3 by 1.26% but increase H_2SO_4

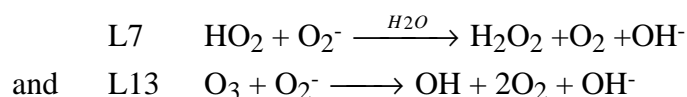
by 16.7% and decrease O₃/NO_z by 12.8% under the Rural conditions. While SO₂, O₃ and NO_y are also less sensitive to R.H., other species and indicators exhibit much higher sensitivities to R.H., with values greater than 1 x 10⁻¹. This is because the fates of these species and indicators are governed by OH, which is mainly produced through reaction of O(¹D)+H₂O (G11) and highly depends on the ambient concentration of water vapor.

4.2.2 Aqueous-Phase Chemistry

4.2.2.1 Sensitivity to Aqueous-Phase Kinetic Reactions

The 25 most influential aqueous-phase reactions on gas-phase O₃ concentrations under various cloudy conditions are shown in Table 10. Various aqueous-phase reactions play an important role under relatively clean (i.e., Remote and Marine) and moderately-polluted (i.e., Rural) conditions, with their sensitivities comparable to other dominant gas-phase reactions. The sensitivities of O₃ formation to aqueous-phase reaction rate constants are at least one order of magnitude smaller than other dominant gas-phase reactions under the Urban and Heavily-polluted conditions. Most aqueous-phase reactions have negative effects on gas-phase O₃ formation throughout the simulation time because these reactions accelerate the rates of scavenging of various gas-phase species including many O₃-precursors. As a result, the formation rate of O₃ drops from 0.3 to 0.0 ppb hr⁻¹, 2.25 to 0.6 ppb hr⁻¹, 2.2 to 0.75 ppb hr⁻¹, 9.07 to 5.75 ppb hr⁻¹, and 5.88 to 3.05 ppb hr⁻¹ under cloudy Remote, Marine, Rural, Urban and Heavily-polluted conditions, respectively, as compared to the corresponding clear air conditions.

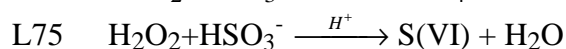
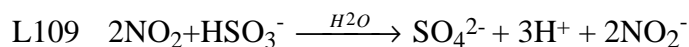
The major aqueous-phase reactions include HO₂ + O₂⁻ (L7), O₃ + O₂⁻ (L13), SO₃²⁻+O₃ (L74), CH₂(OH)₂+OH (L50), HSO₃⁻+H₂O₂ (L75), HO₂+HO₂ (L6), and S(IV)+HO₂ (L105) under all conditions; H₂O₂+O₃ (L16) under relatively clean conditions; and SO₅⁻+O₂⁻ (L82), 2NO₂+HSO₃⁻ (L109), and HCHO+SO₃²⁻ (L112) under polluted conditions. Reactions L6, L7, L13, L16, L74, and L112 act as aqueous-phase sinks for HO₂, H₂O₂, O₃ and HCHO, thus decrease O₃ formation. Other reactions such as L50, L75, L82, L105, L109 can affect O₃ in a variety of ways. For example, L75 has a negative impact under polluted conditions but positive under relatively clean conditions. L50 shows an opposite impact. Two of these reactions



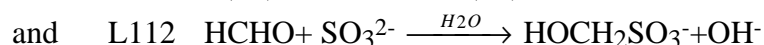
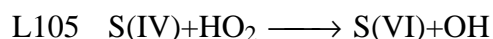
are the predominant aqueous-phase reactions under all conditions except the Heavily-polluted conditions. Followed the dissolution equilibrium of HO₂ and O₃ between gas and aqueous-phases, the self-reaction of dissolved HO₂ (L7) destroys gas and aqueous-phase HO₂ and L13 reduces not only gas and aqueous-phase O₃, but more importantly gas and aqueous-phase HO₂. Being the dominant aqueous-phase sinks for HO₂ and O₃, impact of L7 and L13 is comparable to or even larger than their major gas-phase sink reactions such

as $\text{O}_3 + \text{NO}$ (G3), $\text{NO} + \text{HO}_2$ (G28) and $\text{NO}_2 + \text{OH}$ (G26). These two reactions significantly reduce the gas-phase concentration of HO_2 and O_3 , thus exhibit a negative impact on O_3 formation. These results are in good agreement with the work of Walcek et al. (1997), in which they found a 30-90% reduction in local O_3 formation rates due predominantly to the two aqueous-phase reactions L7 and L13 when excluding other trace metal reactions with dissolved HO_2 under cloudy conditions.

Two aqueous-phase reactions are predominant under the Heavily-polluted conditions:



Although the rate of L109 is just 0.02% NO_2 /hour, it results in a lifetime of NO_2 in the aqueous-phase in the order of 1 s due to the low solubility of NO_2 , thus NO_2 plays an important role in the aqueous-phase chemistry when its concentrations are high. This reaction has a positive impact on O_3 formation by consuming HSO_3^- thus lowering the rates of other negatively-influential S(IV) conversion reactions such as $\text{H}_2\text{O}_2 + \text{HSO}_3^-$ (L75), $\text{S(IV)} + \text{HO}_2$ (L105), $\text{HCHO} + \text{SO}_3^{2-}$ (L112) and $\text{O}_3 + \text{SO}_3^{2-}$ (L74). The secondary important reactions under polluted conditions are:



These two reactions reduce HO_2 and HCHO , thus exhibit negative impact on O_3 formation.

Pandis and Seinfeld (1989) identified aqueous-phase reactions important to major aqueous-phase species through a comprehensive sensitivity analysis using the direct decoupled method under the condition representative of a daytime cloudy environment in the northeastern United States. However, no gas-phase reactions were included in their simulations. Neglecting gas-phase reactions could lead to significant difference in chemical behaviors of species, especially when rates of gas-phase reactions are comparable or even higher than corresponding aqueous-phase reactions. Although a strict comparison between our results and their work is impossible because of differences in initial conditions, some reaction rate constants, and mass transfer treatment, Table 11 summarizes the 1-hr average sensitivities of aqueous-phase S(IV) and S(VI) under the five modeled conditions for a synoptic comparison.

As mentioned in Section 4.2.1.2, the formation of H_2O_2 via G32 and G33 in the gas-phase is the major sink for odd hydrogen R_xO_y under the Remote and Marine conditions. Gaseous H_2O_2 can be rapidly scavenged into cloud droplets due to its high solubility, leading to high aqueous-phase H_2O_2 concentrations. With continuous sources (due to G32 and G33) and slow gas-phase sinks (due to G34 and G35), the high aqueous-phase H_2O_2 can be maintained throughout the simulation time. The reaction of $\text{S(IV)} + \text{H}_2\text{O}_2$ (L75) is thus the dominant pathway for oxidation of S(IV) and formation of S(VI) in the aqueous-phase and has a negative effect on aqueous S(IV) and a positive effect on S(VI) throughout the simulation. Other important pathways for conversion of S(IV) to S(VI) include oxidation of S(IV) by HO_2 (L105), O_2 (catalyzed by Fe^{3+}

and Mn^{2+}) (L77) and O_2^- (L106); oxidation of HSO_3^- by OH (L79) and CH_3OOH (L103); and oxidation of SO_3^{2-} by HCHO (L112, when the aqueous concentration of HCHO is relatively high) and O_3 (L74). The reactions of HO_2+O_2^- (L7) and $\text{OH}+\text{H}_2\text{O}_2$ (L5) have positive impacts on S(IV), because they compete with L105 and L75 by consuming HO_2 and H_2O_2 , thus lower the conversion rates of S(IV) to S(VI) via L105 and L75. Effect of $\text{CH}_2(\text{OH})_2+\text{OH}$ (L50) and O_3+O_2^- (L13) on S(IV) and S(VI) can be either positive or negative. L50 consumes OH and produces HO_2 , reducing the rates of aqueous oxidations of S(IV) involving OH but increasing those involving HO_2 and O_2^- . Under the Remote conditions, L13 produces OH^- , which increases the pH and reduces the rates of some pH-dependent reactions that contribute to S(IV) conversion such as L7. Thus L13 has a positive effect on aqueous-phase S(IV). Being a major source for aqueous OH under the Marine conditions (and various polluted conditions, see below), on the other hand, the reaction of O_3+O_2^- (L13) increases the rates of L79 and L105, thus accelerates the conversion of S(IV) to S(VI).

Under various polluted conditions, the reactions of $\text{NO}+\text{HO}_2$ (G28) and $\text{OH}+\text{NO}_2$ (G26) become the dominant sinks for R_xO_y . Gas-phase H_2O_2 dramatically decreases due to relatively high NO_x and the rapid scavenging by cloud droplets. Due to the decreased gaseous H_2O_2 concentration and its high reactivity in the aqueous-phase solution, the aqueous-phase H_2O_2 concentration reaches its maximum ($(3-7) \times 10^{-5}$ M) within the first minute then substantially drops to $\sim 10^{-7}$ M within 10-40 minutes. As a result, the aqueous-phase reaction of $\text{HSO}_3^- + \text{H}_2\text{O}_2$ (L75) is no longer a dominant reaction for conversion of S(IV) to S(VI) after about 40 minutes. Unlike Remote and Marine atmospheres in which L75 acts as an important sink for aqueous-phase OH via depletion of H_2O_2 and dominates the conversion of S(IV) to S(VI) throughout the simulation, L75 becomes a positively-influential reaction for both aqueous-phase OH and S(IV) by decreasing pH and affecting pH-dependent reactions when aqueous H_2O_2 concentrations are substantially lowered (i.e., after ~ 40 minutes) under the polluted conditions. Instead, $\text{S(IV)}+\text{HO}_2$ (L105) becomes the primary pathway for S(IV) conversion. Other important conversion reactions include oxidations of S(IV) by O_2 (catalyzed by Fe^{3+} and Mn^{2+}) (L77); oxidations of HSO_3^- by SO_5^- (L80), SO_4^- (L91), OH (L79), NO_3 (L108), and NO_2 (L109); as well as oxidations of SO_3^{2-} by SO_5^- (L81), HCHO (L112) and O_3 (L74). Other positively-influential reactions are $\text{SO}_5^- + \text{O}_2^-$ (L82), $\text{CH}_2(\text{OH})_2+\text{OH}$ (L50) and HO_2+O_2^- (L7). These reactions can lower the reaction rates of L105 and L79 through reducing dissolved OH and HO_2 , thus indirectly reduce the conversion rates of S(IV).

While these results are generally consistent with the work of Pandis and Seinfeld (1989), notable differences are the direct impact of HO_2 and H_2O_2 on S(IV) and S(VI) through directly converting S(IV) to S(VI) (L105 and L75) and the indirect impact of HO_2 on S(IV) by lowering the dissolved HO_2 ($= \text{HO}_2+\text{O}_2^-$) (L7). The reaction of S(IV) with HO_2 (L105) is the second important pathway for S(IV) conversion under the relatively clean conditions and becomes the first important one under various polluted conditions, whereas it has little effect on S(IV) in the work of Pandis and Seinfeld (1989). L75 consistently decreases the aqueous-phase S(IV) in the work of Pandis and Seinfeld (1989), whereas it can affect S(IV) in a positive way at low H_2O_2 concentrations ($< 10^{-7}$ M) under our modeled polluted conditions. This is because the predicted aqueous-phase HO_2 concentrations under the five modeled conditions range from $(0.9-4) \times 10^{-8}$ molecules/ cm^3 , which are much higher than a value of $\sim 1.0 \times 10^{-9}$ predicted by Pandis and Seinfeld (1989).

In addition, during the first 20 minutes the predicted aqueous H_2O_2 concentrations significantly decrease from 7.0×10^{-5} to 2.0×10^{-5} M, from 5×10^{-5} to 1.7×10^{-6} M, and from 2.9×10^{-5} to 2.7×10^{-8} M under the Rural, Urban and Heavily-polluted conditions, respectively. In contrast, the predicted aqueous H_2O_2 concentrations in Pandis and Seinfeld (1989) maintained at a level of $(0.9-5) \times 10^{-5}$ throughout the 2-hr simulation. The difference in predicted aqueous-phase HO_2 and H_2O_2 concentrations causes a relatively high conversion rate of S(IV) to S(VI) via L105 and sometimes an opposite effect of L75 under our modeled conditions. In addition to these differences, our simulation predicts a positive impact of $\text{HO}_2 + \text{O}_2^-$ (L7) on S(IV), which is just the opposite to that of Pandis and Seinfeld (1989). The negative effect is because this reaction produces H_2O_2 , thus accelerates the oxidation of S(IV) to S(VI) via L75, as interpreted by Pandis and Seinfeld (1989). In our cases, its negative effect on S(IV) through increasing H_2O_2 is overridden by its positive effect through decreasing HO_2 (via L105). Therefore, the net impact of the $\text{HO}_2 + \text{O}_2^-$ reaction is a higher S(IV) and a lower S(VI).

4.2.2.2 Sensitivity to Gas-Aqueous Mass Transfer Coefficients

Equilibrium Constants. Table 12 shows the sensitivities of the predicted gas-phase O_3 concentrations with respect to Henry's Law constants and dissociation equilibrium constants under various conditions. The dissolution of HO_2 (E10) is the dominant negatively-influential reaction on O_3 under all conditions except for the Heavily-polluted conditions under which the gas-phase HO_2 has the lowest average concentrations of 2×10^7 molecules cm^{-3} (i.e., 8×10^{-4} ppb). Other negatively-influential dissolution equilibria include those of O_3 (E17), H_2O_2 (E11), HCHO (E12), and OH (E18). The Henry's law constants of NO_2 (E13) and HCOOH (E5) have positive effects on gaseous O_3 because these two equilibria tend to increase (rather than decrease) gas-phase NO_2 and HCOOH under cloudy conditions. Henry's law constants of HCHO (E12), NO_2 (E13), HCOOH (E5) and SO_2 (E3) become increasingly important as their gas-phase concentrations become higher. The dissociation of HO_2 (D2) plays a dominant role under all modeled conditions, and the importance of the dissociation of H_2SO_3 (D10 and D11), HCHO (D9) and HCOOH (D16) increases as their aqueous-phase concentrations increase.

Mass Accommodation Coefficients. The rates of heterogeneous uptake and chemical transformation of species in clouds are determined by the overall mass transfer processes consisting of gas-phase diffusion, interfacial mass accommodation, effective aqueous-phase solution and reaction, and aqueous-phase diffusion of dissolved species away from the particle surface (Schwartz, 1986; Worsnop et al., 1989). The mass transfer of a specific species can be controlled by any of the above processes, depending on the relative importance of these processes. Under our modeled conditions, most species do not experience appreciable mass-transfer limitation. Some oxidants such as OH , HO_2 and NO_3 are limited by the interfacial mass transfer process due to high solubility and/or high aqueous-phase effective first-order reaction rates. However, the effects of changing individual mass accommodation coefficients, α_i , on overall predictions are mostly negligible. Sensitivity analyses show that most gaseous species except for NO_3 , N_2O_5 , HNO_3 , H_2O_2 and CH_3OOH are not sensitive to changes in α_i , with sensitivities less than 1.0×10^{-4} . This is in consistence

with the findings of other researchers (Schwartz, 1986; Pandis and Seinfeld, 1989). The partitioning of CH_3OOH , H_2O_2 and N_2O_5 between gas and aqueous-phase is appreciably affected by their own α_i , recognizing that the uncertainty factors in the measured α_i vary from 2-3 (DeMore et al., 1994). Their concentrations can decrease by 5%, 9% and 35% when doubling their own α_i , respectively. The effects of α_i on aqueous species are just the opposite to those on correspondingly gases. For example, as a result of higher α of OH, HO_2 , HNO_2 , the aqueous-phase OH, HO_2 , H_2O_2 , C_2O_3 , CH_3O_2 , and CH_3COOH increase due to accelerated mass transfer from the gas to the aqueous-phase. None of these changes, however, has an appreciable influence on gaseous PAN, O_3 and indicators involving NO_y and O_3 such as NO_y and O_3/NO_z . It is noted that, however, changes in α_i can appreciably affect indicators that involve H_2O_2 , HNO_3 and HCHO, such as $\text{H}_2\text{O}_2/\text{HNO}_3$, $\text{H}_2\text{O}_2/\text{HCHO}$, $\text{H}_2\text{O}_2/\text{NO}_y$, HCHO/HNO_3 , HCHO/NO_y and O_3/HNO_3 , with sensitivities on the order of 1.0×10^{-2} . For example, doubling α_{HNO_3} under all polluted conditions can increase $\text{H}_2\text{O}_2/\text{HNO}_3$ by ~8.8%. This is because both H_2O_2 and HNO_3 are relatively sensitive to α_i .

4.2.2.3 Sensitivity to Other Model Parameters

Sensitivities of major gaseous species and indicators to other model parameters such as temperature, R.H., cloud droplet size and liquid water (V_c) are shown in Table 13. Temperature is the predominant parameter affecting overall model predictions under all conditions. A higher temperature causes increases in SO_2 , HNO_3 , H_2SO_4 , OH, HO_2 , PAN, O_3 , total nitrate (TNO_3^-) and decreases in total sulfate (TSO_4^{2-}). While an increase in temperature tends to increase the gas and aqueous-phase source and sink reaction rates of precursors, it decreases their solubilities in the aqueous-phase, thus reduces the rate of mass transfer from the gas-phase to aqueous-phase. Gas-phase concentrations of most species increase as a result of a net increase in their gaseous production rates and/or a decrease in their solubilities in the aqueous-phase. The lower TSO_4^{2-} is due to an increase in the sink of its precursors in the gas and/or aqueous-phase.

Either V_c or R.H. could be the second important parameter, depending on species and their dominant pathways. For species whose gas-phase reactions are dominant such as NO_x , PAN, ISOP, and OH, the effect of R.H. is more important. A higher R.H. produces higher water vapor and OH thus lower NO_x and ISOP. For species undergoing significant aqueous-phase reactions such as SO_2 , HCHO, HO_2 , H_2O_2 , O_3 and species strongly depending on aqueous-phase chemistry such as TSO_4^{2-} and TNO_3^- , V_c is found to be the second important parameter. An increase in V_c greatly increases the gas to aqueous-phase mass transfer and the pH of the solution, thus affects many important species. As a result of a higher V_c , aqueous-phase HNO_3 , PAN, SO_2 , H_2SO_4 , OH, HO_2 , HCHO and O_3 rapidly increase, lowering their corresponding gas-phase concentrations. Although the total amount of sulfate and nitrate also increases, their total concentrations (TNO_3^- and TSO_4^{2-}) decrease due to higher dilution. In addition, a higher V_c results in higher NO_x under most conditions via lowering their oxidation rates by OH, HO_2 , and O_3 . These results are consistent with those of Pandis and Seinfeld (1989).

The cloud droplet size has an effect comparable to those of V_c and R.H. for most species under the Remote, Marine and Rural conditions, it becomes the least important parameter under the Urban and Heavily-polluted conditions. A larger droplet radius has an opposite effect to that of a higher V_c , i.e.,

decreasing the gas to aqueous-phase mass transfer rate. As a result, there remains higher gas-phase concentrations for most species under most conditions. However, gas-phase concentrations of some species such as NO_x , PAN, SO_2 , OH, HO_2 , ISOP and O_3 can actually decrease under certain conditions. This is because there are net increases in the rates of their sinks despite of the decreasing mass transfer rate from the gas to aqueous-phase.

The impact of solar radiation, H_2O or temperature on indicator correlations has not been explored (Sillman, 1995). In our study, various indicators are also found to be highly sensitive to changes in temperature and moderately sensitive to changes in V_c , R.H., and cloud droplet size. An increase in temperature or R.H. tends to increase $\text{H}_2\text{O}_2/\text{HNO}_3$, but decreases both NO_y and O_3/NO_z under all polluted conditions. While an increase in V_c always increases these indicators, cloud droplet size affects them in a variety of ways, depending on the preexisting gas-phase concentrations. Comparison of Table 13 with Table 9 shows that some species and indicators show opposite sensitivities to temperature in the presence of clouds. For example, an increase in temperature results in a lower SO_2 under all clear air conditions, but a higher SO_2 under various cloudy conditions, implying a significant role of sulfur aqueous-phase chemistry on gas-phase SO_2 . Temperature has a positive impact on NO_y and a negative effect on $\text{H}_2\text{O}_2/\text{HNO}_3$ under clear air conditions. However, its effect becomes the opposite under cloudy conditions. Further study is needed to fully understand the role of temperature in the mixed-phase chemistry.

4.2.3 Aerosol Surface Chemistry

4.2.3.1 Sensitivity to Individual Species Uptake Coefficients

The overall heterogeneous loss rates on aerosols strongly depend on individual uptake coefficients, γ_i . Unlike the sensitivities to α_i under cloudy conditions, the predicted sensitivities of various species concentrations to γ_i in the presence of aerosols are higher by 1-3 orders of magnitude. For those species that are assumed to be directly scavenged to the aerosol surface, their concentrations are always anti-correlated with their own γ_i because higher γ_i deplete more gases onto the surface. For example, an increase in γ_{O_3} always decreases gas-phase O_3 . Reactive species are also found to be affected by surface uptake of other species. The most influential aerosol surface reactions to overall model predictions include uptake of HCHO, O_3 , HO_2 , HNO_2 , HNO_3 , NO, NO_2 , NO_3 , N_2O_5 , PAN, OH, H_2O_2 , SO_2 , CH_3O_2 , CH_3OOH and CH_3COOH .

Table 14 shows the sensitivities of various species including reactive nitrogen, odd hydrogen and reactive hydrocarbon to γ_i of the most influential species (with $\bar{S}_{kl} > 1.0 \times 10^{-4}$) under the Heavily-polluted aerosol conditions. For reactive nitrogen species, the most influential γ_i are those of HCHO, O_3 , NO_2 , and N_2O_5 in addition to their own γ_i . An increase of any of these γ_i either increases or decreases predicted gaseous species concentrations depending on its effects on the formation and destruction rates of these species. For example, an increase in γ_{HCHO} or γ_{O_3} can reduce all reactive nitrogen species except for NO. This can be interpreted by the dominant reactions of these species. The dominant sinks for NO are $\text{O}_3 + \text{NO}$ (G3), $\text{C}_2\text{O}_3 + \text{NO}$ (G46) and $\text{HO}_2 + \text{NO}$ (G28) under this condition. An increase in γ_i of O_3 and HCHO can

cause lower gaseous O_3 and HCHO, respectively. Since photolysis of HCHO (G38) is the dominant source of HO_2 , less HCHO results in less HO_2 in the gas-phase. As the result of lower O_3 and HO_2 , the rates of G3 and G28 are lower, which results in a higher NO. On the contrary, G3, G28 and G38 act as sources for NO_2 , NO_3 , and N_2O_5 . Lower gaseous O_3 and HCHO always cause lower formation rates of these species. For HNO_3 and PAN, a lower HCHO reduces the rate of G38, a dominant positively-influential reaction on both, thus leads to lower HNO_3 and PAN production. A lower O_3 causes lower OH and C_2O_3 radicals, thus causes lower HNO_3 and PAN production through decreasing the rates of their sources $OH+NO_2$ (G26) and $C_2O_3+NO_2$ (G47), respectively. Other species that have appreciable impacts on predicted NO_y species concentrations when changing their γ_i include NO, HNO_3 , HO_2 , and PAN.

For odd hydrogen species, the most important species are HCHO, O_3 , HNO_2 , NO, NO_2 , HO_2 , H_2O_2 and CH_3OOH . γ_i of NO, NO_2 , N_2O_5 , HNO_3 and SO_2 always have positive effects on their concentrations because the reactions of NO_x and SO_2 with R_xO_y (e.g., G22, G26, G28, G29, G47, G115) are major sinks for OH. Higher uptake rates for NO_x and SO_2 result in lower rates of these sinks thus higher R_xO_y species. Uptake of N_2O_5 and HNO_3 on aerosol provides additional sinks for NO_x and indirectly affects R_xO_y species. Lowering the rates of sources (e.g., G9-11, G38, G23, G32, G33, G48, and G118), on the other hand, O_3 , HCHO, HNO_2 , HO_2 , PAN, and CH_3O_2 always have negative effects on R_xO_y species.

The ROG species assumed to be directly taken by aerosol surfaces include HCHO, HCOOH, CH_3COOH , CH_3O_2 , CH_3OH , CH_3OOH , and CH_3COOOH . Concentrations of all ROG species are found to be not only directly affected by uptake of these species but also indirectly affected by uptake of other species such as HNO_2 , HO_2 , O_3 , NO, NO_2 , SO_2 , H_2O_2 , and PAN. Increases in the γ_i of HCHO, HNO_2 , HO_2 , O_3 , and H_2O_2 always decrease HCHO, ALD_2 , CRES, OPEN, HCOOH, CH_3COOH and CH_3OH but increase concentrations of other reactive ROG such as PAR, OLE, ETH, TOL, XYL and ISOP. Among all influential species, HCHO is the predominant one, with its effects 1-2 orders of magnitude higher than others. The effect of the lower gaseous HCHO due to a faster direct surface uptake on other species depends on their predominant reactions. For PAR, OLE, ETH, TOL, XYL and ISOP, their reactions with OH are the predominant pathway. In addition, photolysis of HCHO (G38) has a negative effect on these species, more HCHO uptake reduces rate of G38 thus lowers OH and HO_2 , resulting in a lower rate of sink via OH thus higher hydrocarbons in the gas-phase. For ALD_2 , CRES, OPEN, HCOOH, CH_3COOH and CH_3OH , G38 has a positive influence. While the lower rate of G38 results in the lower HO_2 and OH, which tends to increase their concentrations through reduction of their depletion rates by OH (e.g., G43, G66, G70), it also reduces the formation rates of these species such as CH_3COOH through reducing organic radicals. In addition, lower OH and HO_2 also decrease the formation rate of ALD_2 through decreasing the rates of hydrocarbon interconversion reactions such as OLE, PAR and ETH converted to ALD_2 through G57, G58, G52, and G61. As a net result of this competition, the latter effect is predominant, i.e., lowering ALD_2 , CRES, OPEN, HCOOH, CH_3COOH and CH_3OH when increasing γ_{HCHO} .

Table 15(a) shows the sensitivity of O_3 to γ_i of the most influential species under various aerosol conditions. The predicted O_3 becomes more sensitive to changes in γ_i when the pre-existing atmospheric conditions become more polluted (i.e., more aerosol surface available). For example, doubling γ_{HCHO} and

γ_{O_3} has almost no effect on O_3 under the Remote conditions, but it decreases O_3 by 6.3% and 10.4% under the Heavily-polluted conditions, respectively. Although the mechanism remains unclear, the direct destruction of O_3 on aerosols is found to be a dominant surface reaction under all modeled conditions. Stephens et al. (1986) found that the uptake of O_3 most likely occurs on carbonaceous or soot particles on which the adsorbed oxygen atom, which is produced from collision of O_3 with carbon aerosols, can combine with another adsorbed oxygen atom to form O_2 . In addition, one or two oxygen atoms may combine with a carbon atom to produce CO or CO_2 . They further determined that γ_{O_3} on carbonaceous surfaces may be initially high but decreases more than a factor of 10 after repeated exposure resulting in an average γ_{O_3} of 7×10^{-4} , due probably to a saturation of surface sites by oxygenated groups. Fendel et al. (1995) also found that submicron carbon or iron aerosols can destroy O_3 efficiently, with a γ_{O_3} of 4×10^{-4} . In this study, a γ_{O_3} of 1×10^{-4} was used, which is the lower limit in laboratory measurements. The predicted decreases in O_3 concentrations due to 29 aerosol surface uptake reactions are 3%, 12.4% and 26.6% under the Rural, Urban and Heavily-polluted conditions, respectively, of which 18.2%, 37.0% and 39.9% are found to be caused by the direct O_3 destruction on aerosols, respectively. The rest of O_3 decrease is caused by the decrease in O_3 precursors such as NO_2 , HO_2 and HCHO. An increase in γ_i of these species also decreases O_3 because these surface uptake can significantly reduce the rates of O_3 -producing reactions (e.g., G1, G28, G38, G57, G61, and G69). On the contrary, higher γ_{NO} and γ_{SO_2} tend to slightly increase O_3 because their surface reactions compete with their corresponding gas-phase reactions and decrease the rates of the gaseous reactions that contribute to O_3 destruction (e.g., G3, G22, and G115). As a result of all aerosol surface uptake, the O_3 formation rate decreases from 2.2 to 1.6 ppb hr^{-1} , from 9.07 to 4.0 ppb hr^{-1} , from 5.88 to 3.55 ppb hr^{-1} under the Rural, Urban and Heavily-polluted conditions, respectively, as compared to the corresponding clear air conditions.

Since some reactive NO_y species such as N_2O_5 and HNO_3 and R_xO_y species such as H_2O_2 and CH_3OOH are highly sensitive to changes in γ_i , the indicators involving these species are expected to respond to these changes. While NO_y is much less sensitive with most sensitivities less than 1.0×10^{-3} , the sensitivities of O_3/NO_z and H_2O_2/HNO_3 are 1-2 orders of magnitude higher, as shown in Table 15 (b) through (d). O_3/NO_z is sensitive to uptake of HNO_3 , HO_2 , H_2O_2 , HCHO, NO_2 , PAN and O_3 . Similar to the effect on O_3 , an increase in γ_{O_3} always causes a decrease in O_3/NO_z . Higher uptake rates of NO_2 and N_2O_5 can either increase (i.e., Rural and Urban) or decrease (i.e., Heavily-polluted) O_3/NO_z , depending on their combined effects on O_3 and NO_z . The impacts of HCHO, HNO_2 , HO_2 , H_2O_2 , CH_3O_2 , NO, and SO_2 on O_3/NO_z , however, are just the opposite as compared to those on O_3 . In addition, O_3/NO_z becomes sensitive to changes in γ_{HNO_3} and γ_{PAN} , which have little effect on O_3 formation. Since G38 is the dominant positively-influential reaction for both NO_z and O_3 , a decrease in gaseous HCHO concentration reduces the photolytic rate of HCHO, thus decreases NO_z and O_3 . Similarly, decreases in H_2O_2 , CH_3O_2 and HO_2 tend to decrease OH and O_3 concentrations. But they also decrease NO_z concentrations by reducing the formation rates of NO_3 , N_2O_5 , HNO_3 and PAN through reactions with OH. Therefore, the net effect of decreases in HCHO, HO_2 , H_2O_2 and CH_3O_2 is an increase in O_3/NO_z . The responses of H_2O_2/HNO_3 are even more significant because both H_2O_2 and HNO_3 are highly sensitive to changes in their own γ_i . While an increase

in $\gamma_{\text{H}_2\text{O}_2}$ greatly decreases gaseous H_2O_2 thus reduces the indicator, an increase in γ_{HNO_3} decreases gaseous HNO_3 thus causes an increase in the indicator. In addition, this indicator is also sensitive to uptake of HCHO , HO_2 , O_3 , NO_x , N_2O_5 , HNO_2 , and SO_2 .

4.2.3.2 Sensitivity to Temperature and Relative Humidity

Sensitivities of most gaseous species to temperature and R.H. under various aerosol conditions are similar to those under the corresponding clear air conditions shown in Table 9, with slightly higher values. Compared to clear air conditions, however, significant changes in both the magnitudes and the signs are found in sensitivities of NO_y and $\text{H}_2\text{O}_2/\text{HNO}_3$. In particular, a higher temperature causes a decrease in NO_y under all polluted conditions and an increase in $\text{H}_2\text{O}_2/\text{HNO}_3$ under the Heavily-polluted conditions. A higher R.H. causes a higher $\text{H}_2\text{O}_2/\text{HNO}_3$ under the Urban and Heavily-polluted conditions. These are just the opposite to those under the clear air conditions. These changes are similar to those under cloudy conditions (see Table 13), indicating that heterogeneous uptake of H_2O_2 and NO_y species are important to their sensitivities, especially under conditions with large aerosol surfaces.

4.2.4 Effect of Heterogeneous Chemistry on Gas-Phase Chemistry

4.2.4.1 Effect of Clouds and Aerosols on O_3 -Precursor Relations

Gas-Phase Reaction Rate Constants. Heterogeneous chemistry alters the sensitivities of O_3 to various gas-phase reactions through changing their amplitudes and the signs. Figure 4 shows the comparison of the sensitivities of O_3 to gas-phase reaction rate constants in the absence and presence of clouds and aerosols under the Remote and Heavily-polluted conditions after a 2-hr simulation. Under the Remote conditions, cloud chemistry is the dominant process and causes significant changes in sensitivities to gas-phase reactions, whereas the changes in sensitivities are mainly caused by aerosol surface reactions under the Heavily-polluted conditions. The sensitivities are generally smaller under the cloudy and aerosol conditions than those under clear air conditions, rationalizing a lower total gas-phase oxidizing capacity due to additional sinks for many O_3 precursors provided by clouds and aerosols. For example, the sensitivities of reactions of DMS, DMSO and $\text{CH}_3\text{SO}_2\text{H}$ with OH (G82, G89, and G97, respectively) radicals are much lower under the cloudy and aerosol conditions because of lower OH levels. The effect of the gas-phase reaction $\text{CO}+\text{OH}$ (G36) on O_3 formation has not only a different magnitude but also an opposite sign under the Remote cloudy conditions relative to the clear air conditions. It becomes negative under the cloudy conditions. This is because that HO_2 produced by G36 is not converted to OH via G28 under cloudy conditions, instead, it dissolves into cloud droplets, which increases the aqueous-phase concentration of O_2^- , thus speeds up the important aqueous-phase sink of O_3 through its reactions with O_2^- (L13).

O_3 -Precursor Relations. The presence of clouds and aerosols not only changes concentrations of O_3 and its precursors, but also their relations provided that heterogeneous chemistry plays a significant role in

determining their mass budget. Figure 5 shows the comparison of the sensitivities of O_3 to species initial concentrations with and without clouds and aerosols under various polluted conditions after 2-hr simulation. O_3 increases with an increase in NO_2 in the presence of both clouds and aerosols under all conditions and in the presence of each alone under some conditions, which is just the opposite to that in clear air conditions. Under clear air conditions, the formation of HNO_3 (G26) and PAN (G47) through oxidation of NO_2 by OH and C_2O_3 are predominant sink reactions for NO_2 . An increase in NO_2 results in a lower OH, thus a lower O_3 . Although OH still decreases with increasing NO_2 (due to R26) in the presence of clouds and/or aerosols, the fate of OH is no longer the dominant factor of determining the effect of NO_2 on O_3 production. The heterogeneous uptake and subsequent aqueous-phase reactions that affect NO_2 and the relative importance of its gas-phase sinks via G26, G47, and G1 determine its correlation with O_3 . When there are sufficient surface areas, OH and C_2O_3 are reduced due to lower levels of their precursors such as H_2O_2 , HCHO and ALD_2 and the direct surface uptake of OH. This reduction could be so significant (20-48%, see Table 5) under some conditions (i.e., under the Rural and Urban cloudy condition, under the Urban and Heavily-polluted aerosol conditions, and under all polluted conditions with presence of both cloud and aerosols) that G26 and G47 are no longer the major sinks for NO_2 . Instead, G1 becomes the overwhelming sink for NO_2 and leads to O_3 formation followed by G2. Thus, O_3 formation increases with an increase in initial NO_2 under most cloudy and/or pre-existing aerosol conditions. In addition to the change in O_3 - NO_2 relations, O_3 becomes slightly more sensitive to NO under the Heavily-polluted conditions and less sensitive to initial O_3 and various ROG species such as HCHO and ALD_2 under all conditions. For example, for a doubled HCHO, the predicted O_3 only increases by 15.4%, 1.8% and 1.9% in air with clouds alone, aerosols alone and both clouds and aerosols, respectively, as compared to 21.1% in clear air. Higher sensitivity of O_3 to initial NO is due to a slightly higher sensitivity to the rate constant of $NO+O_3$ (G3). O_3 sensitivities to various ROG are lower because the TOC is reduced and O_3 sensitivities to most ROG reactions such as G38 and G43 are appreciably lower, as shown in Figure 4.

4.2.4.2 Effect of Clouds and Aerosols on Sensitivity of Indicators

Significant changes are found in sensitivities of indicators to both reaction rate constants and species initial concentrations due to the cloud chemistry and aerosol surface uptake. Although the sensitivities of NO_y to most gas-phase reactions rate constants are greatly increased in the presence of clouds and/or aerosols, their magnitudes are still smaller by 1-3 orders than those of O_3/NO_z and H_2O_2/HNO_3 , indicating that NO_y is relatively insensitive to reaction rate constants. Figure 6 compares the sensitivities of O_3/NO_z and H_2O_2/HNO_3 to gas-phase reaction rate constants with and without clouds and aerosols under the Heavily-polluted conditions. O_3/NO_z becomes more sensitive to G9-G11, G43-G47, G58, G69, G74, and G76, and less sensitive to G1, G3, G38, G39, G52, and G57. The most significant change is that the impact of the rate constant of NO_2+OH (G26) on O_3/NO_z changes from negative to positive. Under clear air conditions, HNO_3 produced via this reaction remains in the gas-phase and largely increases the denominator, NO_z . Thus a higher rate constant of G26 actually decreases the indicator. When there are sufficient cloud

droplets and/or aerosol particles, HNO_3 can be quickly taken onto these surfaces as soon as it is produced in the gas-phase. In the meanwhile, other NO_x species such as NO_3 , N_2O_5 and PAN can undergo similar uptake and subsequent aqueous-phase reactions, therefore decrease gas-phase NO_x . This decrease is larger than the simultaneous decrease in O_3 due to the surface uptake. As a result, the indicator increases with a higher rate constant of G26. The sensitivities of $\text{H}_2\text{O}_2/\text{HNO}_3$ to many reaction rate constants in the presence of clouds and aerosols are significantly changed in both magnitudes and signs because both H_2O_2 and HNO_3 can be effectively scavenged by clouds and aerosols, and these surface uptake and aqueous-phase chemistry become the predominant pathways for H_2O_2 and HNO_3 .

The changes in these sensitivities cause substantial changes in the sensitivities of the indicators to initial species concentrations, as shown in Figure 7. NO_y becomes less sensitive to NO_2 , but more sensitive to initial O_3 , NO , and ROG species such as HCHO , ALD_2 , and OLE . O_3/NO_x becomes much more sensitive to changes in NO_2 , ALD_2 , OLE , TOL , XYL and ISOP and less sensitive to changes in O_3 , NO , HCHO , and PAR . The changes in sensitivities of $\text{H}_2\text{O}_2/\text{HNO}_3$ to various species are even more significant. $\text{H}_2\text{O}_2/\text{HNO}_3$ becomes extremely sensitive (with $\bar{S}_{kl} > 0.9$) to initial NO , NO_2 , O_3 , and OLE and almost insensitive to H_2O_2 . In addition, the impact of initial O_3 , HCHO , OLE , ETH , TOL , XYL and ISOP on $\text{H}_2\text{O}_2/\text{HNO}_3$ changes from negative under clear air conditions to positive under cloud and/or aerosol conditions. Cloud chemistry and aerosol surface uptake cause significant changes in dominant reactions of H_2O_2 . H_2O_2 is no longer a reservoir for OH and HO_2 (due to G34 and G35). Once produced, H_2O_2 can be rapidly scavenged into cloud droplets or onto aerosol surfaces. In addition, other odd hydrogen species such as OH and HO_2 can also be effectively removed by clouds and aerosols and undergo rapid aqueous-phase reactions. As a result, the gaseous H_2O_2 and OH and HO_2 are substantially lower. While higher NO_2 increases HNO_3 via G26, it also causes further decreases in OH (due to G26), thus a lower H_2O_2 and a subsequent significant decrease in the indicator. The extremely high sensitivity to initial NO , NO_2 , and OLE was caused by the much higher sensitivities to their corresponding reactions (i.e., G26, G28, and G57) shown in Figure 6(b). Similarly, the opposite effect of initial O_3 , HCHO , OLE , ETH , TOL , XYL and ISOP is due to the corresponding changes in sensitivities to their dominant reactions (i.e., G9-11, G38, G57, G58, G61, G63, G69 and G76).

5. Conclusions

A mixed-phase chemistry box model consisting of detailed gas- and aqueous-phase chemistry and a simplified treatment of aerosol surface chemistry was used to study heterogeneous chemistry and its effect on gas-phase chemistry under a variety of atmospheric conditions. A subsequent comprehensive sensitivity analysis was conducted to evaluate the sensitivity of overall model predictions and identify the most influential model parameters that affect O_3 formation, O_3 -precursor relations and photochemical indicators in the mixed-phase chemical system. The results show that heterogeneous processes associated with clouds and aerosols not only reduce many gas-phase species concentrations and the total oxidizing capacity but alter O_3 -precursor relations. Decreases in O_3 and PAN concentrations can be up to 27% and 38%, respectively, with

up to 100% decrease in their formation rates under typical atmospheric conditions. The magnitude of the heterogeneous effects is very sensitive to temperature, R.H., cloud water content and individual uptake coefficients. The effects of clouds and aerosols can be accelerated by a higher water content and higher individual uptake coefficients, respectively. Temperature and R.H. can influence both cloud and aerosol processes in a variety of ways.

The most influential gas-phase reactions to O_3 formation under the relatively clean conditions include the photolytic reactions of NO_2 , O_3 , $HONO$, H_2O_2 , and $HCHO$; the conversion of NO to NO_2 by HO_2 , O_3 , CH_3O_2 , CH_3SCH_2OO and C_2O_3 ; the generation and inter-conversion of OH , HO_2 and RO_2 via reactions $O(^1D)+H_2O$, O_3+HO_2 , and reactions of OH with CH_4 , O_3 , CO , $DMSO$, DMS , CH_3OOH , $HCHO$, ALD_2 , OLE , ETH and PAR ; and the formation and/or dissociation of oxidants and acids such as CH_3OOH , HNO_3 , H_2O_2 , HNO_4 , CH_3SO_2 , H_2SO_4 , $HONO$, PAN , and CH_3SCH_2OO . The most influential gas-phase reactions under various polluted conditions are the photolytic reactions of NO_2 , O_3 , $HONO$, H_2O_2 , $HCHO$, ALD_2 , $OPEN$, and $MGLY$; the conversion of NO to NO_2 by HO_2 , O_3 , C_2O_3 and TO_2 ; the generation and inter-conversion of OH , HO_2 and RO_2 through reactions $O(^1D)+H_2O$, $OLE+O_3$, and reactions of OH with CO , CH_4 , ETH , ALD_2 , PAR , OLE , $ISOP$, TOL , $HCHO$, XYL , and $MGLY$; and the formation and dissociation of HNO_3 , H_2SO_4 , HNO_4 , H_2O_2 and PAN .

Cloud chemistry is a dominant heterogeneous process in relatively clean and moderately polluted atmospheres. The most influential aqueous-phase reactions to O_3 formation under the relatively clean conditions are oxygen-hydrogen reactions of O_2^- with O_3 and HO_2 , HO_2+HO_2 , $H_2O_2+O_3$, $OH+H_2O_2$, $OH+HO_2$, photolysis of H_2O_2 ; sulfur reactions $HSO_3^-+H_2O_2$, $SO_3^{2-}+O_3$, $S(IV)+HO_2$, $HSO_3^-+O_3$, $HOCH_2SO_3^-+OH$; methane oxidation $CH_2(OH)+OH$ and $CH_3O_2+O_2^-$; carbonate reactions of CO_3^- with H_2O_2 and O_2^- and $HCO_3^-+O_2^-$; and nitrate reactions $NO_3^-+Cl^-$. The most influential aqueous-phase reactions under various polluted conditions include oxygen-hydrogen reactions of O_2^- with O_3 and HO_2 , $OH+HO_2$, HO_2+HO_2 ; sulfur reactions of HSO_3^- with H_2O_2 , OH , SO_5^- , NO_2 , and O_3 , reactions of SO_3^{2-} with O_3 , SO_5^- and $HCHO$, reactions of $S(IV)$ with HO_2 and O_2 (catalyzed by Mn^{2+} and Fe^{3+}), reactions of SO_5^- with SO_5^- and O_2^- , $HOCH_2SO_3^-+OH$, and $SO_4^-+HCOO^-$; nitrate reactions NO_3+HO_2 , NO_2+NO_2 and photolysis of NO_3^- ; methane oxidation $CH_2(OH)+OH$ and $HCOO^-+OH$; carbonate reaction $HCO_3^-+O_2^-$. Among these, the reactions of O_2^- with dissolved HO_2 and O_3 are mainly responsible for the decrease in O_3 formation under most cloudy conditions.

Aerosols can be more effective surfaces than clouds in polluted areas when the total surface area is larger than $1000 \mu m^2 cm^{-3}$. The aerosol surface chemistry is very sensitive to the individual uptake coefficients, which are subject to large uncertainties. Among the 29 condensing species, the heterogeneous uptake of O_3 , $HCHO$, HO_2 , NO_2 , NO , N_2O_5 , HNO_2 , HNO_3 , H_2O_2 , SO_2 , CH_3O_2 , PAN , CH_3OOH and CH_3COOH are the most influential aerosol surface reactions. In particular, the significant decrease in O_3 formation in the presence of aerosols is mainly caused by the heterogeneous uptake of O_3 , $HCHO$, HO_2 , H_2O_2 and NO_2 . Further laboratory and field studies are urgently needed to precisely quantify this important parameter and quantify the rates and product yields of these heterogeneous reactions on aerosols.

The O_3 formation is also sensitive to a number of mass transfer coefficients and physical parameters. Under the relatively clean conditions, the Henry's law constants of HO_2 , O_3 , H_2O_2 , and $HCHO$; the

dissociation equilibrium constants of HO_2 and H_2SO_3 ; and the uptake coefficients of O_3 , H_2O_2 , and HO_2 are the most important parameters in determining the mass transfer between the gas and the condensed-phases. Under various polluted conditions, the most influential parameters include the Henry's law constants of HO_2 , HCHO , O_3 , SO_2 , NO_2 , and HCOOH ; the dissociation equilibrium constants of HO_2 , H_2SO_3 , HCHO , and HCOOH ; and the uptake coefficients of O_3 , HCHO , HO_2 , NO_2 , NO , N_2O_5 , HNO_2 , HNO_3 , PAN , H_2O_2 , CH_3O_2 , CH_3OOH , CH_3COOH and SO_2 . Temperature, R.H., cloud water content and droplet size can largely affect O_3 and its precursors in a variety of ways. O_3 formation is relatively insensitive to changes in mass accommodation coefficients of individual species under all modeled conditions.

As a result of changes in gas-phase concentrations and the total oxidizing capacities, the magnitude of photochemical indicators and their sensitivity to model parameters are also largely affected. Presence of clouds and/or aerosols can increase O_3/NO_z and O_3/HNO_3 , decrease NO_y , $\text{H}_2\text{O}_2/\text{NO}_y$, HCHO/NO_y ($\text{HNO}_3/\text{H}_2\text{O}_2/(\text{NO}_x/\text{ROG})$), and affect O_3/NO_y and $\text{H}_2\text{O}_2/\text{HNO}_3$ in both ways under all modeled conditions. The indicators NO_y and O_3/NO_y are relatively insensitive to most model parameters, whereas indicators involving H_2O_2 , HNO_3 , HCHO and NO_z are highly sensitive to changes in initial species concentrations, reaction rate constants, equilibrium constants, uptake coefficients, temperature, R.H., cloud droplet size and water content. While their most influential reactions are similar to those of O_3 , their relative impacts may be different both in signs and amplitudes. Indicators generally have higher sensitivities to ROG reactions and lower sensitivities to NO_x reactions under polluted conditions than less polluted conditions, which coincides with the nature of the indicators as good markers for the O_3 - NO_x -ROG sensitivity. In addition, sensitivities of the indicators to model parameters can be significantly changed when including cloud and aerosol chemistry. Caution should be taken when applying the established threshold values of indicators to determine NO_x - or ROG-sensitive O_3 in regions where large cloud coverage and high aerosol loading are frequently observed.

Our results indicate that the effect of aerosols is similar and comparable to that of clouds when the aerosol loading is large (e.g., in urban atmospheres). However, the predicted aerosol effect is based on the assumption of a non-reversible mass transfer between gas and aerosol surfaces, which may not always be the case in the atmosphere. Future work is needed to refine aerosol treatments by accounting for gas-aerosol equilibria, saturation and reactions on various aerosols. Our results also demonstrate a need to further study the role of heterogeneous chemistry in tropospheric chemistry through sensitivity analysis of a 3-D model. In particular, their impacts on O_3 formation, O_3 -precursor relations and photochemical indicators need to be further studied in 3-D models. Furthermore, we have only evaluated model responses to changes in the chemical mechanism, and there are many other uncertain parameters in the "real" atmosphere such as emission and meteorological conditions. Results from 3-D sensitivity studies will be extremely useful in evaluating O_3 - NO_x -ROG sensitivities and developing integrated control strategies for O_3 and particulate matters in non-attainment regions.

Our work show that large-scale sensitivity analysis of complex computer models is feasible with automatic differentiation tools, although the fully automatic approach currently is quite compute-intensive. Automatic differentiation is a technology in its infancy, so further improvements in tools are expected.

However, exploitation of high-level program or algorithmic structure has been shown to have a dramatic impact on computational cost in certain application studies. Thus, as more experience is gained in the use of AD tools, we expect that synergy between improvements in AD tools and high-level user understanding will decrease the computational cost by orders of magnitude. With improved aerosol treatment and AD tools, a comprehensive 3-D sensitivity analysis will be possible and greatly enhance our understanding of mixed-phase chemical system and their impact on photochemistry in the “real” atmosphere.

6. Acknowledgments

We sincerely thank Dr. Len Peters and his Ph.D. student, Mr. Rahul A. Zaveri, for providing an earlier version of MaTChM. We thank Dr. Rick D. Saylor and Ms. Elaine G. Chapman for early constructive work on MaTChM. We thank Dr. William R. Stockwell and Mr. Carl M. Berkowitz for valuable comments. This work was supported by the DOE’s Office of Health and Environmental Research through Laboratory Directed Research and Development project at Pacific Northwest National Laboratory and the Mathematical, Information, and Computational Sciences Division subprogram of the Office of Computational and Technology Research, U.S. Department of Energy, under Contract W-31-109-Eng-38, at Argonne National Laboratory.

7. References

- Astarita G., *Mass Transfer with Chemical Reaction*, Elsevier, New York, 1967.
- Baldwin, A. C., Reactions of gases on prototype aerosol particle surfaces, in *Heterogeneous Atmospheric Chemistry*, pp. 99-102, AGU Geophysical Monograph 26, edited by Schryer D.R., 1982.
- Baldwin A.C., and D.M. Golden, Heterogeneous atmospheric reactions 2. atom and radical reactions with sulfuric acid, *J. Geophys. Res.*, 85, 2888-2889, 1980.
- Berz M., Bischof C., Corliss G., and Griewank A., Computational differentiation: techniques, applications, and tools, *SIAM, Philadelphia*, PA, 1996.
- Bischof C., Carle A., Corliss G., Griewank A. and Hovland P., ADIFOR generating derivatives codes for Fortran programs, *Scientific Programming*, 1(1), 11-29, 1992.
- Bischof C., Carle A., Khademi P., and Mauer A., The ADIFOR 2.0 system for the automatic differentiation of Fortran 77 programs, *IEEE J. Computational Science and Engineering*, 3(3), 18-32, 1996a.
- Bischof C. and Haghghat M., On hierarchical differentiation, pp. 83-94, in Berz et al., 1996.
- Bischof C., Green L., Haigler K., and Knauff K., Parallel calculation of sensitivity derivatives for aircraft design using automatic differentiation, In *Proceedings of the 5th AIAA/NASA/USAF/ISSMO Symposium on Multidisciplinary Analysis and Optimization*, AIAA 94-4261, pp. 73-84, American Institute of Aeronautics and Astronautics, 1994.

- Bischof C., Khademi, P., Bouaricha, A., and Carle, A., Efficient Computation of Gradients and Jacobians by Transparent Exploitation of Sparsity in Automatic Differentiation, *Optimization Methods and Software*, 7(1), 1-39, 1996b.
- Bischof C., Pusch G., and Knösel R., Sensitivity Analysis of the MM5 weather model using automatic differentiation, *Computers in Physics*, 10(6), 605-612, 1996c.
- Bischof C., Roh L., and Mauer A., ADIC - An extensible automatic differentiation tool for ANSI-C, *Preprint ANL/MCS-P626-1196*, Mathematics and Computer Science Division, Argonne National Laboratory, 1996d.
- Bischof C. and Wu P.-T., Time-parallel computation of pseudo-adjoints for a leapfrog scheme, *Preprint ANL/MCS-P639-0197*, Mathematics and Computer Science Division, Argonne National Laboratory, 1997.
- Bongartz A., J. Kames, U. Schurath, Ch. George, Ph. Mirabel, and J.L. Ponce, Experimental determination of HONO mass accommodation coefficients using two different techniques, *J. Atmos. Chem.*, 18, 149-169, 1994.
- Carle, A., and Fagan, M., Improving Derivative Performance for CFD by using simplified recurrences, pp. 343-352, in Berz et al., 1996.
- Carmichael G.R., A. Sandu and F.A. Potra, Sensitivity analysis for atmospheric chemistry models via automatic differentiation, *Atmos. Environ.* 31(3), 475-489, 1997.
- Cho Y-S, Carmichael, G.R., and Rabitz, H. , Sensitivity Analysis of the Advection-Diffusion Equation, *Atmos. Environ.*, 21, 2589-2598, 1987.
- DeBruyn W.J., J.A. Shorter and P. Davidovits, Uptake of gas phase species methanesulfonic acid, dimethylsulfoxide, and dimethyl sulfone by aqueous surfaces," *J. Geophys. Res.*, 99(D8), 16927-16932, 1994).
- DeMore, W.B., S.P. Sander, D.M. Golden, R.F. Hampson, M.J. Kurylo, C.J. Howard, A.R. Ravishankara, C.E. Kolb, and M.J. Molina, Chemical kinetics and photochemical data for use in stratospheric modeling, Evaluation Number 11, *JPL Publication 94-26*, 1994.
- Davidovits P., M.S. Zahniser, D.R. Worsnop, and C.E. Kolb, How gas molecules enter liquids-a study of heterogeneous gas/liquid interactions, *Atmospheric Chemistry Program Monthly Update*, 4(4), 1-11, 1993.
- Dentener, F.J. *Heterogeneous Chemistry in the Troposphere*, Ph.D. dissertation, The Max-Planck-Institute for Chemistry in Mainz, 1993.
- Dentener, R. and P. Crutzen, Reaction of N₂O₅ on tropospheric aerosols: impact of the global distributions of NO_x, O₃ and OH, *J. Geophys. Res.*, 98, 7149-7163, 1993.
- Dentener, F. J. , G. R. Carmichael and Y. Zhang, J. Lelieveld and P.J. Crutzen, Role of Mineral Aerosol as a Reactive Surface in the Global Troposphere, *J. of Geophys. Res.*, 101(D17), 22869-22889, 1996.
- Dingenen R.V. and F. Raos, Determination of the condensation accommodation coefficient of sulfuric acid on water-sulfuric acid aerosol, *Aerosol Sci. and Tech.*, 15, 93-106, 1991.

- Dunker A., The decoupled direct method for calculating sensitivity coefficients in chemical kinetics, *J. Chem. Phys.*, 81, 2385-2393, 1984.
- Eberhard P. and Bischof C., Automatic Differentiation of Numerical Integration Algorithms, *Preprint ANL/MCS-P621-1196*, Mathematics and Computer Science Division, Argonne National Laboratory, 1996.
- Fendel W., Matter D., Burtscher H. and Schmidt-ott A., Interaction between carbon or iron aerosol particles and ozone, *Atmos. Environ.*, 29(9), 967-973, 1995.
- Fitzgerald J.W., Marine aerosols: a review, *Atmos. Environ.*, 25A(3/4), 533-545, 1991.
- Fuchs N.A. and A.G. Sutugin, Highly Dispersed Aerosols, Ann Arbor Science, Ann Arbor, Mich., 1970.
- Gao D., W.R. Stockwell, J.B. Milford, First-order sensitivity and uncertainty analysis for a regional-scale gas-phase chemical mechanism, *J. Geophys. Res.*, 100(D11), 23153-23166, 1995.
- Gardner J.A., L.R. Watson, Y.G. Adewuyi, P. Davidovits, M.S. Zahniser, D.R. Worsnop, and C.E. Kolb, Measurement of the mass accommodation coefficient of SO₂ (g) on water droplets, *J. Geophys. Res.*, 92, 10887-10895, 1987.
- Gery M.W., G.Z. Whitten, J.P. Killus, and M.C. Dodge, A photochemical kinetics mechanism for urban and regional scale computer modeling, *J. Geophys. Res.*, 94 (D10), 12925-12956, 1989.
- Griewank A., Bischof C., Corliss G., Carle A., and Williamson K., Derivative convergence of iterative equation solvers, *Optimization Methods and Software*, 2, 321-355, 1993.
- Griewank A. and Gorliss G., Automatic differentiation of algorithms: theory, implementation, and application, *SIAM, Philadelphia, PA*, 1991.
- Hanson D.R., J.B. Burkholder, C.J. Howard and A.R. Ravishankara, Measurement of OH and HO₂ radical uptake coefficients on water and sulfuric acid surfaces, *J. Phys. Chem.*, 96, 4979-4985, 1992.
- Hall, M.C. and D.G. Cacuci, Physical interpretation of adjoint functions for sensitivity analysis of atmospheric models, *J. Atmos. Sci.*, 40, 2537-2546, 1983.
- Heikes B.G. and A.M. Thompson, Effects of heterogeneous processes on NO₃, HONO, and HNO₃ chemistry in the troposphere, *J. Geophys. Res.*, 88(C15), 10883-10895, 1983.
- Heymsfield A.J., Microphysical structure of stratiform and cirrus clouds, in *Aerosol-Cloud-Climate Interactions*, Chapter 4, P.V. Hobbs, Eds., Academic Press, Inc., pp 97-121, 1993.
- Hindmarsh, A.C. Odepack, a systematized collection of ode solvers, in *Scientific Computing*, R. S. Stepleman et al. Eds., North-Holland, Amsterdam, pp 55-64, 1983.
- Hovland P., Bischof C., Spiegelman D., and Casella M., Efficient derivative codes through automatic differentiation and interface contraction: An application to biostatistics," *Preprint ANL/MCS-P491-0195*, Mathematics and Computer Science Division, Argonne National Laboratory, 1995. To appear in *SIAM J. Scientific Computing* 18(4), 1997.
- Jaenicke R., Tropospheric aerosols, in *Aerosol-Cloud-Climate Interactions*, P.V. Hobbs, Eds., Academic Press, Inc., pp 1-31, 1993.
- Jayne J.T., P. Davidovits, D.R. Worsnop, M.S. Zahniser, and C.E. Kolb, Uptake of Gas-phase aldehyd and organic acid molecules by water surfaces, *J. Phys. Chem.*, 95, 6329-6336, 1991.

- Jayne J.T., S.X. Duan, P. Davidovits, D.R. Worsnop, M.S. Zahniser, and C.E. Kolb, Uptake of gas-phase aldehydes by water surfaces, *J. Phys. Chem.*, 96, 5452-5460, 1992.
- Judeikis H.S., T.B. Stewart and A.G. Wren, Laboratory studies of heterogeneous reactions of SO₂, *Atmos. Environ.*, 12, 1633-1641, 1978.
- Kirchner W., F. Welter, A. Bongartz, J. Kames, S. Schweighoeffer, and U. Schurath, Trace gas exchange at the air/water interface: measurements of mass accommodation coefficients, *J. Atmos. Chem.*, 10, 427-449, 1990.
- Kurylo M.J., J.A. Kaye, R.F. Hampson, and A.M. Schmoltner, Present state of knowledge of the upper atmosphere 1993: An assessment report, Report to Congress, NASA reference publication 1337, NASA Office of Mission to Planet Earth, Science Division, Washington, D.C., 1994.
- Lee, J. H. and I. N. Tang, Accommodation Coefficient of Gaseous NO₂ on Water Surfaces. *Atmos. Environ.* 22, 1147-1151, 1988.
- Lelieveld J. and P.J. Crutzen, Influences of cloud photochemical processes on tropospheric ozone, *Nature*, 343(18), 227-233, 1990.
- Leu M.T., *Geophys. Res. Lett.* 15, 851-854, 1988.
- Li S.M., K.G. Anlauf and H.A. Wiebe, Heterogeneous nighttime production and deposition of particle nitrate at a rural site in North America during summer 1988, *J. of Geophys. Res.*, 98, 5139-5157, 1993.
- Luria M. and H. Sievering, Heterogeneous and homogeneous oxidation of SO₂ in the remote marine atmosphere, *Atmos. Environ.*, 25A(8), 1489-1496, 1991.
- Lurmann F.W., Carter W.P.L. and Coyner L.A., A surrogate species chemical reaction mechanism for urban-scale air quality simulation models, Volume I and II, *EPA Report Contract 68-02-4104*, ERT, Inc., Newbury Park, and Statewide Air Pollution Research Center, University of California, Riverside, California, 1987.
- Martin L.R., H.S. Judeikis and M. Wun, *J. Geophys. Lett.* 41, 394-396, 1980.
- Milford J.B., D. Gao, A.G. Russell and G.J. McRae, Use of sensitivity analysis to compare chemical mechanisms for air-quality modeling, *Environ. Sci. Technol.* 26, 1179-1189, 1992.
- Milford J.B., D. Gao, S. Sillman, P. Blossey and A. G. Russell, Total reactive nitrogen (NO_y) as an indicator of the sensitivity of ozone to reductions in hydrocarbon and NO_x emissions, *J. Geophys. Res.*, 99(D2), 3533-3542, 1994.
- Mozurkewich, M. and J. G. Calvert, Reaction Probability of N₂O₅ on Aqueous Aerosols. *J. Geophys. Res.* 93, 15889-15896, 1988.
- Mozurkewich M., P.H. McMurry, A. Gupta and J.G. Calvert, Mass accommodation coefficient for HO₂ radicals on aqueous particles, *J. Geophys. Res.*, 92, 4163-4170, 1987.
- Pandis S.N. and J.H. Seinfeld, Sensitivity analysis of a chemical mechanism for aqueous-phase atmospheric chemistry, *J. of Geophys. Res.*, 94(D1), 1105-1126, 1989.
- Ponche, J.L., Ch. George and Ph. Mirabel, Mass transfer at the air/water interface: mass accommodation coefficients of SO₂, HNO₃, NO₂ and NH₃, *J. Atmos. Chem.*, 16, 1-21, 1993.

- Pruppacher H.R. and J.D. Klett, *Microphysics of Clouds and Precipitation*, D. Reidel Publishing Company, pp 9-21, 1980.
- Pruppacher H. R. and J. D. Klett, *Microphysics of Clouds and Precipitation*, Chapter 2, 9-21, D. Reidel Publishing Company, 1980.
- Rall L.B., Automatic differentiation: techniques and applications, *Lecture Notes in Computer Science*, Vol. 120, Springer Verlag, Berlin, 1981.
- Ross H.B. and K.J. Noone, A numerical investigation of the destruction of peroxy radical by Cu ion catalyzed reactions on atmospheric particles, *J. of Atmos. Chem.*, 12, 121-136, 1991.
- Schwartz S.E., Mass transport consideration pertinent to aqueous phase reactions of gases in liquid-water clouds, in *Chemistry of Multiphase Atmospheric System*, W. Jaeschke, Eds., Springer-Verlag Berlin Heidelberg, 1986.
- Sillamnn S., The use of NO_y, H₂O₂, and HNO₃ as indicators for ozone-NO_x-hydrocarbon sensitivity in urban locations, *J. Geophys. Res.*, 100(D7), 14175-14188, 1995.
- Stephens S., J.M. Rossi and D.M. Golden, The heterogeneous reaction of ozone on carbonaceous surfaces, *Int. J. Chem. Kinet.* 18, 1133-1149, 1986.
- Stockwell W.R., A homogeneous gas phase mechanism for use in a regional acid deposition model, *Atmos. Environ.* 20, 1615-1632, 1986.
- Stockwell W. R., P. Middleton, J.S. Chang and X.Y. Tang, The second generation regional acid deposition model chemical mechanism for regional air-quality modeling, *J. Geophys. Res.*, 95, 16343-16367, 1990.
- Stockwell W.R., J.B. Milford, D. Gao and Y.-J. Yang, An analysis of the uncertainties in an atmospheric chemical mechanism, paper # 93-WA-68A.01, in *Proceeding of the 86th Annual Meeting & Exhibition*, Denver, Colorado, June 13-18, 1993.
- Tang I.N., and J.H. Lee, Accommodation coefficients of ozone and SO₂: implications on SO₂ oxidation in cloud water, in *The Chemistry of Acid Rain, ACS Symposium Series 349*, American Chemical Society, Washington, D.C., pp 109-117, 1987.
- Thomas K., D. Kely, D. Mihelcic, A. Volz-Thomas, Mass accommodation coefficients for NO₃ radicals on water: implications for atmospheric oxidation processes, in *Abstracts of International Conference on the Generation of Oxidants on Regional and Global Scales*, University of East Anglia, Norwich, 1989.
- Trainer M., D.D. Parrish, M.P. Buhr, R.B. Norton, F.C. Fehsenfeld, K.G. Anlauf, J.W. Bottenheim, Y.Z. Tang, H.A. Wiebe, J.M. Roberts, R.L. Tanner, L. Newman, V.C. Bowersox, J.F. Meagher, K.J. Olszyna, M.O. Rodgers, T.Wang, H. Berresheim, K.L. Demerjian and U.K. Roychowdhury, Correlation of ozone with NO_y in photochemically aged air, *J. Geophys. Res.*, 98(D2), 2917-2925, 1993.
- Van Doren J.M., L.R. Watson, P. Davidovits, D.R. Worsnop, M.S. Zahniser, and C.E. Kolb, Temperature dependence of the uptake coefficients of HNO₃, HCl, and N₂O₅ by water droplets, *J. Phys. Chem.* ,94, 3265-3269, 1990.
- Walcek C.J., H.-H. Yuan and W.R. Stockwell, The influence of aqueous-phase chemical reactions on O₃ formation in polluted and nonpolluted clouds, *Atmos. Environ.* 31(8), 1221-1237, 1997.
- Whitby K.T., The physical characteristics of sulfur aerosols, *Atmos. Environ.*, 12, 135-159, 1978.

- Worsnop D.R., M.S. Zahniser, C.E. Kolb, J.A. Gardner, L.R. Watson, J.M. V. Doren, J.T. Jayne, and P. Davidovits, Temperature dependence of mass accommodation of SO₂ and H₂O₂ on aqueous surfaces, *J. Phys. Chem.*, 93, 1159-1172, 1989.
- Yin F., D. Grosjean, and J.H. Seinfeld, Photooxidation of dimethyl sulfide and dimethyl disulfide. I: mechanism and development, *J. Atmos. Chem.*, 11, 309-364, 1990.
- Zaveri, R., Development of a comprehensive tropospheric chemistry model for regional and global applications, PhD dissertation, Virginia Polytechnic Institute and State University, Blacksburg, Virginia, US, 1997.
- Zhang, Y., R. D. Saylor, R. C. Easter and E. G. Chapman, Effect of atmospheric heterogeneous processes on gas-phase chemistry, *Proceedings of 89th A&WMA Annual Meeting and Exhibition*, No. 96-FA130B.02, pp. 1-16, Nashville, Tennessee, June 23-28, 1996.

Table 1. Chemical species included in the MaTChM.

No.	Gas-phase species	Representation	No	Aqueous and aerosol species
1	Nitric oxide	NO	1	HNO3
2	Nitrogen dioxide	NO2	2	HNO2
3	Nitrogen trioxide (nitrate radical)	NO3	3	SO2
4	Dinitrogen pentoxide	N2O5	4	H2SO4
5	Nitrous acid	HONO	5	HCOOH
6	Nitric acid	HNO3	6	CH3COOH
7	Peroxynitric acid (HO2NO2)	PNA	7	CO2
8	Oxygen atom (singlet)	O(1D)	8	MSA
9	Oxygen atom (triplet)	O(3P)	9	NH3
10	Hydroxyl radical	OH	10	HO2
11	Ozone	O3	11	H2O2
12	Hydroperoxy radical	HO2	12	HCHO
13	Hydrogen peroxide	H2O2	13	NO2
14	Formaldehyde (CH2=O)	HCHO	14	NO
15	Carbon monoxide	CO	15	NO3
16	High molecular weight aldehydes (RCHO, R>H)	ALD2	16	PAN
17	Peroxyacyl radical (CH3C(O)OO·)	C2O3	17	O3
18	Peroxyacyl nitrate(CH3C(O)OONO2)	PAN	18	OH
19	NO-to-NO2 operation	XO2	19	CH3O2
20	Paraffin carbon bond (C-C)	PAR	20	CH3OH
21	Secondary organic oxy radical	ROR	21	DMS
22	NO-to-nitrate operation	XO2N	22	DMSO
23	Olefinic carbon bond (C=C)	OLE	23	DMSO2
24	Ethene(CH2=CH2)	ETH	24	CH3OOH
25	Toluene(C6H5-CH3)	TOL	25	CH3C(O)OOH
26	Cresol and higher molecular weight phenols	CRES	26	N2O5
27	Toluene-hydroxyl radical adduct	TO2	27	NTR
28	Methylphenoxy radical	CRO	28	HCl
29	High molecular weight aromatic oxidation ring fragment	OPEN	29	Cl
30	Xylene(C6H4-(CH3)2)	XYL		
31	Methylglyoxal (CH3C(O)C(O)H)	MGLY		
32	Isoprene	ISOP		
33	unknown organic oxidation product of nitrogen species	NTR	No	Ionic species
34	Dimethyl sulfide, (CH3)2S	DMS	1	CO3 ⁻
35	Methyl sulfonyl radical	CH3SO2	2	HOCH2SO3 ⁻
36	Methyl sulfonic radical	CH3SO3	3	SO4 ⁻
37	Methane sulfonic acid (CH3SO3H)	MSA	4	SO5 ⁻
38	Dimethyl sulfoxide (CH3)2SO	DMSO	5	HSO5 ⁻
39	Dimethyl sulfone (CH3)2SO2	DMSO2	6	CH2(OH)2
40	Methyl sulfonyl acid	CH3SO2H	7	H ⁺
41	Methyl sulfonyl peroxy radical	CH3S(O)2OO	8	NH4 ⁺
42	Dimethyl sulfide peroxy radical	CH3SCH2OO	9	Fe ³⁺
43	Dimethyl sulfonyl peroxy radical	CH3S(O)2CH2OO	10	Fe(OH) ²⁺
44	Sulfur dioxide	SO2	11	Fe(OH)2 ⁺
45	Sulfuric acid	H2SO4	12	Mn ²⁺
46	Unkown oxidation product of sulfur species	SULF	13	OH ⁻
47	Methane	CH4	14	NO3 ⁻
48	Ethane	C2H6	15	NO2 ⁻
49	Methyl peroxy radical	CH3O2	16	HSO3 ⁻
50	Ethyl peroxy radical formed from alkane	ETHP	17	SO3 ⁼
51	Methyl peroxide	CH3OOH	18	HSO4 ⁻
52	Acetic acid	CH3COOH	19	SO4 ⁼
53	Formic acid	HCOOH	20	HCO3 ⁻
54	Methanol	CH3OH	21	CO3 ⁼
55	Carbon dioxide	CO2	22	O2 ⁻
56	Ammonia	NH3	23	HO2 ⁻
57	Hydrogen chloride	HCl	24	HCOO ⁻
No	Lumped gas-phase species		25	CH3COO ⁻
1	Nitrogen oxides=NO+NO2	NOx	26	CH3SO3 ⁻
2	Total reactive nitrogen=NO+NO2+NO3+N2O5+HNO3+PAN+NTR	NOy	27	ClOH ⁻
3	Total non-NOx reactive nitrogen=NOy-NOx	NOz	28	Cl ⁻
4	Odd hydrogen=OH+HO2+CH3O2+ETHP+C2O3+ROR+TO2+CRO	RxOy	29	Cl2 ⁻

Table 2. Mass accommodation coefficients (α) and uptake coefficients (γ) of species in the MaTChM.

No	Species	α	Reference	$\gamma = \alpha_{\min}$	Reference
1	HNO ₃	1.1E-1	Ponche et al., 1993	2.4E-3	Baldwin, 1982, see note [e]
2	HNO ₂	3.0E-2	Bongartz et al., 1994	5.0E-4	Kirchner et al., 1990, see note [d]
3	SO ₂	5.4E-2	Gardner et al., 1987	2.4E-4	Judeikis et al., 1978
4	H ₂ SO ₄	2.0E-2	Dingenen and Raos, 1991	2.0E-4	see note [c]
5	HCOOH	4.7E-2	Jayne et al., 1991	4.7E-4	see note [c]
6	CH ₃ COOH	4.7E-2	see note [a]	4.7E-4	see note [a]
7	CO ₂	1.0E-4	see note [b]	1.0E-6	see note [c]
8	MSA	9.0E-2	DeBruyn et al., 1994	9.0E-4	see note [c]
9	NH ₃	9.7E-2	Ponche et al., 1993	9.7E-4	see note [c]
10	HO ₂	2.0E-1	Mozurkewich et al., 1987; Kurylo et al., 1994	1.0E-1	Hanson et al., 1992, see note [e]
11	H ₂ O ₂	1.8E-1	Worsnop et al., 1989	7.8E-3	Baldwin, 1982, see note [e]
12	HCHO	2.0E-2	Jayne et al., 1992	1.0E-3	Jayne et al., 1992
13	NO ₂	6.3E-4	Lee and Tang, 1988	3.3E-5	Baldwin, 1982, see note [e]
14	NO	1.0E-5	Leu, 1988	1.0E-5	Baldwin, 1982, see note [e]
15	NO ₃	1.0E-2	see note [b]	1.0E-2	Thomas et al., 1989, see note [e]
16	PAN	1.0E-3	Kirchner et al., 1990	1.0E-4	Kirchner et al., 1990, see note [d]
17	O ₃	5.3E-4	Tang and Lee, 1987	1.0E-4	Fendel et al., 1995
18	OH	8.0E-2	Hanson et al., 1992	4.9E-3	Baldwin and Golden, 1980, see note [e]
19	CH ₃ O ₂	5.0E-2	Dentener, 1993	5.0E-3	Dentener, 1993, see note [d]
20	CH ₃ OH	3.4E-2	Davidovits et al., 1993	3.4E-3	Davidovits et al., 1993, see note [d]
21	DMS	7.4E-2	see note [a]	7.4E-3	see note [a]
22	DMSO	7.4E-2	Davidovits et al., 1993	7.4E-3	Davidovits et al., 1993, see note [d]
23	DMSO ₂	7.9E-2	Davidovits et al., 1993	7.9E-3	Davidovits et al., 1993, see note [d]
24	CH ₃ OOH	2.9E-2	Davidovits et al., 1993	2.9E-4	Davidovits et al., 1993, see note [c]
25	CH ₃ COOOH	2.9E-2	see note [a]	2.9E-4	see note [a]
26	N ₂ O ₅	1.0E-1	Morzurkewich and Calvert, 1988	1.0E-1	Morzurkewich and Calvert, 1988
27	NTR	1.0E-6	Baldwin and Golden, 1980, see note [f]	1.0E-8	see note [c]
28	HCl	1.4E-1	Van Doren et al., 1990	1.0E-2	Kirchner et al., 1990
29	Cl	1.0E-4	Martin et al., 1980	3.0E-5	Martin et al., 1980

- a* α s and γ s of DMS, CH₃COOH and CH₃COOOH are assumed to be the same as those of DMSO, HCOOH and CH₃OOH, respectively.
- b* For species with missing or insufficient α and γ measurement data and for which measurements of analogous compounds do not exist, the values of α are assumed to be 0.01 for soluble species, and 1.E-4 for less soluble species, respectively.
- c* γ is assumed to be a factor of 100 lower than the corresponding α used in this work.
- d* γ is assumed to be a factor of 10 lower than the corresponding measured lower limit of α reported in the reference.
- e* γ is assumed to be a factor of 10 higher than the corresponding measured lower limit of γ reported in the reference.
- f* The mass accommodation coefficient of other nitrogen species (NTR) is assumed to be the same as that of atomic nitrogen in Baldwin and Golden, 1980.

Table 3. Heterogeneous uptake of various species on the surface of aerosols in MaTChM.

No	Heterogeneous surface uptake	Overall heterogeneous loss rate, K_{pi} , s^{-1}				
		Remote	Marine	Rural	Urban	Heavily-polluted
P1.	$\text{HNO}_3(\text{g}) \rightarrow \text{HNO}_3(\text{p})$	2.46E-6	5.19E-6	2.51E-5	2.08E-4	5.90E-4
P2.	$\text{HNO}_2(\text{g}) \rightarrow \text{HNO}_2(\text{p})$	5.39E-7	1.14E-6	5.30E-6	4.38E-5	1.24E-4
P3.	$\text{SO}_2(\text{g}) \rightarrow \text{H}_2\text{SO}_3(\text{p})$	2.55E-7	5.39E-7	2.51E-6	2.07E-5	5.86E-5
P4.	$\text{H}_2\text{SO}_4(\text{g}) \rightarrow \text{H}_2\text{SO}_4(\text{p})$	1.72E-7	3.63E-7	1.69E-6	1.39E-5	3.95E-5
P5.	$\text{HCOOH}(\text{g}) \rightarrow \text{HCOOH}(\text{p})$	5.87E-7	1.24E-6	5.79E-6	4.78E-5	1.35E-4
P6.	$\text{CH}_3\text{COOH}(\text{g}) \rightarrow \text{CH}_3\text{COOH}(\text{p})$	5.12E-7	1.08E-6	5.07E-6	4.19E-5	1.19E-4
P7.	$\text{CO}_2(\text{g}) \rightarrow \text{H}_2\text{CO}_3(\text{p})$	1.29E-8	2.72E-8	1.26E-7	1.04E-6	2.95E-6
P8.	$\text{MSA}(\text{g}) \rightarrow \text{MSA}(\text{p})$	7.71E-7	1.63E-6	7.66E-6	6.34E-5	1.79E-4
P9.	$\text{NH}_3(\text{g}) \rightarrow \text{NH}_4\text{OH}(\text{p})$	1.92E-6	4.05E-6	1.95E-5	1.62E-4	4.59E-4
P10.	$\text{HO}_2(\text{g}) \rightarrow \text{HO}_2(\text{p})$	5.33E-5	1.16E-4	1.20E-3	1.08E-2	3.25E-2
P11.	$\text{H}_2\text{O}_2(\text{g}) \rightarrow \text{H}_2\text{O}_2(\text{p})$	9.28E-6	1.97E-5	1.08E-4	9.12E-4	2.60E-3
P12.	$\text{HCHO}(\text{g}) \rightarrow \text{HCHO}(\text{p})$	1.50E-6	3.17E-6	1.52E-5	1.26E-4	3.56E-4
P13.	$\text{NO}_2(\text{g}) \rightarrow \text{NO}_2(\text{p})$	4.16E-8	8.77E-8	4.07E-7	3.36E-6	9.51E-6
P14.	$\text{NO}(\text{g}) \rightarrow \text{NO}(\text{p})$	2.34E-8	4.94E-8	2.29E-7	1.89E-6	5.35E-6
P15.	$\text{NO}_3(\text{g}) \rightarrow \text{NO}_3(\text{p})$	8.89E-6	1.88E-5	1.03E-4	8.67E-4	2.47E-3
P16.	$\text{PAN}(\text{g}) \rightarrow \text{PAN}(\text{p})$	7.76E-8	1.64E-7	7.60E-7	6.28E-6	1.78E-5
P17.	$\text{O}_3(\text{g}) \rightarrow \text{O}_3(\text{p})$	1.23E-7	2.60E-7	1.21E-6	9.97E-6	2.82E-5
P18.	$\text{OH}(\text{g}) \rightarrow \text{OH}(\text{p})$	8.39E-6	1.78E-5	9.65E-5	8.11E-4	2.31E-3
P19.	$\text{CH}_3\text{O}_2(\text{g}) \rightarrow \text{CH}_3\text{O}_2(\text{p})$	5.49E-6	1.16E-5	5.98E-5	5.00E-4	1.42E-3
P20.	$\text{CH}_3\text{OH}(\text{g}) \rightarrow \text{CH}_3\text{OH}(\text{p})$	4.61E-6	9.74E-6	4.95E-5	4.13E-4	1.17E-3
P21.	$\text{DMS}(\text{g}) \rightarrow \text{DMS}(\text{p})$	6.86E-6	1.45E-5	7.68E-5	6.43E-4	1.83E-3
P22.	$\text{DMSO}(\text{g}) \rightarrow \text{DMSO}(\text{p})$	6.21E-6	1.31E-5	6.86E-5	5.74E-4	1.63E-3
P23.	$\text{DMSO}_2(\text{g}) \rightarrow \text{DMSO}_2(\text{p})$	6.06E-6	1.28E-5	6.68E-5	5.58E-4	1.59E-3
P24.	$\text{CH}_3\text{OOH}(\text{g}) \rightarrow \text{CH}_3\text{OOH}(\text{p})$	3.55E-7	7.49E-7	3.50E-6	2.89E-5	8.18E-5
P25.	$\text{CH}_3\text{C}(\text{O})\text{OOH}(\text{g}) \rightarrow \text{CH}_3\text{C}(\text{O})\text{OOH}(\text{p})$	2.83E-7	5.96E-7	2.78E-6	2.30E-5	6.50E-5
P26.	$\text{N}_2\text{O}_5(\text{g}) \rightarrow 2\text{HNO}_3(\text{p})$	3.87E-5	8.34E-5	7.07E-4	6.23E-3	1.83E-2
P27.	$\text{NTR}(\text{g}) \rightarrow \text{NTR}(\text{p})$	1.62E-10	3.41E-10	1.58E-9	1.31E-8	3.69E-8
P28.	$\text{HCl}(\text{g}) \rightarrow \text{HCl}(\text{p})$	1.17E-5	2.48E-5	1.35E-4	1.13E-3	3.22E-3
P29.	$\text{Cl}(\text{g}) \rightarrow \text{Cl}(\text{p})$	4.30E-8	9.08E-8	4.21E-7	3.48E-6	9.84E-6

Read 2.46E-6 as 2.46×10^{-6} .

Table 4. Initial atmospheric conditions in the model simulations.

(a) Gas and aqueous-phase concentrations (in ppb and M, respectively)

Species	Remote	Marine	Rural	Urban	Heavily-polluted
O ₃	20.0	30.0	40.0	60.0	80.0
H ₂ O ₂	1.0	1.0	1.0	1.0	1.0
NO	7.5×10^{-2}	7.5×10^{-1}	1.5	10.0	100.0
NO ₂	2.5×10^{-2}	2.5×10^{-1}	0.5	1.0	10.0
SO ₂	0.6	0.6	2.0	5.0	10.0
DMS	4.0×10^{-2}	4.0×10^{-2}	0.0	0.0	0.0
HCHO	0.2	1.8	0.2	8.3	27.5
ALD ₂	0.0	0.0	8.3×10^{-2}	11.7	39.0
C ₂ H ₆	0.0	1.9	1.58	9.08	30.3
PAR	0.0	3.1	9.8	177.9	593.1
OLE	0.0	5.6×10^{-1}	0.3	13.2	44.0
ETH	0.0	1.9×10^{-1}	0.6	11.6	38.5
TOL	0.0	3.6×10^{-2}	5.3×10^{-1}	6.0	19.9
XYL	0.0	0.0	7.5×10^{-2}	3.2	10.5
ISOP	0.0	0.0	2.4×10^{-1}	0.5	2.0
CO	80.0	100.0	120.0	150.0	300.0
CH ₄	1.7×10^3	1.7×10^3	1.6×10^3	1.7×10^3	1.7×10^3
CO ₂	3.4×10^5	3.4×10^5	3.4×10^5	3.4×10^5	3.4×10^5
NH ₃	0.1	0.5	0.5	0.5	0.5
HCl	0.5	0.5	0.1	0.0	0.0
Fe(III)(l)	4.0×10^{-7}	4.0×10^{-7}	4.0×10^{-7}	4.0×10^{-7}	4.0×10^{-7}
Mn(II)(l)	2.0×10^{-7}	2.0×10^{-7}	2.0×10^{-7}	2.0×10^{-7}	2.0×10^{-7}
NaCl(l)	1.0×10^{-6}	5.0×10^{-7}	0.0	0.0	0.0

(b) Cloud, aerosol and physical parameters

Model parameters	Remote	Marine	Rural	Urban	Heavily-polluted
Cloud					
droplet radius (μm)	10	10	10	10	10
volumetric water content	4.0×10^{-7}	4.0×10^{-7}	4.0×10^{-7}	4.0×10^{-7}	4.0×10^{-7}
Aerosol [§]					
number (cm^{-3})	1.26×10^2	3.4×10^2	6.65×10^3	1.06×10^5	2.12×10^6
mode 1 radius (μm)	5.00×10^{-3}	5.00×10^{-3}	7.39×10^{-3}	7.00×10^{-3}	6.50×10^{-3}
Log σ	0.204	0.204	0.225	0.255	0.241
number (cm^{-3})	2.25×10^1	6.00×10^1	1.47×10^2	3.20×10^4	3.70×10^4
mode 2 radius (μm)	3.55×10^{-2}	3.55×10^{-2}	2.69×10^{-2}	2.70×10^{-2}	3.1×10^{-2}
Log σ	0.301	0.301	0.557	0.334	0.297
number (cm^{-3})	1.50×10^0	3.10×10^0	1.99×10^3	5.4×10^0	4.9×10^0
mode 3 radius (μm)	3.10×10^{-1}	3.10×10^{-1}	4.19×10^{-2}	4.3×10^{-1}	5.4×10^{-1}
Log σ	0.431	0.431	0.266	0.344	0.328
number (cm^{-3})	1.50×10^2	4.03×10^2	8.78×10^3	1.38×10^5	2.15×10^6
total surface ($\mu\text{m}^2 \text{cm}^{-3}$)	1.39×10^1	2.93×10^1	1.36×10^2	1.13×10^3	3.27×10^3
total volume ($\mu\text{m}^3 \text{cm}^{-3}$)	1.56×10^1	3.23×10^1	2.28×10^1	6.85×10^1	8.95×10^1
Temperature (K)	280	280	280	280	280
Relative humidity%	80	80	80	80	80

§ Aerosol distributions for heavily polluted, urban and marine conditions are based on those of the urban and freeway, urban average, and marine surface background conditions described in Whitby, 1978. Aerosol distribution for rural condition is from Jaenicke, 1993. Aerosol distribution for remote marine condition is assumed to have the same geometric number mean diameter and geometric standard deviation as those of the marine condition, with the number concentration data for remote oceans from Fitzgerald, 1991.

Table 5. 1-hr average concentrations (ppb) of gas-phase species, total sulfate (TSO₄⁼) and total nitrate (TNO₃⁻) in all phases under various conditions. The values in parentheses indicate the percent changes in presence of clouds and/or aerosols relative to gas only conditions.

Condition	NO	NO ₂	HNO ₃	PAN	SO ₂	H ₂ SO ₄	HCHO	ISOP	OH	HO ₂	H ₂ O ₂	O ₃	TSO ₄ ⁼	TNO ₃ ⁻
<i>Remote</i>														
Gas	3.79E-2	4.26E-2	1.66E-2	--	5.82E-1	2.19E-2	2.63E-1	--	1.484E-4	1.09E-2	1.03E+0	2.05E+1	2.19E-2	1.66E-2
Cloud	4.98E-2 (31.5)	4.16E-2 (-2.3)	8.93E-6 (-99.9)	--	1.24E-2 (-97.9)	2.88E-6 (-100.0)	1.13E-1 (-57.0)	--	8.83E-5 (-54.5)	2.22E-3 (-79.6)	1.04E-1 (-89.9)	2.00E+1 (-2.4)	5.90E-1 (2671.9)	7.72E-3 (-53.6)
Aerosol	3.80E-2 (0.3)	4.26E-2 (-0.1)	1.64E-2 (-1.1)	--	5.82E-1 (-0.1)	2.18E-2 (-0.5)	2.61E-1 (-0.6)	--	1.93E-46 (-0.7)	1.08E-3 (-1.1)	9.81E-1 (-4.8)	2.05E+1 (-0.1)	2.30E-2 (4.9)	1.65E-2 (-0.4)
Cloud+ Aerosol	4.98E-2 (31.4)	4.16E-2 (-2.3)	8.91E-6 (-99.9)	--	1.25E-2 (-97.9)	2.87E-6 (-100.0)	1.12E-1 (-57.2)	--	8.83E-5 (-54.6)	2.22E-3 (-79.7)	1.03E-1 (-90.0)	2.00E+1 (-2.4)	5.90E-1 (2672.0)	7.74E-3 (-53.6)
<i>Marine</i>														
Gas	1.99E-1	3.14E-1	2.87E-1	1.58E-1	5.67E-1	4.08E-2	1.39E+0	--	3.54E-4	1.11E-2	9.73E-1	3.37E+1	4.08E-2	2.87E-1
Cloud	3.53E-1 (80.3)	4.37E-1 (40.7)	1.73E-4 (-99.9)	4.40E-2 (-72.7)	5.67E-3 (-99.0)	3.28E-6 (-100.0)	1.04E+0 (-25.3)	--	1.63E-4 (-53.7)	2.73E-3 (-75.2)	1.42E-1 (-85.4)	3.10E+1 (-7.7)	5.96E-1 (1401.1)	1.47E-1 (-49.1)
Aerosol	2.01E-1 (1.2)	3.15E-1 (0.4)	2.81E-1 (-2.1)	1.56E-1 (-1.2)	5.66E-1 (-0.3)	4.04E-2 (-1.1)	1.37E+0 (-1.3)	--	3.50E-4 (-1.0)	1.08E-2 (-2.4)	8.77E-1 (-9.8)	3.36E+1 (-0.2)	4.29E-2 (5.1)	2.86E-1 (-0.5)
Cloud+ Aerosol	3.53E-1 (80.4)	4.37E-1 (40.6)	1.73E-4 (-99.9)	4.38E-2 (-72.8)	5.99E-3 (-99.0)	3.19E-6 (-100.0)	1.02 (-26.2)	--	1.63E-4 (-53.8)	2.71E-3 (-75.4)	1.40E-1 (-85.7)	3.10E+1 (-7.9)	5.96E-1 (1401.0)	1.47E-1 (-49.1)
<i>Rural</i>														
Gas	4.53E-1	7.94E-1	4.23E-1	2.04E-1	1.91E-1	8.57E-2	8.55E-1	1.15E-2	2.91E-4	5.50E-3	9.2E-1	4.27E+1	8.57E-2	4.23E-1
Cloud	5.56E-1 (23.5)	8.98E-1 (13.5)	4.07E-4 (-99.9)	1.40E-1 (-31.0)	4.76E-1 (-75.1)	5.29E-5 (-99.9)	4.43E-1 (-48.2)	2.81E-2 (190.4)	1.83E-4 (-37.0)	2.63E-3 (-51.7)	1.19E-2 (-98.7)	4.13E+1 (-3.2)	1.52E+0 (1751.6)	3.18E-1 (-24.9)
Aerosol	4.73E-1 (4.5)	8.10E-1 (2.1)	3.75E-1 (-11.0)	1.92E-1 (-5.7)	1.89E+0 (-1.1)	7.98E-2 (-6.8)	7.98E-1 (-6.6)	1.30E-2 (16.5)	2.66E-4 (-8.6)	4.73E-3 (-13.5)	5.16E-1 (-43.9)	4.22E+1 (-1.1)	1.19E-1 (39.1)	4.05E-1 (-4.2)
Cloud+ Aerosol	5.61E-1 (24.7)	8.99E-1 (13.6)	3.98E-4 (-99.9)	1.38E-1 (-32.3)	4.84E-1 (-74.7)	5.20E-5 (-99.9)	4.23E-1 (-50.5)	2.91E-2 (202.7)	1.79E-4 (-38.3)	2.53E-3 (-53.4)	1.10E-2 (-98.8)	4.10E+1 (-3.9)	1.52E+0 (1747.4)	3.16E-1 (-25.4)
<i>Urban</i>														
Gas	1.82E+0	5.19E+0	9.91E-1	2.44E+0	4.93E+0	7.24E-2	1.04E+1	1.57E-1	9.15E-5	6.06E-3	9.56E-1	7.18E+1	7.24E-2	9.91E-1
Cloud	2.07E+0 (14.7)	5.52E+0 (6.6)	1.15E-3 (-99.9)	1.98E+0 (-18.5)	2.80E+0 (-43.2)	1.52E-4 (-99.8)	7.97E+0 (-23.6)	1.88E-1 (20.8)	7.35E-5 (-19.7)	4.17E-3 (-30.4)	3.06E-3 (-99.7)	6.82E+1 (-5.0)	2.16E+0 (2977.7)	9.84E-1 (-0.7)
Aerosol	2.14E+0 (19.2)	5.44E+0 (5.1)	4.76E-1 (-50.9)	1.91E+0 (-21.0)	4.41E+0 (-10.4)	5.35E-2 (-25.4)	6.07E+0 (-41.7)	1.90E-1 (22.6)	6.70E-5 (-26.7)	3.58E-3 (-40.1)	1.23E-2 (-98.7)	6.50E+1 (-9.3)	8.28E-1 (1051.6)	9.55E-1 (-3.3)
Cloud+ Aerosol	2.29E+0 (27.6)	5.60E+0 (8.4)	9.53E-4 (-99.9)	1.69E+0 (-30.4)	2.61E+0 (-47.0)	1.16E-4 (-99.8)	5.13E+0 (-50.7)	2.09E-1 (35.7)	6.06E-5 (-33.9)	3.00E-3 (-49.7)	1.94E-3 (-99.9)	6.31E+1 (-12.0)	2.51E-1 (3472.2)	1.01E+0 (2.1)
<i>Heavily-Polluted</i>														
Gas	2.41E+1	7.51E+1	5.52E+0	4.02E+0	9.93E+1	6.99E-2	2.85E+1	1.04E+0	4.30E-5	8.63E-4	9.45E-1	8.35E+1	6.99E-2	5.52E+0
Cloud	2.47E+1 (2.3)	7.32E+1 (-2.5)	7.46E-3 (-99.9)	3.71E+0 (-7.6)	8.17E+1 (-17.7)	3.87E-4 (-99.4)	2.39E+1 (-16.2)	1.08E+0 (4.0)	3.99E-5 (-6.8)	7.75E-4 (-10.4)	3.25E-5 (-100.0)	7.97E+1 (-4.6)	1.73E+0 (2463.3)	7.37E+0 (33.3)
Aerosol	2.78E+1 (15.6)	6.87E+1 (-8.5)	1.01E+0 (-80.7)	2.65E+0 (-33.2)	7.24E+1 (-27.1)	3.77E-2 (-45.0)	6.73E+0 (-76.4)	1.22E+0 (18.1)	2.53E-5 (-40.9)	4.09E-4 (-52.4)	2.0E-5 (-100.0)	6.63E+1 (-20.4)	4.00E+0 (5670.9)	8.26E+0 (51.0)
Cloud+ Aerosol	2.78E+1 (15.6)	6.84E+1 (-8.9)	4.55E-3 (-99.9)	2.68E+0 (-32.7)	5.99E+1 (-39.7)	2.05E-4 (-99.7)	7.18E+0 (-74.8)	1.22E+0 (17.8)	2.63E-5 (-38.7)	4.22E-4 (-50.8)	1.59E-5 (-100.0)	6.60E+1 (-20.8)	4.96E+0 (7135.1)	9.85E+0 (79.8)

Table 6. Predicted photochemical indicators under various polluted atmospheric conditions and the changes in the presence of clouds and/or aerosols relative to the base value under clear air conditions at the end of the 2-hr simulation.

Indicators	Scenarios	Conditions					
		Rural		Urban		Heavily-polluted	
		Indicator value	Relative change	Indicator value	Relative change	Indicator value	Relative change
NO _y	Gas	2.00E+0		1.10E+1		1.10E+2	
	Cloud	1.59E+0	-2.05E-1	9.71E+0	-1.17E-1	9.99E+1	-9.18E-2
	Aerosol	1.95E+0	-2.50E-2	1.01E+1	-8.18E-2	9.78E+1	-1.11E-1
	Cloud+Aerosol	1.59E+0	-2.05E-1	9.63E+0	-1.25E-1	9.64E+1	-1.24E-1
O ₃ /NO _y	Gas	2.19E+1		7.05E+0		8.31E-1	
	Cloud	2.64E+1	2.06E-1	7.49E+0	6.24E-2	8.64E-1	3.97E-2
	Aerosol	2.21E+1	9.10E-3	6.72E+0	-4.68E-2	6.86E-1	-1.75E-1
	Cloud+Aerosol	2.61E+1	1.92E-1	6.81E+0	-3.40E-2	6.94E-1	-1.65E-1
O ₃ /NO _z	Gas	4.62E+1		1.47E+1		6.48E+0	
	Cloud	1.52E+2	2.29E+0	2.26E+1	5.37E-1	1.41E+1	1.18E+0
	Aerosol	5.08E+1	9.96E-2	1.91E+1	2.99E-1	1.32E+1	1.04E+0
	Cloud+Aerosol	1.53E+2	2.31E+0	2.45E+1	6.67E-1	1.60E+1	1.47E+0
O ₃ /HNO ₃	Gas	8.01E+1		5.97E+1		1.22E+1	
	Cloud	1.18E+5	1.47E+3	6.99E+4	1.17E+3	1.15E+4	9.42E+2
	Aerosol	9.11E+1	1.37E-1	1.29E+2	1.16E+0	6.92E+1	4.67E+0
	Cloud+Aerosol	1.20E+5	1.50E+3	7.67E+4	1.28E+3	1.59E+4	9.50E+3
H ₂ O ₂ /NO _y	Gas	4.50E-1		8.64E-2		8.45E-3	
	Cloud	8.06E-3	-9.82E-1	4.04E-4	-9.95E-1	3.23E-7	-1.00E+0
	Aerosol	2.15E-1	-5.22E-1	4.16E-4	-9.95E-1	1.23E-7	-1.00E+0
	Cloud+Aerosol	7.29E-3	-9.84E-1	2.29E-4	-9.97E-1	1.46E-7	-1.00E+0
H ₂ O ₂ /HNO ₃	Gas	1.64E+0		1.00E+0		1.24E-1	
	Cloud	3.62E+1	2.11E+1	3.77E+0	2.77E+0	4.31E-3	-9.65E-1
	Aerosol	8.84E-1	-4.61E-1	8.00E-3	-9.92E-1	1.24E-5	-9.99E-1
	Cloud+Aerosol	3.34E+1	1.94E+1	2.58E+0	1.58E+0	3.35E-3	-9.73E-1
HCHO/NO _y	Gas	4.64E-1		9.49E-1		2.62E-1	
	Cloud	3.03E-1	-3.47E-1	8.49E-1	-1.05E-1	2.44E-1	-6.87E-2
	Aerosol	4.38E-1	-5.60E-2	5.47E-1	-4.24E-1	5.24E-2	-8.00E-1
	Cloud+Aerosol	2.85E-1	-3.86E-1	4.96E-1	-4.77E-1	5.84E-2	-7.77E-1
(HNO ₃ /H ₂ O ₂)/ (NO _x /ROG)	Gas	2.74E-1		1.18E-1		6.80E-2	
	Cloud	2.23E-4	-9.99E-1	1.04E-4	-9.99E-1	7.50E-5	-9.99E-1
	Aerosol	2.43E-1	-1.13E-1	5.20E-2	-5.59E-1	9.92E-3	-8.54E-1
	Cloud+Aerosol	2.18E-4	-9.99E-1	8.87E-5	-9.99E-1	4.37E-5	-9.99E-1

Table 7. 1-hr average sensitivities of O₃ with respect to gas-phase reaction rate constants under clear air conditions.

Rank	Remote		Marine		Rural		Urban		Heavily-polluted	
	Rxn. #	\bar{S}_{kl}	Rxn. #	\bar{S}_{kl}	Rxn. #	\bar{S}_{kl}	Rxn. #	\bar{S}_{kl}	Rxn. #	\bar{S}_{kl}
1	G28	2.01E-2	G1	6.03E-2	G11	4.67E-2	G38	1.20E-1	G3	-2.58E-1
2	G1	1.86E-2	G3	-4.92E-2	G10	-4.67E-2	G43	-1.14E-1	G1	2.77E-1
3	G3	-1.29E-2	G28	4.40E-2	G9	4.47E-2	G1	1.10E-1	G38	1.85E-1
4	G116	6.44E-3	G26	-3.25E-2	G1	4.13E-2	G3	-1.06E-1	G26	-1.75E-1
5	G117	4.38E-3	G11	2.26E-2	G26	-4.10E-2	G57	8.05E-2	G57	1.23E-1
6	G118	-4.05E-3	G10	-2.26E-2	G3	-3.87E-2	G26	-6.34E-2	G43	-8.70E-2
7	G26	-3.94E-3	G9	2.17E-2	G36	1.54E-2	G11	5.12E-2	G45	5.07E-2
8	G33	-3.33E-3	G38	2.10E-2	G116	1.50E-2	G10	-5.12E-2	G47	-4.11E-2
9	G32	-2.81E-3	G116	1.97E-2	G28	1.32E-2	G9	4.90E-2	G46	4.11E-2
10	G13	-2.62E-3	G36	1.46E-2	G38	1.04E-2	G47	-4.60E-2	G58	4.01E-2
11	G34	2.29E-3	G43	-9.41E-3	G61	8.65E-3	G46	4.60E-2	G61	3.93E-2
12	G12	-1.50E-3	G33	-8.24E-3	G34	8.48E-3	G61	3.31E-2	G69	3.79E-2
13	G36	1.33E-3	G32	-6.95E-3	G47	-7.96E-3	G45	2.99E-2	G52	3.38E-2
14	G38	1.12E-3	G47	-6.72E-3	G46	7.94E-3	G69	2.82E-2	G39	-2.74E-2
15	G29	-7.65E-4	G46	6.61E-3	G43	-6.15E-3	G28	2.35E-2	G11	2.61E-2
16	G30	7.48E-4	G117	6.29E-3	G52	6.14E-3	G52	2.23E-2	G10	-2.61E-2
17	G97	-5.59E-4	G34	6.03E-3	G74	5.21E-3	G58	2.08E-2	G9	2.49E-2
18	G89	-5.58E-4	G118	-5.64E-3	G57	3.72E-3	G74	1.74E-2	G74	1.71E-2
19	G11	5.36E-4	G37	4.84E-3	G76	3.52E-3	G39	-1.68E-2	G28	1.50E-2
20	G10	-5.36E-4	G39	-3.72E-3	G29	-3.20E-3	G29	-1.47E-2	G29	-1.46E-2
21	G85	3.70E-4	G29	-3.58E-3	G30	3.12E-3	G30	1.42E-2	G30	1.44E-2
22	G9	3.07E-4	G30	3.43E-3	G63	2.26E-3	G37	6.24E-3	G4	-1.42E-2
23	G122	-2.55E-4	G13	-3.04E-3	G37	2.05E-3	G34	6.14E-3	G63	1.11E-2
24	G22	-2.25E-4	G57	2.88E-3	G22	-1.99E-3	G63	5.54E-3	G76	9.99E-3
25	G23	1.88E-4	G61	2.55E-3	G69	1.90E-3	G36	4.17E-3	G2	8.87E-3
26	G39	-9.66E-5	G52	2.35E-3	G33	-1.85E-3	G76	4.16E-3	G37	8.84E-3
27	G82	9.60E-5	G22	-1.65E-3	G73	-1.84E-3	G116	3.14E-3	G65	-4.78E-3
28	G37	-8.24E-5	G12	-1.55E-3	G23	1.78E-3	G73	-2.89E-3	G64	4.78E-3
29	G86	-6.43E-5	G23	1.44E-3	G32	-1.56E-3	G64	2.31E-3	G7	-4.60E-3
30	G88	6.28E-5	G35	7.64E-4	G13	-1.51E-3	G65	-2.30E-3	G71	4.47E-3

Table 8. 1-hr average sensitivities of odd hydrogen R_xO_y with respect to gas-phase reaction rate constants under clear air conditions.

Rank	Remote		Marine		Rural		Urban		Heavily-polluted	
	Rxn. #	\bar{S}_{kl}	Rxn. #	\bar{S}_{kl}	Rxn. #	\bar{S}_{kl}	Rxn. #	\bar{S}_{kl}	Rxn. #	\bar{S}_{kl}
1	G9	3.65E-1	G9	5.16E-1	G11	1.03E+0	G38	8.42E-1	G38	7.17E-1
2	G11	3.52E-1	G11	5.05E-1	G10	-1.03E+0	G28	-5.80E-1	G28	-6.53E-1
3	G10	-3.52E-1	G10	-5.05E-1	G9	1.03E+0	G43	-5.69E-1	G26	-6.21E-1
4	G118	-1.80E-1	G38	2.90E-1	G28	-4.99E-1	G11	4.03E-1	G57	4.48E-1
5	G33	-1.62E-1	G116	1.72E-1	G26	-4.27E-1	G10	-4.03E-1	G43	-3.21E-1
6	G116	1.49E-1	G33	-1.61E-1	G116	2.54E-1	G9	4.02E-1	G117	-2.54E-1
7	G32	-1.37E-1	G32	-1.36E-1	G38	2.46E-1	G57	3.60E-1	G58	2.34E-1
8	G34	1.28E-1	G117	-1.09E-1	G36	2.02E-1	G1	-3.20E-1	G3	2.34E-1
9	G117	-1.22E-1	G34	1.06E-1	G34	1.63E-1	G3	2.88E-1	G1	-2.28E-1
10	G28	8.71E-2	G118	-9.78E-2	G1	-1.61E-1	G26	-2.77E-1	G45	2.09E-1
11	G36	-6.94E-2	G37	-8.74E-2	G3	1.41E-1	G117	-2.48E-1	G69	1.72E-1
12	G38	5.26E-2	G39	-6.87E-2	G117	-1.38E-1	G47	-2.45E-1	G39	-1.65E-1
13	G37	-1.95E-2	G26	-6.81E-2	G74	1.12E-1	G69	2.26E-1	G47	-1.57E-1
14	G1	-1.50E-2	G47	-5.06E-2	G47	-1.06E-1	G46	2.24E-1	G46	1.42E-1
15	G35	-1.26E-2	G36	4.16E-2	G46	9.31E-2	G45	2.10E-1	G9	1.23E-1
16	G26	-1.25E-2	G28	-4.06E-2	G61	9.13E-2	G58	1.79E-1	G61	1.21E-1
17	G3	1.03E-2	G46	3.73E-2	G43	-8.30E-2	G74	1.72E-1	G11	1.21E-1

Table 9. 1-hr average sensitivities of gas-phase species and photochemical indicators with respect to temperature (Temp.) and relative humidity (R.H.) under various clear air conditions.

Species or indicators	Model parameters	Atmospheric conditions				
		Remote	Marine	Rural	Urban	Heavily-polluted
NO ₂	Temp.	2.37E+0	-1.81E+0	-4.94E+0	-2.65E+0	9.79E-1
	R.H.	-3.96E-2	-2.10E-1	-3.22E-1	-1.34E-1	-7.40E-2
SO ₂	Temp.	-1.47E-1	-3.33E-1	-7.44E-1	-1.50E-1	-4.97E-2
	R.H.	-9.02E-3	-1.54E-2	-3.13E-2	-3.73E-3	-8.01E-3
HNO ₃	Temp.	6.62E+0	6.35E+0	1.42E+1	9.66E+0	6.30E+0
	R.H.	3.08E-1	2.02E-1	5.80E-1	2.19E-1	1.36E-1
H ₂ SO ₄	Temp.	5.18E+0	6.21E+0	1.67E+1	1.03E+1	7.06E+0
	R.H.	2.99E-1	2.62E-1	7.01E-1	2.54E-1	1.13E-1
OH	Temp.	5.48E+0	5.79E+0	1.60E+1	1.02E+1	7.47E+0
	R.H.	2.87E-1	2.18E-1	6.69E-1	2.62E-1	1.27E-1
HO ₂	Temp.	7.79E+0	1.37E+1	2.86E+1	1.92E+1	1.15E+1
	R.H.	1.20E-1	3.37E-1	1.00E+0	3.95E-1	1.20E-1
PAN	Temp.	--	5.71E+0	1.33E+1	8.23E+0	4.51E+0
	R.H.	--	3.75E-1	6.91E-1	2.76E-1	1.18E-1
O ₃	Temp.	3.48E-2	7.29E-1	1.26E+0	2.29E+0	1.12E+0
	R.H.	-2.80E-3	1.43E-2	4.49E-2	4.96E-2	2.52E-2
NO _y	Temp.	--	--	1.41E-1	3.02E-1	9.93E-2
	R.H.	--	--	-8.60E-3	-3.45E-3	-3.66E-3
O ₃ /NO _z	Temp.	--	--	-1.28E+1	-6.93E+0	-4.75E+0
	R. H.	--	--	-5.67E-1	-2.10E-1	-1.02E-1
H ₂ O ₂ /HNO ₃	Temp.	--	--	-1.43E+1	-9.22E+0	-6.36E+0
	R.H.	--	--	-5.76E-1	-1.99E-1	-1.37E-1

Table 10. 1-hr average sensitivities of O₃ with respect to aqueous-phase reaction rate constants under various cloudy conditions.

Rank	Remote		Marine		Rural		Urban		Heavily-polluted	
	Rxn. #	\bar{S}_{kl}	Rxn. #	\bar{S}_{kl}	Rxn. #	\bar{S}_{kl}	Rxn. #	\bar{S}_{kl}	Rxn. #	\bar{S}_{kl}
1	L13	-3.14E-3	L7	-7.76E-3	L7	-7.08E-3	L7	-1.22E-2	L109	6.13E-3
2	L7	-5.96E-4	L13	-4.96E-3	L13	-2.46E-3	L13	-2.52E-3	L75	-1.31E-3
3	L74	-3.86E-5	L75	6.78E-4	L74	-7.21E-4	L105	-1.93E-3	L105	-6.65E-4
4	L50	-3.70E-5	L74	-2.19E-4	L75	6.45E-4	L6	-8.36E-4	L112	-6.62E-4
5	L75	3.29E-5	L6	-1.82E-4	L82	-4.52E-4	L112	-7.60E-4	L7	-4.71E-4
6	L16	-2.13E-5	L105	-1.02E-4	L6	-3.29E-4	L109	7.35E-4	L13	-3.24E-4
7	L6	-1.92E-5	L50	-8.52E-5	L105	-3.03E-4	L82	-4.93E-4	L74	-2.60E-4
8	L105	1.65E-5	L1	5.20E-5	L79	-1.92E-4	L50	4.84E-4	L50	1.30E-4
9	L64	-1.17E-5	L112	-4.64E-5	L85	1.55E-4	L74	-4.38E-4	L44	1.16E-4
10	L49	-9.16E-6	L57	3.83E-5	L57	9.48E-5	L114	-3.36E-4	L32	1.16E-4
11	L5	-8.91E-6	L19	-3.37E-5	L80	9.01E-5	L85	1.90E-4	L99	8.78E-5
12	L1	6.89E-6	L18	-3.31E-5	L3	-8.88E-5	L79	-1.73E-4	L114	-8.24E-5
13	L73	-6.85E-6	L20	3.27E-5	L50	8.48E-5	L99	1.60E-4	L82	-8.10E-5
14	L3	-5.21E-6	L49	-2.49E-5	L81	8.19E-5	L18	-1.55E-4	L73	-6.78E-5
15	L57	-4.38E-6	L114	-2.28E-5	L77	6.93E-5	L46	-9.43E-5	L6	-5.58E-5
16	L82	2.16E-6	L16	-1.88E-5	L91	6.36E-5	L91	-8.47E-5	L91	-4.63E-5
17	L77	1.81E-6	L64	-1.61E-5	L18	-5.40E-5	L93	-7.91E-5	L85	4.13E-5
18	L4	-1.61E-6	L77	1.53E-5	L19	-4.74E-5	L19	-7.11E-5	L93	-4.02E-5
19	L23	-1.52E-6	L82	-1.36E-5	L109	4.43E-5	L59	7.08E-5	L31	3.95E-5
20	L21	-1.51E-6	L25	-1.25E-5	L20	4.40E-5	L77	7.04E-5	L46	-3.79E-5
21	L18	-1.38E-6	L5	1.25E-5	L96	-3.58E-5	L106	-6.82E-5	L59	2.79E-5
22	L22	1.35E-6	L73	-1.17E-5	L73	-3.26E-5	L80	6.29E-5	L79	-2.38E-5
23	L19	-1.34E-6	L3	-1.14E-5	L106	3.19E-5	L20	6.09E-5	L18	-1.78E-5
24	L20	1.32E-6	L54	1.11E-5	L25	-3.10E-5	L73	-5.66E-5	L43	-1.45E-5
25	L85	-1.19E-6	L79	-1.07E-5	L24	2.86E-5	L57	2.89E-5	L97	-1.31E-5

Table 11. 1-hr average sensitivities of aqueous-phase S(IV) and S(VI) with respect to aqueous-phase reaction rate constants under various cloudy conditions.

(a) S(IV)

Rank	Remote		Marine		Rural		Urban		Heavily-polluted	
	Rxn. #	\bar{S}_{kl}	Rxn. #	\bar{S}_{kl}	Rxn. #	\bar{S}_{kl}	Rxn. #	\bar{S}_{kl}	Rxn. #	\bar{S}_{kl}
1	L75	-3.52E+0	L75	-4.52E+0	L75	2.95E-1	L105	-1.66E-1	L105	-2.84E-2
2	L105	-2.69E-1	L105	-4.23E-1	L105	-2.14E-1	L75	6.17E-2	L112	-1.58E-2
3	L7	1.32E-1	L7	1.52E-1	L82	6.17E-2	L77	-2.27E-2	L109	-1.44E-2
4	L5	5.65E-2	L77	-9.33E-2	L77	-5.53E-2	L50	2.26E-2	L77	-1.23E-2
5	L77	-5.50E-2	L112	-6.09E-2	L91	-5.27E-2	L82	2.07E-2	L50	1.02E-2
6	L79	-4.14E-2	L74	-4.08E-2	L80	-5.23E-2	L112	-1.91E-2	L75	6.56E-3
7	L103	-2.15E-2	L79	-3.51E-2	L81	-3.95E-2	L79	-1.82E-2	L91	-6.32E-3
8	L50	-1.88E-2	L106	-3.03E-2	L79	-3.89E-2	L80	-1.43E-2	L80	-5.75E-3
9	L13	1.70E-2	L114	-2.10E-2	L74	-3.51E-2	L7	1.38E-2	L82	4.91E-3
10	L106	-8.54E-3	L50	1.99E-2	L7	3.26E-2	L91	-1.08E-2	L108	-3.39E-3

(b) S(VI)

Rank	Remote		Marine		Rural		Urban		Heavily-polluted	
	Rxn. #	\bar{S}_{kl}	Rxn. #	\bar{S}_{kl}	Rxn. #	\bar{S}_{kl}	Rxn. #	\bar{S}_{kl}	Rxn. #	\bar{S}_{kl}
1	L75	8.60E-2	L75	7.22E-2	L75	-1.14E-1	L105	2.47E-1	L105	1.40E-1
2	L105	6.41E-2	L105	6.56E-2	L105	8.49E-2	L75	-7.79E-2	L109	7.18E-2
3	L7	-3.45E-3	L7	-3.93E-3	L82	-2.47E-2	L50	-3.86E-2	L77	6.02E-2
4	L77	1.31E-3	L112	-3.27E-3	L77	2.20E-2	L77	3.34E-2	L50	-4.44E-2
5	L5	-1.26E-3	L114	2.30E-3	L91	2.11E-2	L82	-3.13E-2	L91	3.08E-2
6	L79	9.91E-4	L50	-2.26E-3	L80	2.09E-2	L79	2.71E-2	L80	2.84E-2
7	L103	3.85E-4	L77	1.40E-3	L81	1.58E-2	L80	2.15E-2	L82	-2.46E-2
8	L50	3.22E-4	L13	1.09E-3	L79	1.55E-2	L7	-2.15E-2	L114	1.81E-2
9	L13	-2.81E-4	L74	6.06E-4	L74	1.40E-2	L91	1.61E-2	L108	1.66E-2
10	L106	2.07E-4	L106	4.92E-4	L7	-1.30E-2	L74	1.28E-2	L75	1.62E-2

Table 12. 1-hr average sensitivities of O₃ with respect to equilibrium constants under various cloudy conditions. Only those sensitivities greater than 1.0E-4 are shown.

(a) Dissolution equilibrium constant (i.e., Henry's Law constant)

Rank	Remote		Marine		Rural		Urban		Heavily-polluted	
	Rxn. #	\bar{S}_{kl}	Rxn. #	\bar{S}_{kl}	Rxn. #	\bar{S}_{kl}	Rxn. #	\bar{S}_{kl}	Rxn. #	\bar{S}_{kl}
1	E10	-4.38E-3	E10	-2.11E-2	E10	-1.83E-2	E10	-3.16E-2	E12	-3.01E-2
2	E17	-3.23E-3	E17	-5.28E-3	E17	-3.39E-3	E12	-1.53E-2	E13	6.61E-3
3	E11	-1.20E-4	E12	-1.51E-3	E3	-9.77E-4	E17	-3.13E-3	E3	4.25E-3
4	E18	-1.02E-4	E11	-3.36E-4	E12	-5.31E-4	E3	-2.37E-3	E10	-2.24E-3
5			E3	-2.03E-4	E18	-1.96E-4	E13	7.57E-4	E17	-6.86E-4
6			E18	-1.35E-4			E5	2.43E-4	E5	1.10E-4
7							E7	-1.43E-4		

(b) Dissociation equilibrium constant

Rank	Remote		Marine		Rural		Urban		Heavily-polluted	
	Rxn. #	\bar{S}_{kl}	Rxn. #	\bar{S}_{kl}	Rxn. #	\bar{S}_{kl}	Rxn. #	\bar{S}_{kl}	Rxn. #	\bar{S}_{kl}
1	D2	-3.75E-3	D2	-1.28E-2	D2	-1.01E-2	D2	-1.55E-2	D10	4.26E-3
2			D11	-2.64E-4	D10	-9.73E-4	D10	-2.34E-3	D11	-9.25E-4
3			D10	-2.03E-4	D11	-6.63E-4	D11	-1.18E-3	D2	-9.10E-4
4							D9	7.62E-4	D9	6.65E-4
5							D4	-3.58E-4	D16	1.21E-4
6							D16	2.62E-4		

Table 13. 1-hr average sensitivities of species and photochemical indicators with respect to temperature (Temp.), relative humidity (R.H.), cloud droplet radius (Rdrop.) and cloud liquid water (V_c) under various cloudy conditions. TSO_4^{2-} and TNO_3^- are the total sulfate and nitrate in all phases, respectively.

Species	Model parameters	Atmospheric conditions				
		Remote	Marine	Rural	Urban	Heavily-polluted
NO ₂	Temp.	2.52E+0	-6.76E-1	-2.86E+0	-2.54E+0	6.51E-1
	R.H.	-2.33E-2	-1.04E-1	-1.79E-1	-9.29E-2	-5.81E-3
	Rdrop.	4.52E-3	-7.56E-2	-4.69E-2	-2.70E-2	2.08E-3
	V_c	-9.55E-3	7.32E-2	6.14E-2	5.82E-2	-1.27E-3
SO ₂	Temp.	4.09E+1	5.08E+1	5.05E+0	3.89E+0	1.93E+0
	R.H.	-4.81E-1	-5.41E-1	-3.25E-1	-6.67E-2	-1.61E-3
	Rdrop.	1.71E-2	1.46E-1	-7.37E-2	9.00E-2	-7.94E-3
	V_c	-6.98E-1	-1.05E+0	-3.88E-1	-2.45E-1	-7.28E-2
HNO ₃	Temp.	1.81E+1	1.38E+1	1.56E+1	1.10E+1	8.28E+0
	R.H.	7.30E-1	4.06E-1	5.04E-1	1.84E-1	1.28E-1
	Rdrop.	2.23E+0	2.21E+0	2.08E+0	1.98E+0	1.91E+0
	V_c	-1.30E+0	-1.33E+0	-1.23E+0	-1.15E+0	-1.07E+0
H ₂ SO ₄	Temp.	1.56E+1	8.11E+0	2.00E+1	1.16E+1	4.68E+0
	R.H.	9.87E-2	1.29E-1	2.96E-1	1.59E-1	5.35E-2
	Rdrop.	4.31E-1	1.05E+0	1.29E+0	1.04E+0	6.02E-1
	V_c	-1.16E+0	-1.29E+0	-1.43E+0	-1.11E+0	-8.45E-1
OH	Temp.	1.82E+1	1.70E+1	2.09E+1	1.35E+1	9.32E+0
	R.H.	7.55E-1	5.10E-1	6.84E-1	2.63E-1	1.31E-1
	Rdrop.	3.17E-1	3.76E-1	2.17E-1	8.93E-2	-5.62E-4
	V_c	-2.49E+0	-4.01E-1	-2.94E-1	-1.91E-1	-6.65E-2
HO ₂	Temp.	2.71E+1	2.41E+1	3.00E+1	2.28E+1	1.43E+1
	R.H.	5.06E-1	4.29E-1	7.16E-1	3.27E-1	1.23E-1
	Rdrop.	4.37E-1	4.73E-1	2.37E-1	1.36E-1	-2.92E-3
	L.W.	-6.33E-1	-6.07E-1	-4.24E-1	-3.18E-1	-1.06E-1
PAN	Temp.	--	2.34E+1	1.63E+1	1.15E+1	5.97E+0
	R.H.	--	8.89E-1	6.91E-1	2.89E-1	1.24E-1
	Rdrop.	--	7.46E-1	1.97E-1	9.37E-2	2.00E-3
	V_c	--	-7.41E-1	-2.58E-1	-1.95E-1	-6.30E-2
O ₃	Temp.	7.21E-2	6.63E-1	8.95E-1	2.56E+0	1.39E+0
	R.H.	-2.12E-3	1.03E-2	2.22E-2	4.18E-2	2.59E-2
	Rdrop.	3.86E-3	2.16E-2	9.03E-3	1.94E-2	-1.26E-3
	V_c	-6.04E-3	-2.69E-2	-1.69E-2	-4.35E-2	-2.67E-2
TSO ₄ ²⁻	Temp.	-9.38E-1	-5.33E-1	-2.04E+0	-5.20E+0	-7.73E+0
	R.H.	1.29E-2	1.06E-2	1.28E-1	9.82E-2	1.15E-2
	Rdrop.	3.86E-4	-3.51E-3	2.95E-2	-1.49E-1	5.95E-3
	V_c	-9.84E-1	-9.91E-1	-8.47E-1	-6.53E-1	-6.87E-1
TNO ₃ ⁻	Temp.	1.85E+1	1.59E+1	1.88E+1	1.29E+1	9.41E+0
	R.H.	6.91E-1	4.57E-1	6.18E-1	1.99E-1	8.70E-2
	Rdrop.	2.13E-1	3.57E-1	1.59E-1	4.82E-2	-2.61E-2
	V_c	-1.22E+0	-1.37E+0	-1.22E+0	-1.12E+0	-1.03E+0
NO _y	Temp.	--	--	-3.10E+0	-1.04E+0	-6.22E-1
	R.H.	--	--	-1.07E-1	-2.10E-2	-6.68E-3
	Rdrop.	--	--	-2.78E-2	-5.47E-1	1.91E-3
	V_c	--	--	3.96E-2	1.42E-2	2.58E-3
O ₃ /NO _z	Temp.	--	--	-1.60E+1	-9.74E+0	-5.38E+0
	R.H.	--	--	-6.36E-1	-2.46E-1	-9.81E-2
	Rdrop.	--	--	-1.83E-1	-7.54E-2	-5.38E-2
	V_c	--	--	2.31E-1	1.51E-1	3.81E-2
H ₂ O ₂ /HNO ₃	Temp.	--	--	3.86E+1	3.40E+1	1.85E+1
	R.H.	--	--	6.96E-1	4.54E-1	1.70E-1
	Rdrop.	--	--	-2.09E+0	-2.41E+0	-1.91E+0
	V_c	--	--	7.89E-1	7.95E-1	8.15E-1

Table 15. 1-hr average sensitivities of O₃ and indicators to uptake coefficients of individual species under various aerosol conditions. Only those sensitivities greater than 1.0E-4 are shown.

(a) O₃

Rank	Remote		Marine		Rural		Urban		Heavily-polluted	
	Species	\bar{S}_{kl}	Species	\bar{S}_{kl}	Species	\bar{S}_{kl}	Species	\bar{S}_{kl}	Species	\bar{S}_{kl}
1	O ₃	-6.55E-4	O ₃	-1.31E-3	O ₃	-6.30E-3	O ₃	-4.67E-2	O ₃	-1.04E-1
2			H ₂ O ₂	-2.76E-4	HO ₂	-2.13E-3	HCHO	-2.49E-2	HCHO	-6.34E-2
3			HO ₂	-2.54E-4	H ₂ O ₂	-1.74E-3	HO ₂	-1.28E-2	NO ₂	-8.06E-3
4					HCHO	-3.59E-4	H ₂ O ₂	-1.43E-3	NO	7.51E-3
5							CH ₃ O ₂	-3.56E-4	HO ₂	-3.47E-3
6							NO	3.46E-4	N ₂ O ₅	-2.15E-3
7							NO ₂	-2.98E-4	HNO ₂	-1.28E-3
8							N ₂ O ₅	-2.96E-4	H ₂ O ₂	-2.79E-4
9							HNO ₂	-2.23E-4	SO ₂	1.98E-4
10							SO ₂	2.08E-4		

(b) NO_y

Rank	Rural		Urban		Heavily-polluted	
	Species	\bar{S}_{kl}	Species	\bar{S}_{kl}	Species	\bar{S}_{kl}
1	HNO ₃	-1.31E-2	HNO ₃	-2.19E-2	NO ₂	-3.55E-2
2	NO ₂	-1.13E-3	NO ₂	-1.11E-2	HNO ₃	-9.09E-3
3	HO ₂	7.86E-4	HCHO	4.59E-3	NO	-8.92E-3
4	H ₂ O ₂	6.99E-4	N ₂ O ₅	-3.18E-3	HCHO	7.21E-3
5	N ₂ O ₅	-6.19E-4	PAN	-3.06E-3	O ₃	2.89E-3
6	NO	-4.08E-4	NO	-2.83E-3	N ₂ O ₅	-2.78E-3
7	PAN	-1.91E-4	HO ₂	2.45E-3	PAN	-1.27E-3
8	HNO ₂	-1.69E-4	O ₃	1.17E-3	HO ₂	4.29E-4
9	HCHO	1.50E-4	HNO ₂	-3.18E-4	HNO ₂	-2.23E-4
10			H ₂ O ₂	2.92E-4		

(c) O₃/NO_z

Rank	Rural		Urban		Heavily-polluted	
	Species	\bar{S}_{kl}	Species	\bar{S}_{kl}	Species	\bar{S}_{kl}
1	HNO ₃	3.72E-2	HNO ₃	8.18E-2	HNO ₃	2.22E-1
2	HO ₂	1.96E-2	HCHO	7.71E-2	HCHO	1.76E-1
3	H ₂ O ₂	1.75E-2	HO ₂	4.53E-2	O ₃	-8.08E-2
4	O ₃	-4.34E-3	O ₃	-3.73E-2	PAN	2.96E-2
5	HCHO	2.02E-3	PAN	1.11E-2	NO ₂	-1.03E-2
6	SO ₂	-5.90E-4	H ₂ O ₂	6.10E-3	HO ₂	1.01E-2
7	N ₂ O ₅	5.40E-4	HNO ₂	1.22E-3	HNO ₂	6.96E-3
8	HNO ₂	3.86E-4	CH ₃ O ₂	1.03E-3	NO	4.73E-3
9	CH ₃ O ₂	2.71E-4	SO ₂	-9.12E-4	H ₂ O ₂	9.61E-4
10	N ₂ O ₅	2.38E-4	N ₂ O ₅	8.94E-4	SO ₂	-9.29E-4
11	NO ₂	1.75E-4	NO	3.25E-4	N ₂ O ₅	-2.60E-4
12	OH	1.31E-4			CH ₃ O ₂	2.01E-4

(d) H₂O₂/HNO₃

Rank	Rural		Urban		Heavily-polluted	
	Species	\bar{S}_{kl}	Species	\bar{S}_{kl}	Species	\bar{S}_{kl}
1	H ₂ O ₂	-5.48E-1	H ₂ O ₂	-3.46E+0	H ₂ O ₂	-2.99E+0
2	HNO ₃	6.49E-2	HNO ₃	4.63E-1	HNO ₃	9.01E-1
3	HO ₂	2.02E-2	HCHO	-6.19E-2	HCHO	-3.44E-1
4	HCHO	2.06E-3	HO ₂	-1.64E-2	O ₃	-1.13E-1
5	O ₃	1.99E-3	NO ₂	1.59E-2	NO ₂	8.37E-2
6	SO ₂	-6.10E-4	O ₃	-9.60E-3	NO	3.09E-2
7	NO ₂	5.40E-4	N ₂ O ₅	8.05E-3	HO ₂	-1.75E-2
8	N ₂ O ₅	4.91E-4	NO	4.21E-3	N ₂ O ₅	1.07E-2
9	HNO ₂	4.39E-4	HNO ₂	5.31E-4	HNO ₂	-3.93E-3
10	CH ₃ O ₂	2.86E-4	CH ₃ O ₂	-3.90E-4	SO ₂	-7.52E-4
11	NO	1.93E-4	SO ₂	-2.80E-4	PAN	-4.97E-4
12					CH ₃ O ₂	-4.06E-4

Appendix A-1. Gas-phase reactions in MaTChM, taken from Zaveri (1997) and references therein.

No.	Reaction	Rate constant, $\text{cm}^3 \text{ molecule}^{-1} \text{ s}^{-1}$
<u>Inorganic Reactions</u>		
G1.	$\text{NO}_2 + h\nu \rightarrow \text{NO} + \text{O}(^3\text{P})$	Radiation Dependent
G2.	$\text{O}(^3\text{P}) \xrightarrow{o^2, M} \text{O}_3$	$1.4\text{E}+03 \exp(1175/\text{T})$
G3.	$\text{O}_3 + \text{NO} \rightarrow \text{NO}_2$	$1.8\text{E}-12 \exp(-1370/\text{T})$
G4.	$\text{O}(^3\text{P}) + \text{NO}_2 \rightarrow \text{NO}$	$9.3\text{E}-12$
G5.	$\text{O}(^3\text{P}) + \text{NO}_2 \xrightarrow{M} \text{NO}_3$	$1.6\text{E}-13 \exp(687/\text{T})$
G6.	$\text{O}(^3\text{P}) + \text{NO} \xrightarrow{M} \text{NO}_2$	$2.2\text{E}-13 \exp(602/\text{T})$
G7.	$\text{O}_3 + \text{NO}_2 \rightarrow \text{NO}_3$	$1.2\text{E}-13 \exp(-2450/\text{T})$
G8.	$\text{O}_3 + h\nu \rightarrow \text{O}(^3\text{P})$	Radiation Dependent
G9.	$\text{O}_3 + h\nu \rightarrow \text{O}(^1\text{D})$	Radiation Dependent
G10.	$\text{O}(^1\text{D}) \xrightarrow{M} \text{O}(^3\text{P})$	$1.19\text{E}+08 \exp(390/\text{T})$
G11.	$\text{O}(^1\text{D}) + \text{H}_2\text{O} \rightarrow 2\text{OH}$	$2.2\text{E}-10$
G12.	$\text{O}_3 + \text{OH} \rightarrow \text{HO}_2$	$1.6\text{E}-12 \exp(-940/\text{T})$
G13.	$\text{O}_3 + \text{HO}_2 \rightarrow \text{OH}$	$1.4\text{E}-14 \exp(-580/\text{T})$
G14.	$\text{NO}_3 + h\nu \rightarrow .89\text{NO}_2 + .89\text{O} + .11\text{NO}$	Radiation Dependent
G15.	$\text{NO}_3 + \text{NO} \rightarrow 2\text{NO}_2$	$1.3\text{E}-11 \exp(250/\text{T})$
G16.	$\text{NO}_3 + \text{NO}_2 \rightarrow \text{NO} + \text{NO}_2$	$2.5\text{E}-14 \exp(-1230/\text{T})$
G17.	$\text{NO}_3 + \text{NO}_2 \xrightarrow{M} \text{N}_2\text{O}_5$	$5.3\text{E}-13 \exp(256/\text{T})$
G18.	$\text{N}_2\text{O}_5 + \text{H}_2\text{O} \rightarrow 2\text{HNO}_3$	$1.3\text{E}-21$
G19.	$\text{N}_2\text{O}_5 \xrightarrow{M} \text{NO}_3 + \text{NO}_2$	$3.5\text{E}+14 \exp(-10897/\text{T})$
G20.	$\text{NO} + \text{NO} \xrightarrow{o^2} 2\text{NO}_2$	$1.8\text{E}-20 \exp(530/\text{T})$
G21.	$\text{NO} + \text{NO}_2 + \text{H}_2\text{O} \rightarrow 2\text{HONO}$	$4.4\text{E}-40$
G22.	$\text{OH} + \text{NO} \xrightarrow{M} \text{HONO}$	$4.5\text{E}-13 \exp(806/\text{T})$
G23.	$\text{HONO} + h\nu \rightarrow \text{OH} + \text{NO}$	Radiation Dependent
G24.	$\text{OH} + \text{HONO} \rightarrow \text{NO}_2$	$6.6\text{E}-12$
G25.	$\text{HONO} + \text{HONO} \rightarrow \text{NO} + \text{NO}_2$	$1.0\text{E}-20$
G26.	$\text{OH} + \text{NO}_2 \xrightarrow{M} \text{HNO}_3$	$1.0\text{E}-12 \exp(713/\text{T})$
G27.	$\text{OH} + \text{HNO}_3 \xrightarrow{M} \text{NO}_3$	$5.1\text{E}-15 \exp(1000/\text{T})$
G28.	$\text{HO}_2 + \text{NO} \rightarrow \text{OH} + \text{NO}_2$	$3.7\text{E}-12 \exp(240/\text{T})$
G29.	$\text{HO}_2 + \text{NO}_2 \xrightarrow{M} \text{PNA}$	$1.2\text{E}-13 \exp(749/\text{T})$
G30.	$\text{PNA} \xrightarrow{M} \text{HO}_2 + \text{NO}_2$	$4.8\text{E}+13 \exp(-10121/\text{T})$
G31.	$\text{OH} + \text{PNA} \rightarrow \text{NO}_2$	$1.3\text{E}-12 \exp(380/\text{T})$
G32.	$\text{HO}_2 + \text{HO}_2 \rightarrow \text{H}_2\text{O}_2$	$5.9\text{E}-14 \exp(1150/\text{T})$
G33.	$\text{HO}_2 + \text{HO}_2 + \text{H}_2\text{O} \rightarrow \text{H}_2\text{O}_2$	$2.2\text{E}-38 \exp(5800/\text{T})$
G34.	$\text{H}_2\text{O}_2 + h\nu \rightarrow 2\text{OH}$	Radiation Dependent
G35.	$\text{OH} + \text{H}_2\text{O}_2 \rightarrow \text{HO}_2$	$3.1\text{E}-12 \exp(-187/\text{T})$
G36.	$\text{CO} + \text{OH} \xrightarrow{o^2} \text{HO}_2$	$2.2\text{E}-13$
<u>Formaldehyde Reactions</u>		
G37.	$\text{FORM} + \text{OH} \xrightarrow{o^2} \text{HO}_2 + \text{CO}$	$1.0\text{E}-11$
G38.	$\text{FORM} + h\nu \xrightarrow{2 o^2} 2\text{HO}_2 + \text{CO}$	Radiation Dependent
G39.	$\text{FORM} + h\nu \rightarrow \text{CO}$	Radiation Dependent
G40.	$\text{FORM} + \text{O}(^3\text{P}) \rightarrow \text{OH} + \text{HO}_2 + \text{CO}$	$3.0\text{E}-11 \exp(-1550/\text{T})$
G41.	$\text{FORM} + \text{NO}_3 \xrightarrow{o^2} \text{HNO}_3 + \text{HO}_2 + \text{CO}$	$6.3\text{E}-16$

Read $1.4\text{E}+03 \exp(1175/\text{T})$ as $1.4 \times 10^3 \text{ e}^{1175/\text{T}}$.

Appendix A-1. continued.

No.	Reaction	Rate constant, cm ³ molecule ⁻¹ s ⁻¹
<u>Higher Molecular Weight Aldehyde Reactions</u>		
G42.	ALD2 + O(³ P) $\xrightarrow{o^2}$ C2O3 + OH	1.2E-11 exp(-986/T)
G43.	ALD2 + OH → C2O3	7.0E-12 exp(250/T)
G44.	ALD2 + NO ₃ $\xrightarrow{o^2}$ C2O3 + HNO ₃	2.5E-15
G45.	ALD2 + <i>hν</i> $\xrightarrow{2 o^2}$ CH ₃ O ₂ + HO ₂ + CO	Radiation dependent
G46.	C2O3 + NO $\xrightarrow{o^2}$ CH ₃ O ₂ + NO ₂	5.4E-12 exp(250/T)
G47.	C2O3 + NO ₂ → PAN	8.0E-20 exp(5500/T)
G48.	PAN → C2O3 + NO ₂	9.4E+16 exp(-14000/T)
G49.	C2O3 + C2O3 → 2CH ₃ O ₂ + O ₂	2.0E-12
G50.	C2O3 + HO ₂ → .79CH ₃ O ₂ + .79OH	6.5E-12
<u>Alkane Reactions</u>		
G51.	C2H6 + OH → ETHP	T ² 1.37E-17 exp(-444/T)
G52.	PAR + OH → .87XO2 + .13XO2N + .11HO ₂ + .11ALD2 + .76ROR - .11PAR	8.1E-13
G53.	ROR → 1.1ALD2 + .96XO2 + .94HO ₂ + .04XO2N + .02ROR - 2.1PAR	1.0E+15 exp(-8000/T)
G54.	ROR → HO ₂	1.6E+3
G55.	ROR + NO ₂ → NITRATES	1.5E-11
<u>Alkene Reactions</u>		
G56.	OLE + O(³ P) → .63ALD2 + .38HO ₂ + .28XO2 + .3CO + .2HCHO + .02XO2N + .22PAR + .2OH	1.2E-11 exp(-324/T)
G57.	OLE + OH → CH ₃ O ₂ + ALD2 - PAR	5.2E-12 exp(504/T)
G58.	OLE + O ₃ → .5ALD2 + .524HCHO + .33CO + .228HO ₂ + .1OH + .216CH ₃ O ₂ - PAR	1.4E-14 exp(-2105/T)
G59.	OLE + NO ₃ → 91XO2 + HCHO + ALD2 + .09XO2N + NO ₂ - PAR	7.7E-15
G60.	ETH + O(³ P) → .3HCHO + .7CH ₃ O ₂ + CO + HO ₂ + .3OH	1.0E-11 exp(-792/T)
G61.	ETH + OH → XO2 + 1.56HCHO + HO ₂ + .22ALD2	2.0E-12 exp(411/T)
G62.	ETH + O ₃ → HCHO + .42CO + .12HO ₂	1.3E-14 exp(-2633/T)
<u>Aromatic Reactions</u>		
G63.	TOL + OH → .08XO2 + .36CRES + .44HO ₂ + .56TO2	2.1E-12 exp(322/T)
G64.	TO2 + NO → .9NO2 + .9OPEN + .9HO ₂	8.1E-12
G65.	TO2 → CRES	4.2
G66.	CRES + OH → .4CRO + .6XO2 + .6HO ₂ + .3OPEN	4.1E-11
G67.	CRES + NO ₃ → CRO + HNO ₃	2.2E-11
G68.	CRO + NO ₂ → NITRATES	1.4E-11
G69.	XYL + OH → .7OH + .5XO2 + .2CRES + .8MGLY + 1.1PAR + .3TO2	1.7E-11 exp(116/T)
G70.	OPEN + OH → XO2 + C2O3 + 2HO ₂ + 2CO + HCHO	3.0E-11
G71.	OPEN + <i>hν</i> → C2O3 + CO + HO ₂	Radiation dependent
G72.	OPEN + O ₃ → .03ALD2 + .62C2O3 + .7HCHO + .03XO2 + .69CO + .08OH + .76HO ₂ + .2MGLY	5.4E-17 exp(-500/T)
G73.	MGLY + OH → XO2 + C2O3	1.7E-11
G74.	MGLY + <i>hν</i> → C2O3 + CO + HO ₂	Radiation dependent
<u>Isoprene Reactions</u>		
G75.	ISOP + O(³ P) → .6HO ₂ + .8ALD2 + .55OLE + .5XO2 + .5CO + .45ETH + .9PAR	1.8E-11
G76.	ISOP + OH → HCHO + XO2 + .67HO ₂ + .4MGLY + .2C2O3 + ETH + .2ALD2 + .13XO2N	9.6E-11
G77.	ISOP + O ₃ → HCHO + .4ALD2 + .55ETH + .2MGLY + .06CO + .1PAR + .44HO ₂ + .1OH	1.2E-17
G78.	ISOP + NO ₃ → XO2N + NITRATES	3.2E-13
<u>Operator Reactions</u>		
G79.	XO2 + NO → NO ₂	8.1E-12
G80.	XO2 + XO2 → Products	1.7E-14 exp(1300/T)
G81.	XO2N + NO → NITRATES	6.8E-13

Appendix A-1. Continued.

No.	Reaction	Rate constant, cm ³ molecule ⁻¹ s ⁻¹
<u>Condensed DMS Chemistry</u>		
G82.	DMS + OH → CH ₃ SCH ₂ OO + H ₂ O	9.64E-12 exp(-234/T)
G83.	DMS + NO ₃ → CH ₃ SCH ₂ OO + HNO ₃	1.40E-13 exp(500/T)
G84.	DMS + O(³ P) → CH ₃ SO ₂ + CH ₃ O ₂	.26E-11 exp(409/T)
G85.	DMS + OH → aCH ₃ SO ₂ + aCH ₃ O ₂ + (1-a)DMSO + (1-a)HO ₂	1.7E-12 (see note)
G86.	CH ₃ SCH ₂ OO + NO → CH ₃ SO ₂ + HCHO + NO ₂	8.0E-12
G87.	CH ₃ SCH ₂ OO + CH ₃ O ₂ → CH ₃ SO ₂ + CH ₃ O + HCHO	1.8E-13
G88.	CH ₃ SCH ₂ OO + HO ₂ → CH ₃ SCH ₂ OOH	1.5E-12
G89.	DMSO+OH→bCH ₃ SO ₂ H+bCH ₃ O ₂ +(1-b)DMSO ₂ + (1-b)HO ₂	5.8E-11 (see note)
G90.	DMSO ₂ + OH → CH ₃ S(O) ₂ CH ₂ OO + H ₂ O	1.0E-14
G91.	CH ₃ S(O) ₂ CH ₂ OO + NO → CH ₃ SO ₂ + HCHO + NO ₂	5.0E-12
G92.	CH ₃ S(O) ₂ CH ₂ OO + CH ₃ O ₂ → CH ₃ SO ₂ + HCHO + CH ₃ O	1.8E-13
G93.	CH ₃ S(O) ₂ CH ₂ OO+HO ₂ →CH ₃ S(O) ₂ CH ₂ OOH+O ₂	1.5E-12
G94.	CH ₃ SO ₂ H + HO ₂ → CH ₃ SO ₂ + H ₂ O ₂	1.0E-15
G95.	CH ₃ SO ₂ H + NO ₃ → CH ₃ SO ₂ + HNO ₃	1.0E-13
G96.	CH ₃ SO ₂ H + CH ₃ O ₂ → CH ₃ SO ₂ + CH ₃ OOH	1.0E-15
G97.	CH ₃ SO ₂ H + OH → CH ₃ SO ₂ + H ₂ O	1.6E-11
G98.	CH ₃ SO ₂ H + CH ₃ SO ₃ → CH ₃ SO ₂ + MSA	1.0E-13
G99.	CH ₃ SO ₂ \xrightarrow{M} SO ₂ + CH ₃ O ₂	4.53E+13exp(-8656/T)
G100.	CH ₃ SO ₂ + NO ₂ → CH ₃ SO ₃ + NO	1.0E-14
G101.	CH ₃ SO ₂ + O ₃ → CH ₃ SO ₃ + O ₂	1.0E-15
G102.	CH ₃ SO ₂ + HO ₂ → CH ₃ SO ₃ + OH	2.5E-13
G103.	CH ₃ SO ₂ + CH ₃ O ₂ →CH ₃ SO ₃ +CH ₃ O+ O ₂	2.5E-13
G104.	CH ₃ SO ₂ + OH → MSA	5.0E-11
G105.	CH ₃ SO ₂ + O ₂ \xrightarrow{M} CH ₃ S(O) ₂ OO	2.6E-18
G106.	CH ₃ S(O) ₂ OO \xrightarrow{M} CH ₃ SO ₂ + O ₂	3.3
G107.	CH ₃ S(O) ₂ OO + NO → CH ₃ SO ₃ + NO ₂	1.0E-11
G108.	CH ₃ S(O) ₂ OO+CH ₃ O ₂ →CH ₃ SO ₃ +CH ₃ O+O ₂	5.5E-12
G109.	CH ₃ S(O) ₂ OO+HO ₂ →CH ₃ S(O) ₂ OOH+O ₂	2.0E-12
G110.	CH ₃ SO ₃ \xrightarrow{M} H ₂ SO ₄ + CH ₃ O ₂	1.6E-1
G111.	CH ₃ SO ₃ + NO ₂ → MSA + HNO ₃	3.0E-15
G112.	CH ₃ SO ₃ + NO → MSA + HNO ₂	3.0E-15
G113.	CH ₃ SO ₃ + HO ₂ → MSA + O ₂	5.0E-11
G114.	CH ₃ SO ₃ + HCHO $\xrightarrow{o^2}$ MSA+HO ₂ +CO	1.6E-15
G115.	SO ₂ + OH \xrightarrow{M} H ₂ SO ₄ +HO ₂	Troe expression
<u>Methane and Methylperoxyl Radical Reactions</u>		
G116.	CH ₄ + OH $\xrightarrow{o^2}$ CH ₃ O ₂	T ² 6.95E-18exp(-1280/T)
G117.	CH ₃ O ₂ + NO → HCHO + HO ₂ + NO ₂	4.2E-12 exp(180/T)
G118.	CH ₃ O ₂ + HO ₂ → CH ₃ OOH	7.7E-14 exp(1300/T)
G119.	CH ₃ O ₂ + CH ₃ O ₂ → 1.5HCHO + HO ₂	1.9E-13 exp(220/T)
G120.	CH ₃ O ₂ + C ₂ O ₃ → HCHO + .5HO ₂ + .5CH ₃ O ₂ + CH ₃ OOH	9.6E-13 exp(220/T)
G121.	CH ₃ OOH + hν → HCHO + HO ₂ + OH	5.57E-06
G122.	CH ₃ OOH+OH→.5CH ₃ O ₂ +.5HCHO+.5OH	1.0E-11
G123.	ETHP + NO → ALD2 + HO ₂ + NO ₂	4.2E-12 exp(180/T)
G124.	ETHP + HO ₂ → Products	7.7E-14 exp(1300/T)
G125.	ETHP + C ₂ O ₃ → ALD2 + .5HO ₂ + .5CH ₃ O ₂ + .5CH ₃ COOH	3.4E-13 exp(220/T)

Note: a = 5E+5/(5E+5 + [O₂] X 3E-12); b = 1.5E+7/(1.5E+7 + [O₂] X 1.2E-12)

Appendix A-2. Aqueous-phase reactions in MaTChM, taken from Zaveri (1997) and references therein.

No.	Reaction	Rate Constant, $M^{\text{a}}s^{-1}$
<u>Oxygen-Hydrogen Chemistry</u>		
L1.	$H_2O_2 + hn \rightarrow 2OH$	5.4E-7
L2.	$O_3 + hn \xrightarrow{H_2O} H_2O_2 + O_2$	1.2E-5
L3.	$OH + HO_2 \rightarrow H_2O + O_2$	$1.07E+12 \exp(-1500/T)$
L4.	$OH + O_2^- \rightarrow OH^- + O_2$	$1.53E+12 \exp(-1500/T)$
L5.	$OH + H_2O_2 \rightarrow H_2O + HO_2$	$8.12E+9 \exp(-1700/T)$
L6.	$HO_2 + HO_2 \rightarrow H_2O_2 + O_2$	$2.40E+9 \exp(-2365/T)$
L7.	$HO_2 + O_2^- \xrightarrow{H_2O} H_2O_2 + O_2 + OH^-$	$1.53E+10 \exp(-1500/T)$
L8.	$O_2^- + O_2^- \xrightarrow{2H_2O} H_2O_2 + O_2 + 2OH^-$	3.0E-1
L9.	$HO_2 + H_2O_2 \rightarrow OH + O_2 + H_2O$	5.0E-1
L10.	$O_2^- + H_2O_2 \rightarrow OH + O_2 + OH^-$	1.3E-1
L11.	$OH + O_3 \rightarrow HO_2 + O_2$	2.0E+9
L12.	$HO_2 + O_3 \rightarrow OH + 2O_2$	5.0E+3
L13.	$O_2^- + O_3 \rightarrow OH + 2O_2 + OH^-$	$2.30E+11 \exp(-1500/T)$
L14.	$OH^- + O_3 \xrightarrow{H_2O} O_2^- + HO_2$	7.0E+1
L15.	$HO_2^- + O_3 \rightarrow OH + O_2^- + O_2$	2.8E+6
L16.	$H_2O_2 + O_3 \rightarrow H_2O + 2O_2$	$7.8E-3 [O_3]^{-0.5}$
<u>Carbonate Chemistry</u>		
L17.	$HCO_3^- + OH \rightarrow H_2O + CO_3^-$	$9.11E+9 \exp(-1910/T)$
L18.	$HCO_3^- + O_2^- \rightarrow HO_2^- + CO_3^-$	1.5E+6
L19.	$CO_3^- + O_2^- \xrightarrow{H_2O} HCO_3^- + O_2 + OH^-$	$6.14E+10 \exp(-1500/T)$
L20.	$CO_3^- + H_2O_2 \rightarrow HO_2 + HCO_3^-$	$1.03E+10 \exp(-2820/T)$
<u>Chlorine Chemistry</u>		
L21.	$Cl^- + OH \rightarrow ClOH^-$	$6.6E+11 \exp(-1500/T)$
L22.	$ClOH^- \rightarrow Cl^- + OH$	6.1E+9
L23.	$ClOH^- \xrightarrow{H^+} Cl + H_2O$	$2.1E+10 [H^+]$
L24.	$Cl \xrightarrow{H_2O} ClOH^- + H^+$	1.3E+3
L25.	$HO_2 + Cl_2^- \rightarrow 2Cl^- + O_2 + H^+$	$6.91E+11 \exp(-1500/T)$
L26.	$O_2^- + Cl_2^- \rightarrow 2Cl^- + O_2$	$1.53E+11 \exp(-1500/T)$
L27.	$HO_2 + Cl \rightarrow Cl^- + O_2 + H^+$	$4.76E+11 \exp(-1500/T)$
L28.	$H_2O_2 + Cl_2^- \rightarrow 2Cl^- + HO_2 + H^+$	$1.14E+10 \exp(-3370/T)$
L29.	$H_2O_2 + Cl \rightarrow Cl^- + HO_2 + H^+$	4.5E+7
L30.	$OH^- + Cl_2^- \rightarrow 2Cl^- + OH$	$1.02E+10 \exp(-2160/T)$
<u>Nitrite and Nitrate Chemistry</u>		
L31.	$NO + NO_2 \xrightarrow{H_2O} 2NO_2^- + 2H^+$	$3.07E+10 \exp(-1500/T)$
L32.	$NO_2 + NO_2 \xrightarrow{H_2O} NO_2^- + NO_3^- + 2H^+$	$1.53E+10 \exp(-1500/T)$
L33.	$NO + OH \rightarrow NO_2^- + H^+$	$3.07E+12 \exp(-1500/T)$
L34.	$NO_2 + OH \rightarrow NO_3^- + H^+$	$2.0E+11 \exp(-1500/T)$
L35.	$HNO_2 + hn \rightarrow NO + OH$	3.7E-5
L36.	$NO_2^- + hn \xrightarrow{H_2O} NO + OH + OH^-$	6.3E-6
L37.	$HNO_2 + OH \rightarrow NO_2 + H_2O$	$1.53E+11 \exp(-1500/T)$
L38.	$NO_2^- + OH \rightarrow NO_2 + OH^-$	$1.53E+12 \exp(-1500/T)$
L39.	$HNO_2 + H_2O_2 \xrightarrow{H^+} NO_3^- + 2H^+ + H_2O$	$3.66E+13 \exp(-6700/T) [H^+]$
L40.	$NO_2^- + O_3 \rightarrow NO_3^- + O_2$	$6.72E+15 \exp(-6950/T)$
L41.	$NO_2^- + CO_3^- \rightarrow NO_2 + CO_3^{2-}$	4.0E+5

Read $1.07E+12 \exp(-1500/T)$ as $1.07 \times 10^{12} e^{-1500/T}$.

Appendix A-2. continued.

No.	Reaction	Rate constant, $M^n s^{-1}$
L42.	$NO_2^- + Cl_2^- \rightarrow NO_2 + 2Cl^-$	$3.84E+10 \exp(-1500/T)$
L43.	$NO_2^- + NO_3 \rightarrow NO_2 + NO_3^-$	$1.84E+11 \exp(-1500/T)$
L44.	$NO_3^- + hn \xrightarrow{H_2O} NO_2 + OH + OH^-$	1.8E-7
L45.	$NO_3 + hn \rightarrow NO + O_2$	0.0
L46.	$NO_3 + HO_2 \rightarrow NO_3^- + H^+ + O_2$	$6.90E+11 \exp(-1500/T)$
L47.	$NO_3 + O_2^- \rightarrow NO_3^- + O_2$	$1.53E+11 \exp(-1500/T)$
L48.	$NO_3 + H_2O_2 \rightarrow NO_3^- + HO_2 + H^+$	$1.20E+10 \exp(-2800/T)$
L49.	$NO_3 + Cl^- \rightarrow NO_3^- + Cl$	$1.53E+10 \exp(-1500/T)$
<u>Methane Oxidation Chain</u>		
L50.	$CH_2(OH)_2 + OH \xrightarrow{o^2} HCOOH + HO_2 + H_2O$	$3.10E+11 \exp(-1500/T)$
L51.	$CH_2(OH)_2 + O_3 \rightarrow \text{Products}$	1.0E-1
L52.	$HCOOH + OH \xrightarrow{o^2} CO_2 + HO_2 + H_2O$	$2.45E+10 \exp(-1500/T)$
L53.	$HCOOH + H_2O_2 \rightarrow \text{Product} + H_2O$	$1.63E+2 \exp(-5180/T)$
L54.	$HCOOH + NO_3 \xrightarrow{o^2} NO_3^- + H^+ + CO_2 + HO_2$	$9.68E+9 \exp(-3200/T)$
L55.	$HCOOH + O_3 \rightarrow CO_2 + HO_2 + OH$	5.0
L56.	$HCOOH + Cl_2^- \xrightarrow{o^2} CO_2 + HO_2 + 2Cl^- + H^+$	$1.24E+10 \exp(-4300/T)$
L57.	$HCOO^- + OH \xrightarrow{o^2} CO_2 + HO_2 + OH^-$	$3.84E+11 \exp(-1500/T)$
L58.	$HCOO^- + O_3 \rightarrow CO_2 + OH + O_2^-$	1.0E+2
L59.	$HCOO^- + NO_3 \xrightarrow{o^2} NO_3^- + CO_2 + HO_2$	$9.21E+9 \exp(-1500/T)$
L60.	$HCOO^- + CO_3^- \xrightarrow{o^2, H_2O} CO_2 + HCO_3^- + HO_2 + OH^-$	$9.92E+9 \exp(-3400/T)$
L61.	$HCOO^- + Cl_2^- \xrightarrow{o^2} CO_2 + HO_2 + 2Cl^-$	$1.17E+10 \exp(-2600/T)$
L62.	$CH_3C(O)O_2NO_2 \rightarrow NO_3^- + \text{Products}$	4.0E-4
L63.	$CH_3O_2 + HO_2 \rightarrow CH_3OOH + O_2$	$1.01E+10 \exp(-3000/T)$
L64.	$CH_3O_2 + O_2^- \xrightarrow{H_2O} CH_3OOH + O_2 + OH^-$	$1.07E+10 \exp(-1600/T)$
L65.	$CH_3OOH + hn \xrightarrow{o^2} HCHO + OH + HO_2$	5.40E-7
L66.	$CH_3OOH + OH \rightarrow CH_3O_2 + H_2O$	$8.11E+9 \exp(-1700/T)$
L67.	$CH_3OH + OH \rightarrow HCHO + HO_2 + H_2O$	$6.91E+8 \exp(-1500/T)$
L68.	$CH_3OH + CO_3^- \xrightarrow{o^2} HCHO + HO_2 + HCO_3^-$	$9.40E+9 \exp(-4500/T)$
L69.	$CH_3OH + Cl_2^- \xrightarrow{o^2} HCHO + HO_2 + H^+ + 2Cl^-$	$9.04E+9 \exp(-4400/T)$
L70.	$CH_3OOH + OH \rightarrow HCHO + OH + H_2O$	$7.98E+9 \exp(-1800/T)$
L71.	$CH_3OH + NO_3 \xrightarrow{o^2} NO_3^- + H^+ + HCHO + HO_2$	$1.20E+10 \exp(-2800/T)$
<u>Sulfur Chemistry</u>		
L72.	$H_2SO_3 + O_3 \rightarrow S(VI)$	2.4E+4
L73.	$HSO_3^- + O_3 \rightarrow S(VI)$	$4.24E+13 \exp(-5530/T)$
L74.	$SO_3^{2-} + O_3 \rightarrow S(VI)$	$7.43E+16 \exp(-5280/T)$
L75.	$HSO_3^- + H_2O_2 \xrightarrow{H^+} S(VI) + H_2O$	$2.9E+10 [H^+] \exp(-1950/T)$ (1 + 16[H+])
L76.	$HSO_3^- + H_2O_2 \xrightarrow{HX} S(VI) + H_2O$	$3.53E+7 [HCOOH]_1 \exp(-1720/T)$ $1.91E+8 [CH_3COOH]_1 \exp(-2620/T)$
L77.	$S(IV) \xrightarrow{o^2, Mn^{2+}, Fe^{3+}} S(VI)$	pH 0-5, $2.6E+3 [Fe^{3+}] + 7.5E+$ $2 [Mn^{2+}] + 1.0E+10 [Fe^{3+}][Mn^{2+}]$ pH >5, $7.5E+2 [Mn^{2+}] + 2E10 [Fe^{3+}][Mn^{2+}]$
L78.	$SO_3^{2-} + OH \xrightarrow{o^2} SO_5^- + OH^-$	$7.06E+11 \exp(-1500/T)$
L79.	$HSO_3^- + OH \xrightarrow{o^2} SO_5^- + H_2O$	$6.44E+11 \exp(-1500/T)$
L80.	$SO_5^- + HSO_3^- \xrightarrow{o^2} HSO_5^- + SO_5^-$	$9.88E+9 \exp(-3100/T)$

Appendix A-2. Continued.

No.	Reaction	Rate constant, $M^n s^{-1}$
L81.	$SO_5^- + SO_3^{2-} \xrightarrow{o^2} HSO_5^- + SO_5^-$	$1.07E+10 \exp(-2000/T)$
L82.	$SO_5^- + O_2^- \xrightarrow{H_2O} HSO_5^- + OH^- + O_2$	$1.53E+10 \exp(-1500/T)$
L83.	$SO_5^- + HCOOH \xrightarrow{o^2} HSO_5^- + CO_2 + HO_2$	$1.06E+10 \exp(-5300/T)$
L84.	$SO_5^- + HCOO^- \xrightarrow{o^2} HSO_5^- + CO_2 + O_2^-$	$9.45E+9 \exp(-4000/T)$
L85.	$SO_5^- + SO_5^- \rightarrow 2SO_4^{2-} + O_2$	$3.07E+10 \exp(-1500/T)$
L86.	$HSO_5^- + HSO_3^- \xrightarrow{H^+} 2SO_4^{2-} + 3H^+$	$6.27E+14 \exp(-4750/T)$
L87.	$HSO_5^- + OH^- \rightarrow SO_5^- + H_2O$	$9.99E+9 \exp(-1900/T)$
L88.	$HSO_5^- + SO_4^{2-} \rightarrow SO_5^- + SO_4^{2-} + H^+$	$5.0E+4$
L89.	$HSO_5^- + NO_2^- \rightarrow HSO_4^- + NO_3^-$	$1.52E+9 \exp(-6650/T)$
L90.	$HSO_5^- + Cl^- \rightarrow SO_4^{2-} + \text{Product}$	$3.38E+7 \exp(-7050/T)$
L91.	$SO_4^- + HSO_3^- \xrightarrow{o^2} SO_4^{2-} + H^+ + SO_5^-$	$2.00E+11 \exp(-1500/T)$
L92.	$SO_4^- + SO_3^{2-} \xrightarrow{o^2} SO_4^{2-} + SO_5^-$	$8.13E+10 \exp(-1500/T)$
L93.	$SO_4^- + HO_2 \rightarrow SO_4^{2-} + H^+ + O_2$	$7.67E+11 \exp(-1500/T)$
L94.	$SO_4^- + O_2^- \rightarrow SO_4^{2-} + O_2$	$7.67E+11 \exp(-1500/T)$
L95.	$SO_4^- + OH^- \rightarrow SO_4^{2-} + OH$	$1.23E+10 \exp(-1500/T)$
L96.	$SO_4^- + H_2O_2 \rightarrow SO_4^{2-} + H^+ + HO_2$	$9.86E+9 \exp(-2000/T)$
L97.	$SO_4^- + NO_2^- \rightarrow SO_4^{2-} + NO_2$	$1.35E+11 \exp(-1500/T)$
L98.	$SO_4^- + HCO_3^- \rightarrow SO_4^{2-} + H^+ + CO_3^-$	$1.04E+10 \exp(-2100/T)$
L99.	$SO_4^- + HCOO^- \xrightarrow{o^2} SO_4^{2-} + CO_2 + HO_2$	$2.61E+10 \exp(-1500/T)$
L100.	$SO_4^- + Cl^- \rightarrow SO_4^{2-} + Cl$	$3.07E+10 \exp(-1500/T)$
L101.	$SO_4^- + HCOOH \xrightarrow{o^2} SO_4^{2-} + H^+ + CO_2 + HO_2$	$1.21E+10 \exp(-2700/T)$
L102.	$S(IV) + CH_3C(O)O_2NO_2 \rightarrow S(VI)$	$6.7E-3$ see note [a]
L103.	$HSO_3^- + CH_3OOH \xrightarrow{H^+} SO_4^{2-} + 2H^+ + \text{Products}$	$6.56E+12 \exp(-3800/T)$
L104.	$HSO_3^- + CH_3C(O)OOH \rightarrow SO_4^{2-} + H^+ + \text{Products}$	$3.37E+13 \exp(-4000/T)$ see note [a]
L105.	$S(IV) + HO_2 \rightarrow S(VI) + OH$	$1.0E+6$
L106.	$S(IV) + O_2^- \xrightarrow{H_2O} S(VI) + OH + OH^-$	$1.0E+5$
L107.	$SO_4^- + CH_3OH \xrightarrow{o^2} SO_4^{2-} + HCHO + H^+ + HO_2$	$1.05E+10 \exp(-1800/T)$
L108.	$2HSO_3^- + NO_3^- \xrightarrow{o^2} NO_3^- + 2H^+ + SO_4^{2-} + SO_4^-$	$1.0E+8$
L109.	$2NO_2 + HSO_3^- \xrightarrow{H_2O} SO_4^{2-} + 3H^+ + 2NO_2^-$	$2.0E+6$
L110a.	$S(IV) + N(III) \rightarrow S(VI) +$	$pH \leq 3 \quad 1.42E+2 [H^+]^{0.5}$
L110b.	$2HSO_3^- + NO_2^- \rightarrow OH^- + HDS$	$pH > 3 \quad 4.76E+3 [H^+] \exp(-6100/T)$
L111.	$HCHO + HSO_3^- \rightarrow HOCH_2SO_3^-$	$4.01E+9 \exp(-4900/T)$
L112.	$HCHO + SO_3^{2-} \xrightarrow{H_2O} HOCH_2SO_3^- + OH^-$	$1.05E+10 \exp(-1800/T)$
L113.	$HOCH_2SO_3^- + OH^- \rightarrow SO_3^{2-} + HCHO + H_2O$	$1.30E+10 \exp(-4500/T)$
L114.	$HOCH_2SO_3^- + OH^- \xrightarrow{o^2} SO_5^- + HCHO + H_2O$	$2.15E+11 \exp(-1500/T)$
L115.	$HSO_3^- + Cl_2^- \xrightarrow{o^2} SO_5^- + 2Cl^- + H^+$	$5.22E+10 \exp(-1500/T)$
L116.	$SO_3^{2-} + Cl_2^- \xrightarrow{o^2} SO_5^- + 2Cl^-$	$2.45E+10 \exp(-1500/T)$
L117.	$DMS + OH^- \rightarrow 0.5DMSO + 0.5DMS + 0.5H_2O$	$1.9E+10$
L118.	$DMS + H_2O_2 \rightarrow DMSO + H_2O$	$3.5E-2$
L119.	$DMS + O_3 \rightarrow DMSO + O_2$	$6.72E+15 \exp(-4832/T)$
L120.	$DMSO + O_3 \rightarrow DMSO_2 + O_2$	5.7

a For non-elementary rate expression, $[S(IV)] = [SO_2]_w$; $[S(VI)] = [H_2SO_4]_w$;
 $[N(III)] = [HNO_2]_w$.

Appendix A-3. Dissolution equilibria in MaTChM, taken from Zaveri (1997) and references therein.

No.	Dissolution Equilibria	Henry's Law Constant, H [$M_{(l)}/M_{(g)}$]
E1.	$\text{HNO}_3(\text{g}) \rightleftharpoons \text{HNO}_3(\text{l})$	$5.1\text{E}+6 \exp(8700\text{FT})$
E2.	$\text{HNO}_2(\text{g}) \rightleftharpoons \text{HNO}_2(\text{l})$	$1.2\text{E}+3 \exp(4780\text{FT})$
E3.	$\text{SO}_2(\text{g}) \rightleftharpoons \text{H}_2\text{SO}_3$	$3.0\text{E}+1 \exp(3120\text{FT})$
E4.	$\text{H}_2\text{SO}_4(\text{g}) \rightleftharpoons \text{H}_2\text{SO}_4(\text{l})$	$1.0\text{E}+3$
E5.	$\text{HCOOH}(\text{g}) \rightleftharpoons \text{HCOOH}(\text{l})$	$9.04\text{E}+4 \exp(5700\text{FT})$
E6.	$\text{CH}_3\text{COOH}(\text{g}) \rightleftharpoons \text{CH}_3\text{COOH}(\text{l})$	$1.0\text{E}+3$ (assumed)
E7.	$\text{CO}_2(\text{g}) \rightleftharpoons \text{H}_2\text{CO}_3$	$8.31\text{E}-1 \exp(2420\text{FT})$
E8.	$\text{MSA}(\text{g}) \rightleftharpoons \text{MSA}(\text{l})$	$1.0\text{E}+3$ (assumed)
E9.	$\text{NH}_3(\text{g}) \rightleftharpoons \text{NH}_4\text{OH}$	$1.38\text{E}+3 \exp(4181\text{FT})$
E10.	$\text{HO}_2(\text{g}) \rightleftharpoons \text{HO}_2(\text{l})$	$4.89\text{E}+4 \exp(6640\text{FT})$
E11.	$\text{H}_2\text{O}_2(\text{g}) \rightleftharpoons \text{H}_2\text{O}_2(\text{l})$	$2.44\text{E}+1 \exp(7514/T - 13.63)$
E12.	$\text{HCHO}(\text{g}) \rightleftharpoons \text{HCHO}(\text{l})$	$1.54\text{E}+5 \exp(6460\text{FT})$
E13.	$\text{NO}_2(\text{g}) \rightleftharpoons \text{NO}_2(\text{l})$	$2.44\text{E}-1 \exp(2500\text{FT})$
E14.	$\text{NO}(\text{g}) \rightleftharpoons \text{NO}(\text{l})$	$4.64\text{E}-2 \exp(1480\text{FT})$
E15.	$\text{NO}_3(\text{g}) \rightleftharpoons \text{NO}_3(\text{l})$	$3.67\text{E}+2$
E16.	$\text{PAN}(\text{g}) \rightleftharpoons \text{PAN}(\text{l})$	$7.1\text{E}+1 \exp(5910\text{FT})$
E17.	$\text{O}_3(\text{g}) \rightleftharpoons \text{O}_3(\text{l})$	$2.76\text{E}-1 \exp(2300\text{FT})$
E18.	$\text{OH}(\text{g}) \rightleftharpoons \text{OH}(\text{l})$	$6.10\text{E}+2 \exp(5280\text{FT})$
E19.	$\text{CH}_3\text{O}_2(\text{g}) \rightleftharpoons \text{CH}_3\text{O}_2(\text{l})$	$1.46\text{E}+2 \exp(5600\text{FT})$
E20.	$\text{CH}_3\text{OH}(\text{g}) \rightleftharpoons \text{CH}_3\text{OH}(\text{l})$	$5.38\text{E}+3 \exp(4900\text{FT})$
E21.	$\text{DMS}(\text{g}) \rightleftharpoons \text{DMS}(\text{l})$	$1.17\text{E}-4 \exp(3480/T)$
E22.	$\text{DMSO}(\text{g}) \rightleftharpoons \text{DMSO}(\text{l})$	$2.44\text{E}+7$
E23.	$\text{DMSO}_2(\text{g}) \rightleftharpoons \text{DMSO}_2(\text{l})$	$1.0\text{E}+4$ (assumed)
E24.	$\text{CH}_3\text{OOH}(\text{g}) \rightleftharpoons \text{CH}_3\text{OOH}(\text{l})$	$5.55\text{E}+3 \exp(5610\text{FT})$
E25.	$\text{CH}_3\text{C}(\text{O})\text{OOH}(\text{g}) \rightleftharpoons \text{CH}_3\text{C}(\text{O})\text{OOH}(\text{l})$	$1.15\text{E}+4 \exp(6170\text{FT})$
E26.	$\text{N}_2\text{O}_5(\text{g}) \rightarrow 2\text{HNO}_3(\text{w})$	$1.0\text{E}+4$ (assumed)
E27.	$\text{NTR}(\text{g}) \rightleftharpoons \text{NTR}(\text{l})$	1.0 (assumed)
E28.	$\text{HCl}(\text{g}) \rightleftharpoons \text{HCl}(\text{l})$	$1.77\text{E}+4 \exp(2020\text{FT})$
E29.	$\text{Cl}(\text{g}) \rightleftharpoons \text{Cl}(\text{l})$	$1.77\text{E}+4 \exp(2020\text{FT})$

Appendix A-4. Dissociation equilibria in MaTChM, taken from Zaveri (1997) and references therein.

No.	Dissociation Equilibrium	Dissociation Constant, M or M atm ⁻¹
D1.	$\text{H}_2\text{O} \rightleftharpoons \text{H}^+ + \text{OH}^-$	$1.00\text{E-}14 \exp(-6716\text{FT})$
D2.	$\text{HO}_2(\text{l}) \rightleftharpoons \text{H}^+ + \text{O}_2^-$	$3.50\text{E-}5$
D3.	$\text{H}_2\text{O}_2(\text{l}) \rightleftharpoons \text{HO}_2^- + \text{H}^+$	$2.2\text{E-}12 \exp(-3730\text{FT})$
D4.	$\text{H}_2\text{CO}_3 \rightleftharpoons \text{HCO}_3^- + \text{H}^+$	$4.46\text{E-}7 \exp(-1000\text{FT})$
D5.	$\text{HCO}_3^- \rightleftharpoons \text{CO}_3^{2-} + \text{H}^+$	$4.48\text{E-}11 \exp(-1760\text{FT})$
D6.	$\text{HNO}_3(\text{l}) \rightleftharpoons \text{NO}_3^- + \text{H}^+$	15.4
D7.	$\text{HNO}_2(\text{l}) \rightleftharpoons \text{NO}_2^- + \text{H}^+$	$5.1\text{E-}4 \exp(-1260\text{FT})$
D8.	$\text{NH}_4\text{OH} \rightleftharpoons \text{NH}_4^+ + \text{OH}^-$	$1.75\text{E-}5 \exp(-450\text{FT})$
D9.	$\text{HCHO}(\text{l}) \rightleftharpoons \text{CH}_2(\text{OH})_2(\text{l})$	$1.82\text{E+}3 \exp(4020\text{FT})$
D10.	$\text{H}_2\text{SO}_3 \rightleftharpoons \text{HSO}_3^- + \text{H}^+$	$1.23\text{E-}2 \exp(1960\text{FT})$
D11.	$\text{HSO}_3^- \rightleftharpoons \text{SO}_3^{2-} + \text{H}^+$	$6.61\text{E-}8 \exp(1500\text{FT})$
D12.	$\text{H}_2\text{SO}_4(\text{l}) \rightleftharpoons \text{HSO}_4^- + \text{H}^+$	$1.00\text{E+}3$
D13.	$\text{HSO}_4^- \rightleftharpoons \text{SO}_4^{2-} + \text{H}^+$	$1.02\text{E-}2 \exp(2720\text{FT})$
D14.	$\text{HCl}(\text{l}) \rightleftharpoons \text{H}^+ + \text{Cl}^-$	$1.74\text{E+}6 \exp(6900\text{FT})$
D15.	$\text{Cl}_2 \rightleftharpoons \text{Cl} + \text{Cl}^-$	$5.26\text{E-}6$
D16.	$\text{HCOOH}(\text{l}) \rightleftharpoons \text{HCOO}^- + \text{H}^+$	$1.78\text{E-}4 \exp(-20\text{FT})$
D17.	$\text{CH}_3\text{COOH}(\text{l}) \rightleftharpoons \text{CH}_3\text{COO}^- + \text{H}^+$	$1.0\text{E-}4$
D18.	$\text{CH}_3\text{SO}_3\text{H} \rightleftharpoons \text{CH}_3\text{SO}_3^- + \text{H}^+$	$6.31\text{E-}2$

Note: $\text{FT} = (1/\text{T} - 1/298)$, T in Kelvin, Read $5.1\text{E+}6 \exp(8700\text{FT})$ as $5.1 \times 10^6 \exp(8700(1/\text{T}-1/298))$.